Methods for Pricing Pre-Earnings Equity Options and Leveraged ETF Options

Marco Santoli

Submitted in partial fulfillment of the
requirements for the degree
of Doctor of Philosophy
in the Graduate School of Arts and Sciences

COLUMBIA UNIVERSITY

2015

ABSTRACT

Methods for Pricing Pre-Earnings Equity Options and Leveraged ETF Options

Marco Santoli

In this thesis, we present several analytical and numerical methods for two financial engineering problems: 1) accounting for the impact of an earnings announcement on the price and implied volatility of the associated equity options, and 2) analyzing the price dynamics of leveraged exchange-traded funds (LETFs) and valuation of LETF options. Our pricing models capture the main characteristics of these options, along with jumps and stochastic volatility in the underlying asset. We illustrate our results through numerical implementation and calibration using market data.

In the first part, we model the pricing of equity options around an earnings announcement (EA). Empirical studies have shown that an earnings announcement can lead to an immediate price shock to the company stock. Since many companies also have options written on their stocks, the option prices should reflect the uncertain price impact of an upcoming EA before expiration. To represent the shock due to earnings, we incorporate a random jump on the announcement date in the dynamics of the stock price. We consider different distributions of the scheduled earnings jump as well as different underlying stock price dynamics before and after the EA date. Our main contributions include analytical option pricing formulas when the underlying stock price follows the Kou model along with a double-exponential or Gaussian EA jump on the announcement date. Furthermore, we derive analytic bounds and asymptotics for the pre-EA implied volatility under various models. The calibration results demonstrate adequate fit of the entire implied volatility surface prior to an announcement. The comparison of the risk-neutral distribution of the EA jump to its historical counterpart is also discussed. Moreover, we discuss the valuation and exercise strategy of pre-EA American options, and present an analytical approximation

and numerical results.

The second part focuses on the analysis of LETFs. We start by providing a quantitative risk analysis of LETFs with an emphasis on the impact of leverage ratios and investment horizons. Given an investment horizon, different leverage ratios imply different levels of risk. Therefore, the idea of an admissible range of leverage ratios is introduced. For an admissible leverage ratio, the associated LETF satisfies a given risk constraint based on, for example, the value-at-risk (VaR) and conditional VaR. Moreover, we discuss the concept of admissible risk horizon so that the investor can control risk exposure by selecting an appropriate holding period. The intra-horizon risk is calculated, showing that higher leverage can significantly increase the probability of an LETF value hitting a lower level. This leads us to evaluate a stop-loss/take-profit strategy for LETFs and determine the optimal take-profit given a stop-loss risk constraint. In addition, the impact of volatility exposure on the returns of different LETF portfolios is investigated.

In the last chapter, we study the pricing of options written on LETFs. Since LETFs on the same reference index share the same source of risk, it is important to consider a consistent pricing methodology of these options. In addition, LETFs can theoretically experience a loss greater than 100%. In practice, some LETF providers design the fund so that the daily returns are capped both downward and upward. We incorporate these features and model the reference index by a stochastic volatility model with jumps. An efficient numerical algorithm based on transform methods to value options under this model is presented. We illustrate the accuracy of our pricing algorithm by comparing it to existing methods. Calibration using empirical option data shows the impact of leverage ratio on the implied volatility. Our method is extended to price American-style LETF options.

Table of Contents

List of Figures

List of Tables

Acknowledgments

First and foremost, I am deeply grateful to my academic advisor Professor Tim Leung. His continuous support, guidance and encouragement truly made this dissertation possible. Professor Leung excels as an advisor in many ways. Not only is he knowledgeable and resourceful, but he is also patient, supportive and readily available regardless of his very busy schedule. His forthright and effective feedback was invaluable to my research. Furthermore, I am appreciative of his patience in allowing me to work on my own ideas and to develop as an independent researcher. Professor Leung, with his incessant pursuit of academic and intellectual excellence is, and will always be, an inspiration to me.

I am grateful to my committee, Professors Karl Sigman, Xuedong He, Agostino Capponi and Jamol Pender. I kindly thank them for participating in my thesis defense committee, and for the feedback received on my dissertation.

During my doctoral program at Columbia University, I had the pleasure and privilege to interact with exceptional individuals who inspired and motivated me, as well as helped me build stronger foundations on which to continue my intellectual journey. The list would be too long to mention them all, but special thanks go to Professors Donald Goldfarb, Martin Haugh, Soulaymane Kachani, Garud Iyengar, Ward Whitt and Dr. Mike Lipkin. I thank the entire faculty of the Industrial Engineering and Operations Research department at Columbia University, for providing me with top of the class lectures and for their availability.

I kindly thank Adina Brooks, Jenny Mak, Jaya Mohanty, Darbi Roberts, Krupa Thakore and others in the department staff and school administration. Their friendly help and availability is unmatched and allowed me to focus on my research. A special thanks to Adina Brooks who helped me to a great extent when I was managing the Columbia Quantitative Network student group. Without her guidance, the group could not have been as successful as it was.

I thank my college Professors Marco Frittelli, Franco Gallone and Marco Bramanti. These remarkable characters and excellent teachers guided, motivated and supported my efforts. They played a crucial role in my pursuit of a doctoral education and I will always be sincerely grateful to them. This dissertation would not have been possible without their vision.

My sincerest thanks go to many friends and colleagues, several of whom are also Ph.D. fellows: Arseniy Kukanov, Aditi Dandapani, Shyam Chandramouli, Jinbeom Kim, Ningyuan Chen, Yin Lu, Aya Wallwater, Peter Maceli, Cun Mu, Carlos Abad, Cecilia Zenteno, Rodrigo Carrasco, Juan Li, Yujiao Chen, Xin Li, Alex Michalka, Andrew Ahn, Itai Feigenbaum, Akshay Shah, Federico Meloni, Daniele Alfonsi, Liuyu Chen, Paulina Mangubat, Lorenzo Mortaro, Vaibhav Bhandari, Suraj Malladi, Eric Wu and Eric A. Wu, Rahim Damji, Rajiv Chopra, Stefano Mosso and many others who are not on this list but to whom I am grateful for their friendship and support. I also thank my aunt and uncle, Luisa Miglioranzi and Claudio Menini, for their generosity and kindness. A special thanks goes to my girlfriend Kristen Toms, for her genuine friendship and support, especially during the most challenging times.

Last but not least, I am deeply indebted to my parents, Claudio Santoli and Giuliana Miglioranzi. Their love and guidance is an inspiration. I will always be grateful, and I dedicate my contributions to them.

To my parents.

Chapter 1

Introduction

> In theory, theory and practice are the same.
> But in practice, they are very different.
>
> *Casey Stengel*

This thesis studies analytical and numerical methods for two financial engineering problems: 1) accounting for the impact of an earnings announcement on the price and implied volatility of the associated equity options, and 2) analyzing the price dynamics of leveraged exchange-traded funds (LETFs) and valuation of LETF options. Our valuation models capture the main characteristics of these options such as the dynamic behavior of the implied volatility (IV) of equity options observed prior to an earnings event. One of the main challenge in analyzing these problems is that candidate pricing models often lose some of their analytical tractability. This is especially true when stochastic volatility and jumps in the underlying are accounted for. We demonstrate through numerical implementation and calibration using market data that the proposed models are able to produce the desired characteristic of these options, while allowing for efficient computation.

1.1 Earnings Announcement

Public companies routinely release summaries of their operations and performance, including income statements, balance sheets, and other reports. Such events are commonly referred to as *earnings announcements*. In the market session following a scheduled an-

nouncement[1], empirical studies (see, for example, Patell and Wolfson (1984)) suggest that the opening stock price can move drastically. For instance, Dubinsky and Johannes (2006) study a sample of stocks and report that the variance of stock price returns on the earnings announcement date is over five times greater than those on other dates. In addition to the immediate price impact, earnings releases may also affect the drift of the stock price over a longer horizon. This empirical observation is commonly referred to as the post-earnings-announcement drift; see Chordia and Shivakumar (2006) and references therein.

Since many public companies also have options written on their stock prices, this motivates us to investigate the problem of pricing equity options prior to an earnings announcement (EA). As options are intrinsically forward-looking contracts, their prices should account for the uncertain stock price impact of an upcoming earnings release. A natural question is how to extract some information on such an impact from observed options prices, especially a few days before the announcement. Since traders often quote or study the implied volatility (IV) for each option, in practice it is also important to better understand the behavior of the *pre-earnings announcement implied volatility* (PEAIV). For example, one of the main features of the PEAIV is that it tends to rise, often rather drastically, until the announcement date (see Figures 2.1 and 2.2 in Chapter 2). These empirical observations call for the development of new pricing models that account for these phenomena.

In Chapter 2, we analyze an option pricing framework that accounts for the price impact of an earnings announcement, with emphasis on the behavior of the implied volatility prior to the event. Specifically, we introduce a random-sized jump scheduled on the earnings announcement date to represent the shock to the company stock price. The introduction of a jump related to earnings is consistent with prior empirical studies (Maheu and McCurdy (2004); Piazzesi (2005); Dubinsky and Johannes (2006); Lee and Mykland (2008)). We first apply this idea to the Black and Scholes (1973) (BS) model, where we obtain formulas for the pre-EA European option price, its IV and various Greeks. In this model, we find that the IV increases with a specific pattern as time approaches the announcement date. We further incorporate additional random-time jumps in the stock price by extending the Kou (2002)

[1]Earnings reports are commonly released after the market closes. Therefore, the price impact of earnings are first reflected at the beginning of the next market session.

double-exponential (DE) jump-diffusion model to incorporate an EA jump. Specifically, we assume that the EA jump size for the log stock price is either a DE or Gaussian random variable. In both cases, analytic option pricing formulas are derived and used to generate IVs. We also extend the Heston (1993) stochastic volatility model and show how to price options via transform methods under the extended framework. The methodology is rather general and therefore large classes of models, including Lévy, can be priced in a similar way.

To better understand the behavior of the PEAIV, we derive analytic bounds and asymptotics of the IV for extreme strikes under a general class of stock price models with an EA jump. In the bounds, we observe the explicit dependence on EA jump parameters and a common time-dependence of the PEAIV across these models. In addition, we calibrate a number of models, namely the extended Heston and Kou models with an EA jump, to market option prices. Our results demonstrate a more adequate fit of the entire PEAIV surface, as compared to the same models without the EA jump. Furthermore, we extract the risk-neutral distribution of the EA jump and compare it to its historical distribution. The discrepancy between the two distributions can be interpreted as a risk premium for the jump risk due to earnings. We conclude the first part by analyzing the pricing of American options before and after an EA date. For implementation, we discuss a numerical method as well as an analytical approximation based on the work of Barone-Adesi and Whaley (1987). The results of Chapter 2 are adapted from Leung and Santoli (2014).

1.2 Leveraged ETFs

The exchange-traded fund (ETF) market has grown substantially in recent years. As of November 30, 2014, the US ETF industry consisted of 1,450 funds with over $1.9 trillion in assets under management (AUM)[2]. Equity ETFs constitute the majority of AUM, with over $1.5 trillion, followed by fixed income and commodity ETFs, with over $320 billion and $53 billion respectively. Within the ETF market, leveraged ETFs (LETFs) have gained

[2] "2015 ETF and Investment Outlook" by David Mazza et al., SPDR ETF Strategy & Consulting, State Street Global Advisors

popularity among investors with over $61 billion AUM as of October 31, 2014[3]. LETFs are typically designed to replicate multiples of the daily returns of some underlying index or benchmark. For example, the ProShares Ultra S&P 500 (SSO) is expected to generate twice the daily returns of the S&P 500 index, minus a small expense fee. Moreover, investors can take a bearish position on the underlying index by going long an inverse LETF (i.e. a LETF with a negative leverage ratio). An example is the ProShares UltraShort S&P 500 (SDS) on the S&P 500 with leverage ratio of -2. In addition, both long and short triple LETFs are available for various underlyings. For many investors, LETFs are a highly accessible and liquid instrument. They also tend to be more effective during periods of large momentum and low volatility.

On the other hand, LETFs have drawn a number of criticisms. Some argue that they tend to underperform over extended (quarterly or annual) investment horizons, as compared to the nominal multiple of the underlying index returns (see Figures 3.1 and 3.2 in Chapter 3). This underperformance has been attributed to ill-timed rebalancing, returns compounding, and the use of derivatives to replicate returns. In a discrete-time model, Cheng and Madhavan (2009) illustrate that the LETF value can erode due to its dependence on the realized variance of the underlying index, coupled with daily re-balancing. Avellaneda and Zhang (2010) also discuss the path-dependent performance and potential tracking errors of LETFs under both discrete-time and continuous-time frameworks. In fact, the SEC has issued an alert announcement regarding the riskiness of LETFs[4] and investigated whether LETFs would create a feedback effect, leading to increased market volatility[5].

From the perspective of an LETF holder, it is thus crucial to understand the roles of leverage ratios and investment horizons in the risk and return of the fund. In Chapter 3, we provide a quantitative risk analysis of LETFs with an emphasis on the impact of leverage and investment horizon. A number of market observations suggest that value erosion is more severe for highly leveraged ETFs. As an example, we compare the empirical returns of several major LETFs based on the S&P 500 index against multiples of the unleveraged ETF.

[3] "Short & Leveraged ETFs/ETPs Global Flows Report", Boost ETP, a WisdomTree Company.

[4] See http://www.sec.gov/investor/pubs/leveragedetfs-alert.htm

[5] See "SEC Looks Into Effect of ETFs on Market," Wall Street Journal, September 7, 2011.

The performance of LETFs generally declines as the investment horizon or the (absolute) leverage ratio increase. This motivates the analysis of the risk impact of leverage as well as risk horizon. Given an investment horizon, different leverage ratios imply different levels of risk. Therefore, we introduce the idea of an admissible range of leverage ratios. These are the leverage ratios for which the associated LETFs satisfy a given risk constraint based on, for example, the value-at-risk (VaR) and conditional VaR. This idea can help investors exclude LETFs that are deemed too risky. Moreover, we discuss the concept of admissible risk horizon so that the investor can control risk exposure by selecting an appropriate holding period. In addition, we compute the intra-horizon risk and find that higher leverage can significantly increase the probability of the LETF value hitting a lower level. This leads us to evaluate a stop-loss/take-profit strategy for LETFs. In particular, we determine the optimal take-profit level given a stop-loss risk constraint. Lastly, we investigate the impact of volatility exposure on the returns of different LETF portfolios. The results of Chapter 3 are adapted from Leung and Santoli (2012).

In Chapter 4, we shift our focus to the pricing of options written on LETFs. While existing models can arguably be used to price options written on a particular LETF, the mere existence of LETFs with the same reference index—but with different leverage ratios—raises the question of how to price these options in a consistent manner. In practice, ETF providers that offer leveraged funds on a particular index or security always create a group of LETFs to track different multiples of the underlier's returns. In most cases, 6 ETFs related to positive and negative multiples—from 1x to 3x—are offered. Therefore, LETFs that are designed to track the same underlying asset, e.g. the S&P500 index, ultimately share the same source of risk.

In our work, we propose a methodology for the pricing of options where the reference index is modeled by a Heston stochastic volatility model with jumps in the underlying. Our choice is motivated by the tractability of this model as well as its ability to reproduce, to a certain extent, observed features of the implied volatility surface. We start our analysis by considering the pricing problem when the reference index follows a Heston process without jumps. In this relevant case, the LETF price also follows the Heston dynamics. This simple yet significant result allows for tractability and efficient numerical pricing of options

on LETFs. Thus, we analyze a practical calibration example under this framework and discuss our results. More specifically, we obtain the option prices for 6 LETFs on the reference S&P500 index and calibrate a Heston model on each of them separately. We then obtain the reference index model parameters implied by each of this calibrations—and their respective IV surfaces—and compare them to each other. We find that the model parameters agree to a significant extent, with the exception of a non-negligible difference between long and short LETFs. We then proceed by including random jumps in the dynamics of the reference index. In contrast to the basic Heston model, the LETF dynamics are no longer of the same kind. While the continuous part of the dynamics is still Heston, the jump part is generally not of the same kind as that of the reference index. As a consequence, the model loses some of its tractability and a new pricing algorithm is required. We propose a numerical transform method and show that it is possible to price the options with the same computational complexity as in the Heston case, as well as for general distributions of the jump size. To prove the validity of our results, we then analyze a pricing example and compare it with results from the literature. We find that our algorithm performs well and with improved accuracy compared to existing methods.

Furthermore, we model other features relevant to the problem of consistent pricing of LETF options. LETF providers may buy insurance against adverse moves in the underlier (see Section 4.3 for a detailed discussion and references). Managers can pay for this protection by capping the LETF gains during favorable moves of the reference index. We thus incorporate the effects of such caps and floors on the LETF returns dynamics. We are able to include these effects in our pricing algorithm and evaluate their effects on the pricing of LETF options. Next, we consider the impact of discrete rebalancing of the LETF on the pricing of the options. Once again, we present accurate and efficient algorithms to incorporate this effect with the pricing of options and show a few examples under the Black and Scholes (1973), Merton (1976) and Bates (1996) (SVJ) models. We show that, in several cases, a rebalancing frequency of 1 day likely causes negligible effects on option prices. Finally, we show how to price American options written on LETFs under Lévy models by adopting the same methodology used to price European options.

Chapter 2

Accounting for Earnings in the Pricing of Equity Options

> There are known knowns. These are things we know that we know. There are known unknowns. That is to say, there are things that we know we don't know. But there are also unknown unknowns. There are things we don't know we don't know.
>
> *Donald Rumsfeld*

In this chapter, we study the pricing of equity options prior to an earnings announcement. In particular, we introduce a valuation framework whereby the shock to the company stock price is modeled by a random-sized jump scheduled on the earnings announcement date. In Section 2.1, we present some empirical observations on the implied volatility evolution days before and after an earnings announcement. Section 2.2 summarizes the existing literature on the pricing of pre-earnings equity options and discusses our contribution. In Section 2.3, we extend the Black-Scholes model by incorporating a scheduled, random EA jump in the stock price, and derive the corresponding implied volatility function and Greeks. In Section 2.4, we incorporate EA jumps in other models, including the Kou and Heston models. Among our results, we provide an analytic formula for the option price under the extended Kou model. In Section 2.5, bounds and asymptotics for the IV surface under various models are derived. Here, we find that a characteristic pattern for the evolution

of the IV is shared across different models. Section 4.2 illustrates the calibration results based on the extended BS, Kou, and Heston models. We also compare the risk-neutral and historical distributions of jumps due to earnings announcements. In Section 4.4, we study the valuation of American options prior to an earnings announcement. The results of this chapter are adapted from Leung and Santoli (2014).

2.1 Market Observations

We start by looking at the behavior of price and implied volatility in the days preceding an earnings announcement. In Figure 2.1, we show the price and IV of the front month (i.e. with the nearest maturity date) at-the-money (ATM) call option written on IBM. Following an earnings announcement on July 17, 2013, the option expires on the Friday in the same week. As we can see on the bottom panel, the IV increases rapidly from 30% to over 70% as time approaches the earnings announcement, and then drops significantly to close to 20% after the earnings report is released. At the same time, the ATM call price stays well above zero even though the time to maturity is very short (Figure 2.1 (top)). Moreover, we observe that the IV reaches a maximum just before an earnings event.

Let us briefly discuss the intuitions behind these observations. First, the market price of an option expiring after an earnings announcement reflects the possibility of a jump in the stock price on the announcement date. Since the Black-Scholes formula, which is used to convert option prices to IVs, assumes a log-normal model for the underlying price without jumps, the only way to account for the deterministically timed yet random jump in the stock price is to apply a higher volatility parameter. Furthermore, since the volatility parameter in the Black-Scholes formula is coupled with time-to-maturity, an even higher volatility parameter is needed as time progresses. As a result, even though the stock price may not experience a higher (historical) volatility or clear directional movements before earnings, the (risk-neutral) IV tends to increase. However, as soon as the earnings announcement is made, the jump in the stock price is realized and the volatility effect will also disappear.

To illustrate that the increasing PEAIV is more than a coincidence, in Figure 2.2 (top) we plot the time series of the IV of the ATM call option for IBM from January 1996 to

August 2013. In the same figure, we mark in red the IV values on days during which earnings announcements were made. As we can see, spikes in volatility most often coincide with the earnings release dates. We can also gain some insight from the shape of the implied volatility surface. In Figure 2.2 (bottom), we show the IV surface of IBM on July 15, 2013, two days before an earnings release. It is also clear that the front month options, which have 1 day to expiration, have very high volatility. The implied volatility is significantly lower for longer-term options, suggesting a less pronounced effect of the upcoming earnings announcement.

2.2 Related Studies

There is a wealth of literature in empirical finance and accounting that examines how earnings announcements affect stock and option prices. Most of the studies focus on the informational content, market reactions and price patterns associated with earnings releases. Systematic reviews of the empirical studies can be found in Dubinsky and Johannes (2006), Barth et al. (2011), Rogers et al. (2009) and Billings and Jennings (2011). For the price impact of news on futures, we refer to Chatrah et al. (2009) and references therein. Below, we summarize a number of related studies that focus on option prices prior to an earnings announcement.

The model by Patell and Wolfson (1981) (PW) is among the first empirical studies on the prices of options in the presence of an earnings announcement. They build on the pricing models of Black and Scholes (1973) and Merton (1973), and assume the instantaneous volatility as a deterministic piece-wise constant function of time, with two volatility levels over two time windows around the earnings release in order to reflect the uncertainty surrounding the earnings impact. Since their seminal work, other papers have adopted the same model or its variations and performed empirical tests (see Donders and Vorst (1996), Isakov and Perignon (2001), Barth et al. (2011), among others). In particular, Barth et al. (2011) extend PW's model by allowing the deterministic piece-wise constant volatility to take different values before, during, and after the announcement date. In all these empirical studies, there are no jumps incorporated in the stock price at anytime. Moreover, without

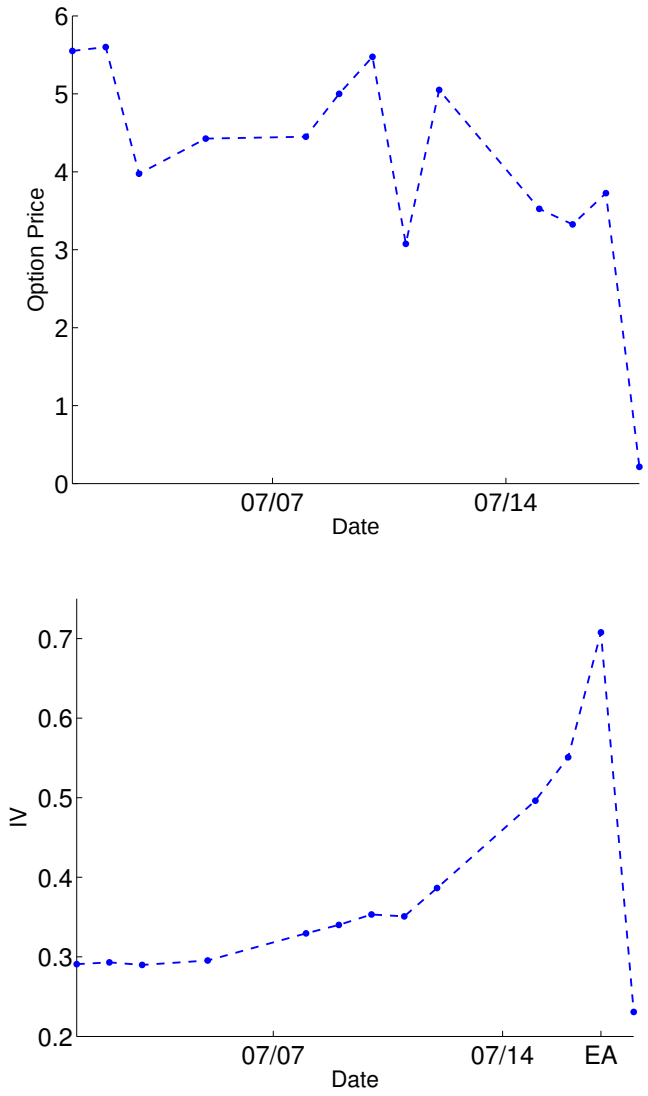

Figure 2.1: The price (top) and implied volatility (bottom) of the front month ATM option on IBM with expiration date July 19, 2013. The earnings announcement date is July 17, 2013.

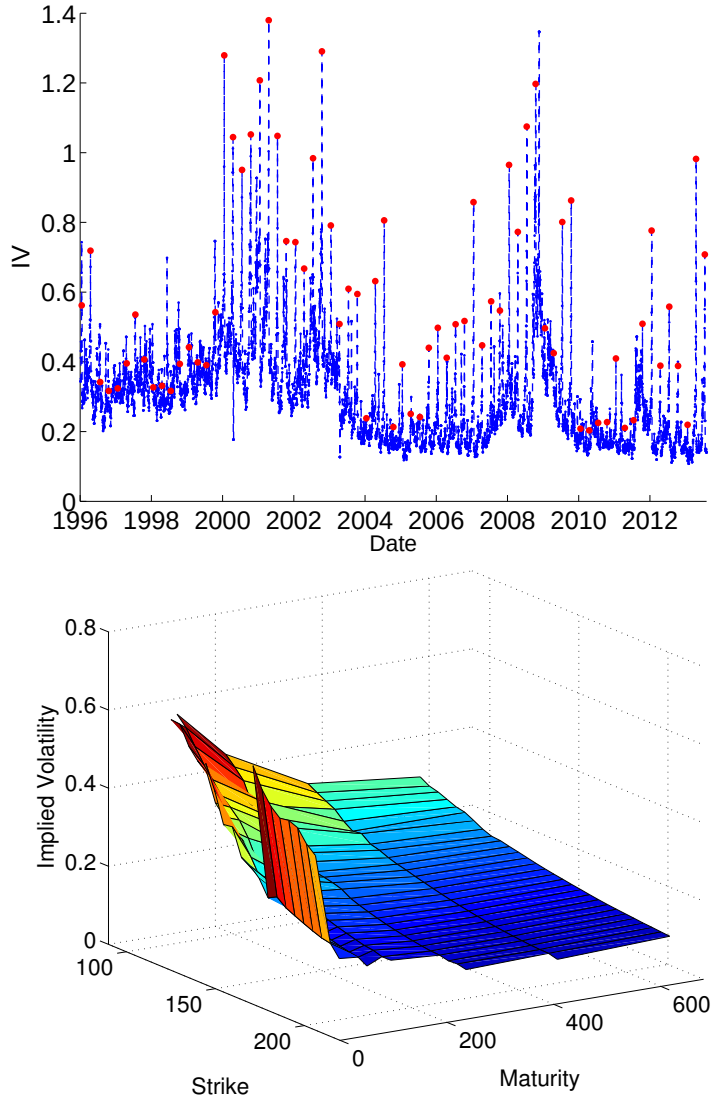

Figure 2.2: The time series (top) of the IV of the front month ATM call on IBM. The red dots mark the value of the IV on EA dates. The IV surface (bottom) of IBM at the market close on July 15, 2013, two days before an EA.

stochastic volatility or jumps in the stock price, the IV will not exhibit any skew, though this is commonly observed in the options market.

In this dissertation, we adopt a different approach by incorporating a deterministic-time random jump in the stock price dynamics. We consider different distributions of the scheduled earnings jump as well as different underlying stock price dynamics before and after the EA date. Our study generalizes that of Dubinsky and Johannes (2006), which focuses on the BS model with a Gaussian EA jump and provide a formula for the time-deterministic implied volatility function. Our main contributions include analytical option pricing formulas when the underlying stock price admits doubly exponential jumps over time (the Kou model), along with a double-exponential or Gaussian EA jump on the announcement date (see Theorem 2.4.1). Furthermore, we derive analytic bounds and asymptotics for the pre-EA implied volatility under various models (see Propositions 2.5.1 and 2.5.2). In addition, we study the pricing of pre-earnings American options under the Kou model and discuss an analytic approximation to the option price by extending the method of Barone-Adesi and Whaley (1987).

Our analysis draws motivation from empirical studies and market observations to introduce more sophisticated models that help reproduce the entire implied volatility surface accurately and tractably. For calibration, we employ recent options data from the whole observed IV surface, instead of ATM only options used in Dubinsky and Johannes (2006). Using earnings data from 1994 to 2013, we also compare the risk-neutral distribution of the EA jump to its historical distribution. The framework and methods introduced herein can be readily generalized to other option pricing models. They can also be useful for monitoring the PEAIV, and estimating the historical and risk-neutral distributions of the EA jump and the associated risk premium.

2.3 Black-Scholes Model with an EA Jump

The effect of a scheduled earnings announcement on the stock price is modeled by a deterministic-time random-size price jump in the price dynamics. Naturally, this modification can be applied to virtually any model, and we start with an extension of the Black

and Scholes (1973) model.

Let $(W_t)_{t\geq 0}$ be a standard Brownian motion defined on the risk-neutral probability space $(\Omega, \mathcal{F}, \mathbb{Q})$. Throughout, we assume a constant risk-free rate $r \geq 0$. Let T_e be the EA date, and we call the r.v. Z_e the EA jump, which is the jump size of the log stock price immediately after the earnings announcement. We assume Z_e to be independent of W. Under the risk-neutral measure, the company stock price $(S_t)_{t\geq 0}$ evolves according to

$$\frac{dS_t}{S_{t_-}} = rdt + \sigma dW_t + d\left(1_{\{t\geq T_e\}}\left(e^{Z_e} - 1\right)\right), \tag{2.3.1}$$

where $1_{\{\cdot\}}$ denotes the indicator function, r is the positive constant interest rate, and σ represents the constant volatility. The martingale condition $S_0 = \mathbb{E}\left\{e^{-rt}S_t\right\},\ 0 \leq t \leq T$, where $\mathbb{E}\{\cdot\}$ denotes the expectation under $\mathbb{Q}$, implies that $\mathbb{E}\left\{e^{Z_e}\right\} = 1$.

In this section, we assume that Z_e is *normally* distributed. This yields closed form expressions for the price and the IV surface. The martingale condition $\mathbb{E}\left\{e^{Z_e}\right\} = 1$ implies that $Z_e \sim N\left(-\frac{\sigma_e^2}{2}, \sigma_e^2\right)$, so the EA jump is parametrized by σ_e only. We notice that, for $T \geq T_e$,

$$\log\left(\frac{S_T}{S_t}\right) \sim N\left(\left(r - \frac{\sigma^2}{2} - \frac{\sigma_e^2}{2(T-t)}\right)(T-t),\ \sigma^2(T-t) + \sigma_e^2\right). \tag{2.3.2}$$

Therefore, the price of a European call with strike K and maturity T is given by

$$C(t, S_t) = C_{BS}\left(T - t, S_t; \sqrt{\sigma^2 + \frac{\sigma_e^2}{T-t}}, K, r\right), \quad 0 \leq t < T_e, \tag{2.3.3}$$

where $C_{BS}(\tau, S; \sigma, K, r)$ represents the usual BS formula with time to maturity τ and spot price S.

2.3.1 Implied Volatility

The price formula (2.3.3) allows us to express the implied volatility (IV) as the deterministic function

$$I(t; K, T) = \begin{cases} \sqrt{\sigma^2 + \frac{\sigma_e^2}{T-t}} & 0 \leq t < T_e, \\ \sigma & T_e \leq t < T. \end{cases} \tag{2.3.4}$$

As we can see, although the IV surface, for a fixed time t, is flat across strikes, it has a decreasing term structure in T. In addition, the IV for any particular option increases in

time as we approach the earnings announcement. Alternatively, the option price formula (2.3.3) can be obtained as if the stock has no jump and follows the dynamics

$$\frac{dS_t}{S_t} = rdt + I\left(t; K, T\right) dW_t.$$

This model is used in Patell and Wolfson (1981), who assume $I\left(t; K, T\right)$ to be a deterministic, piece-wise constant function to reflect the impact of earnings on the implied volatility.

In Figure 2.3 (top), we compare the IV function in (2.3.4) for fixed (K, T), against the IV time series of the front month ATM IBM option[1] with expiration date 7/19/2013. The parameters of the model have been chosen by a least-square regression[2]. As we can see, the observed ATM IV and the model IV increase in a similar fashion. In the same figure (bottom), we also compare the IV function in (2.3.4) for fixed (t, K), against the term structure of the IV of the ATM IBM call option on 7/17/2013—just before the earnings announcement and one day before the expiration date. Again, the parameters of the model are obtained via an additional least-square regression and they differ from the ones obtained from the IV time series analysis. The model term structure approximates the observed one even if the IV surface presents no skew and a term structure which allows only for the functional form (2.3.4).

2.3.2 Greeks

In order to understand the sensitivity of options prices approaching the earnings announcement, we derive and analyze the Greeks based on the price function (2.3.3).

For a call or put with maturity T after the EA date T_e, the Delta and Gamma are the simply the Black-Scholes Delta and Gamma functions, but with the volatility parameter set at higher value $I(t)$, for $t < T_e$. On the other hand, we notice that there are two parameters related to the volatility of the stock price. Consequently, in addition to the

[1]The IVs of the ATM call and put are observed to be very close but not identical. Each point of the time series represents the average of the two IVs.

[2]More precisely, given the observed time-series of the IV, $\sigma_{IV,t}$, we perform the in-sample, linear regression $\sigma_{IV,t} = \sigma^2 + \sigma_e^2/(T-t)$ to obtain the parameters σ^2 and σ_e^2.

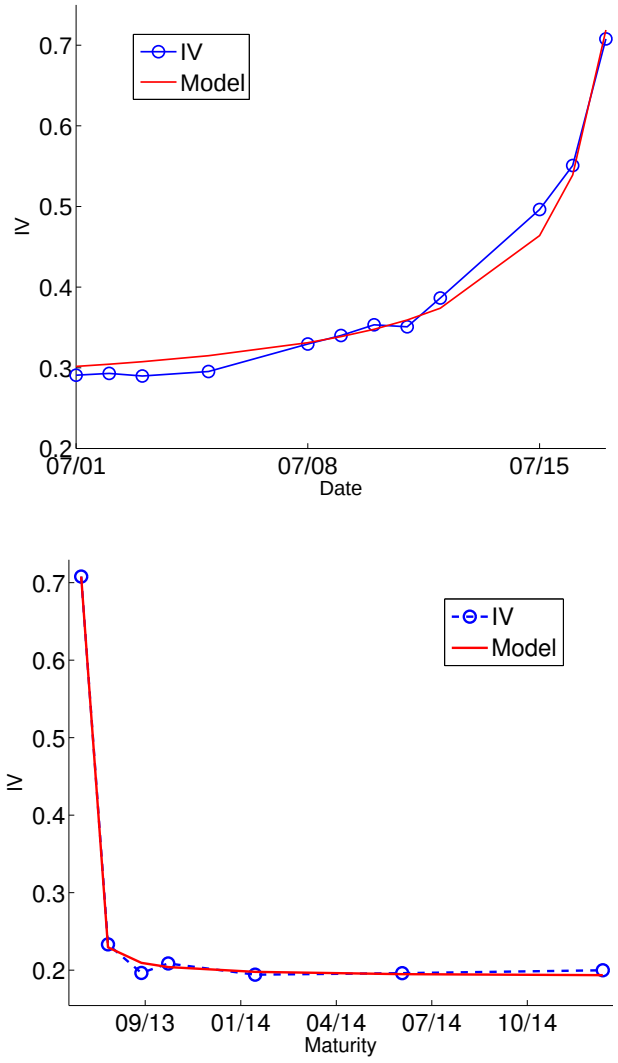

Figure 2.3: Left: The IV function (2.3.4) (solid line) prior to an EA, with $\sigma = 0.2538$, $\sigma_e = 0.0424$ and expiration date 7/19/2013, as compared to the market-observed IV (circle) of the front month IBM ATM option with the same expiration date. Right: The term structure of the IV (solid) according to (2.3.4), with $\sigma = 0.1912$, $\sigma_e = 0.0429$, on 7/17/2013, compared to the market-observed term structure (circle) for ATM IBM options on the same date.

standard Black-Scholes Vega, we introduce the *EA-Vega*

$$\mathcal{V}_e \equiv \frac{\partial C}{\partial \sigma_e} = \frac{1}{\sqrt{T-t}\sqrt{\frac{\sigma^2(T-t)}{\sigma_e^2}+1}}\mathcal{V}_{BS}\left(T-t,S;I\left(t\right),K,r\right),$$

where $\mathcal{V}_{BS}\left(\tau,S;\sigma,K,r\right) = S\phi\left(d_1\right)\sqrt{\tau}$ represents the usual Black-Scholes Vega function with spot price S and time-to-maturity τ.

For the Theta of a call, we obtain

$$\Theta \equiv \frac{\partial C}{\partial t} = \Theta_{BS}\left(T-t,S;I\left(t\right),K,r\right)+\frac{1}{2I(t)}\left(\frac{\sigma_e}{T-t}\right)^2\mathcal{V}_{BS}\left(T-t,S;I(t),K,r\right), \quad 0\leq t<T. \tag{2.3.5}$$

where $\Theta_{BS}\left(\tau,S;\sigma,K,r\right) = -S\frac{\sigma}{2\sqrt{\tau}}\phi\left(d_1\right) - rKe^{-r\tau}\Phi\left(d_2\right)$ is the Black-Scholes Theta function. First, we note that $\Theta_{BS}\left(T-t,S;I(t),K,r\right) \leq \Theta \leq 0$. The left part of the inequality is a direct consequence of (2.3.5) while the right part is a consequence of the fact that the option price is decreasing in time. On the other hand, it is not true in general that $\Theta \leq \Theta_{BS}\left(S,K,r,T-t,\sigma\right)$. This means that the option may lose value less rapidly over time than an option priced with a lower volatility. To illustrate this point, we suppose $r=0$, and the Black-Scholes PDE implies that

$$\frac{\partial C}{\partial t} = -\sigma^2S^2\frac{\partial^2 C}{\partial S^2} = -\sigma^2S^2\Gamma_{BS}\left(T-t,S;I(t),K,0\right).$$

Conversely, we have $\Theta_{BS}\left(T-t,S;\sigma,K,0\right) = -\sigma^2S^2\Gamma_{BS}\left(T-t,S;\sigma,K,0\right)$. Therefore,

$$\frac{\partial C}{\partial t} - \Theta_{BS}\left(T-t,S;\sigma,K,0\right) = -\sigma^2S^2\left(\Gamma_{BS}\left(T-t,S;I(t),K,0\right)-\Gamma_{BS}\left(T-t,S;\sigma,K,0\right)\right).$$

For ATM options, we have $\Gamma_{BS}\left(T-t,S;\sigma,S,0\right) = \frac{1}{\sqrt{2\pi}\sigma S}e^{-\frac{\sigma^2(T-t)}{2}}$, which is decreasing in σ. This implies that $\frac{\partial C}{\partial t} > \Theta_{BS}\left(T-t,S;\sigma,S,0\right)$ for $\sigma_e > 0$, implying a less rapid time decay in the option value. In fact, the same is true for other puts and calls whose Γ_{BS} is decreasing in σ.

In Figure 2.4 (top), we illustrate Θ as a function of the spot price for a call with 5 days to maturity. For comparison, we plot two additional benchmarks based on the BS Theta with different volatility parameter values $I(0)$ and σ, respectively. As expected from (2.3.5), the time-decay of the call price is less severe than $\Theta_{BS}\left(T,S;I(0),K,r\right)$. In addition, for spot prices near the strike K, we observe that $\Theta > \Theta_{BS}\left(T,S;\sigma,S,r\right) > \Theta_{BS}\left(T,S;I(0),S,r\right)$.

Figure 2.4 (bottom) shows how Θ changes in time for an ATM ($S = K = 100$) call, up to one day before earnings. Again, we notice the same dominance of Theta's, but their differences increase as time approaches the EA date. Interestingly, Θ, which accounts for the EA jump, appears to be significantly more constant as compared to the other two BS Theta's.

2.4 Incorporating EA Jumps into Other Models

Although the extended BS model (2.3.1) is capable of showing an increasing IV approaching an earnings announcement, the IV has no skew and its term structure only admits the particular two-parameter functional form $\sqrt{\sigma^2 + \frac{\sigma_e^2}{T-t}}$. Furthermore, the stock price may also experience randomly timed jumps which cannot be adequately captured by diffusion. This has motivated many models that incorporate jumps of various distributions into the stock price dynamics, with notable examples in the Merton (1976), Kou (2002), Variance Gamma (Madan and Unal (1998)), CGMY (Carr et al. (2002))) models. In this section, we present an analytic formula for pricing European options under an extension of the jump-diffusion model of Kou (2002), and also discuss the pricing of options prior to an earnings announcement using a transform method.

2.4.1 Extensions of the Kou Model

We consider an extension of the Kou model and derive an analytic formula for the price of a European option with an EA jump. Under this model, the risk-neutral terminal stock price follows

$$\log\left(\frac{S_T}{S_0}\right) = rT - \frac{\sigma^2}{2}T + \sigma W_T - m\kappa T + \sum_{i=1}^{N_T} J_i + 1_{\{t \geq T_e\}}\left(Z_e - \log\left(\mathbb{E}\left\{e^{Z_e}\right\}\right)\right), \quad (2.4.1)$$

where each jump $J_i \sim DE(p, \lambda_1, \lambda_2)$ is *double-exponentially* distributed with the p.d.f. $f_{J_i}(x) = 1_{\{x \geq 0\}} p\lambda_1 e^{-\lambda_1 x} + 1_{\{x \leq 0\}}(1-p)\lambda_2 e^{\lambda_2 x}$. The number of randomly timed jumps is modeled by $N_T \sim \text{Poi}(\kappa T)$. To ensure that the martingale condition holds, we set $m = p\frac{\lambda_1}{\lambda_1 - 1} + (1-p)\frac{\lambda_2}{\lambda_2 + 1} - 1$. We shall consider separately two distributions for the EA log jump size Z_e: (i) double-exponential $Z_e \sim DE(u, \eta_1, \eta_2)$, and (ii) Gaussian $Z_e \sim N\left(0, \sigma_e^2\right)$.

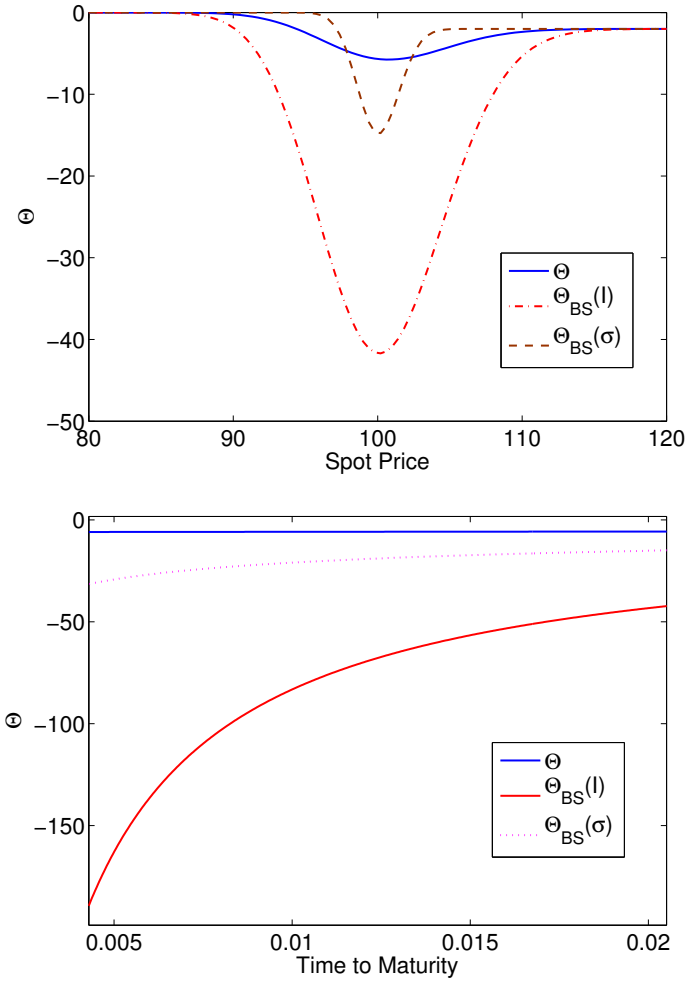

Figure 2.4: The shape of Θ and Θ_{BS} changes w.r.t. the spot price (with $T = \frac{5}{252}$) and time to maturity (with $S = K = 100$). In both panels, we see that Θ for ATM options is less negative than the ordinary BS Theta Θ_{BS}. Common parameters: $r = 0.02,\ \sigma = 0.1,\ \sigma_e = 0.04$.

Let $C(S) = \mathbb{E}\left\{e^{-rT}(S_T - K)^+ | S_0 = S\right\}$ be the price of the European call option at time $t = 0$ when the spot price is S. We now present the price formula when the EA jump Z_e is a double exponential random variable.

Proposition 2.4.1. *Suppose the terminal stock price follows (2.4.1), with $Z_e \sim DE(u, \eta_1, \eta_2)$ and $\eta_1 \neq \lambda_1,\ \eta_2 \neq \lambda_2$. Then, the European call option price is given by*

$$\begin{aligned} C(S) = e^{-\alpha} S \Upsilon \left(S, K, r + \sigma^2, T, \sigma, \hat{\kappa}, \hat{p}, \hat{\lambda}_1, \hat{\lambda}_2, \hat{u}, \hat{w}, \hat{\eta}_1, \hat{\eta}_2\right) \\ - K e^{-rT} \Upsilon \left(S, K, r, T, \sigma, \kappa, p, \lambda_1, \lambda_2, u, w, \eta_1, \eta_2\right), \end{aligned} \tag{2.4.2}$$

where the function Υ is given in Appendix A.1, and the constants are

$$\hat{\eta}_1 = \eta_1 - 1, \quad \hat{\eta}_2 = \eta_2 + 1, \quad \hat{\lambda}_1 = \lambda_1 - 1, \quad \hat{\lambda}_2 = \lambda_2 + 1, \quad \hat{u} = u\frac{\eta_1}{\eta_1 - 1}, \quad w = 1 - u,$$
$$\hat{w} = w\frac{\eta_2}{\eta_2 + 1}, \hat{\kappa} = (m+1)\kappa, \quad \hat{p} = \frac{\lambda_1}{\lambda_1 - 1}\frac{p}{m+1}, \quad \alpha = \log\left(u\frac{\eta_1}{\eta_1 - 1} + w\frac{\eta_2}{\eta_2 + 1}\right).$$

The proof of Proposition 2.4.1 is provided in Appendix A.2. When the jump size parameters of the EA and randomly timed jumps are the same, i.e. $\eta_1 = \lambda_1$ or $\eta_2 = \lambda_2$, an analytic pricing formula can also be derived but omitted here. In practice, the parameters λ_1, λ_2 are usually of an order of magnitude greater than η_1 and η_2, as we will observe from our calibration in Section 4.2.

Alternatively, if the EA jump is *normally* distributed, i.e. $Z_e \sim N\left(0, \sigma_e^2\right)$, then one can directly adapt the result from Kou (2002) to account for the EA jump. Specifically, the EA jump parameter σ_e can be incorporated in the volatility coefficient of the Brownian motion W_T:

$$\log\left(\frac{S_T}{S_0}\right) \overset{d}{=} \left(-\frac{\sigma^2 + \frac{\sigma_e^2}{T}}{2} - m\kappa\right) T + \sqrt{\sigma^2 + \frac{\sigma_e^2}{T}}\, W_T + \sum_{i=1}^{N_T} J_i\,.$$

From this, we see that the resulting analytic formula is in fact identical to the original formula without the EA jump, except with σ replaced by $\sqrt{\sigma^2 + \frac{\sigma_e^2}{T}}$.

The analytic formula (2.4.2) allows for the fast computation of the price, and simultaneously its delta, $\Delta = e^{-\alpha}\Upsilon(\cdot)$, where $\Upsilon(\cdot)$ is the first term on RHS of (2.4.2). In Table

$K \setminus T$	1 Week		1 Month		3 Months		1 Year	
	C	IV	C	IV	C	IV	C	IV
90	11.031	0.799	11.380	0.425	12.348	0.300	16.050	0.239
92.5	8.958	0.767	9.400	0.415	10.529	0.297	14.485	0.239
95	7.048	0.738	7.598	0.407	8.871	0.295	13.027	0.239
97.5	5.357	0.714	6.007	0.401	7.384	0.294	11.675	0.239
100	3.945	0.699	4.651	0.397	6.075	0.293	10.428	0.239
102.5	2.849	0.696	3.536	0.396	4.942	0.292	9.284	0.239
105	2.047	0.704	2.651	0.396	3.979	0.292	8.240	0.238
107.5	1.475	0.719	1.968	0.399	3.173	0.292	7.292	0.238
110	1.069	0.738	1.455	0.403	2.509	0.293	6.434	0.238

Table 2.1: Option prices and IVs under model (2.4.1). Prices are computed via formula (2.4.2). Parameters: $r = 2\%$, $S_0 = 100$, $\kappa = 10$, $p = 0.6$, $\lambda_1 = 60$, $\lambda_2 = 50$, $u = 0.55$, $\eta_1 = 15$, $\eta_2 = 12$, $\sigma = 20\%$.

2.4.1, we apply (2.4.2) to calculate option prices and we report the corresponding implied volatilities. As we can see, the IV decreases as time to maturity increases, which is typical of the IV before an earnings announcement. In addition, the IV skew becomes flatter as maturity increases. In Figure 2.5, we plot the IV of the ATM option when the underlying follows (2.4.1) with either a Gaussian or DE EA jump. For comparison, we have chosen the jumps parameters so that the variances of the Gaussian and DE EA jumps coincide. We notice that the IVs have similar dependence on time. Comparing Figures 2.3 and 2.5, it is natural to wonder whether the IV increases in time in a similar fashion, not only in the extended Black-Scholes and Kou, but also in other models. This motivates us to explore the properties of the IV under different models in Section 2.5.

2.4.2 Pricing via the Characteristic Function

In general, let us write the terminal stock price as $S_T = S_0 e^{X_T + Z_e}$. If X_T and Z_e are independent, and they both admit analytic characteristic functions, then we obtain the characteristic formula of the log-price

$$\Psi(\omega) := \mathbb{E}\left\{ e^{\mathrm{i}\omega \log\left(\frac{S_T}{S_0}\right)} \right\} = e^{\hat{\psi}(\omega) + \psi_e(\omega)},$$

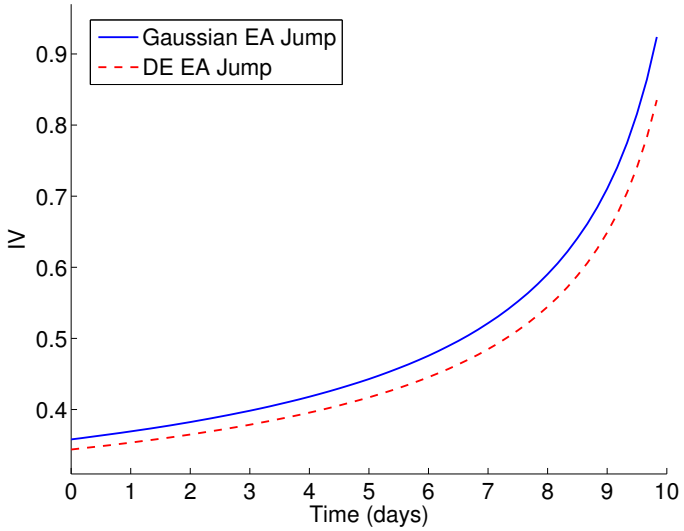

Figure 2.5: The time-series of the ATM option IV under the extended Kou model (2.4.1) when the EA and expiration dates are on the 10th and 11th days respectively. Parameters: $T_e = 14$ days, $T = 15$ days, $r = 2\%$, $S_0 = 100$, $\kappa = 10$, $p = 0.5$, $\lambda_1 = 50$, $\lambda_2 = 50$, $u = 0.5$, $\eta_1 = 25$, $\eta_2 = 25$, $\sigma = 20\%$.

where

$$\hat{\psi}(\omega) := \log\left(\mathbb{E}\left\{e^{\mathrm{i}\omega\log(X_T)}\right\}\right), \quad \text{and} \quad \psi_e(\omega) := \log\left(\mathbb{E}\left\{e^{\mathrm{i}\omega\log(Z_e)}\right\}\right).$$

It is then possible to make use of available methods to price vanilla as well as exotic options. For example, the methods of Carr and Madan (1999), Duffie et al. (2000), Lee (2004), and Raible (2000), among others, can be used to price European options. Alternatively, the methods developed in Jackson et al. (2008) or Lord et al. (2008) can be adapted to price both European and American options in models incorporating the jump Z_e.

In the following sections, we will also consider an extension of the Heston model with dynamics

$$\begin{aligned} \frac{dS_t}{S_t} &= rdt + \sigma_t dW_t + d\left(1_{\{t\geq T_e\}}\left(e^{Z_e}-1\right)\right), \\ d\sigma_t^2 &= \nu\left(\vartheta - \sigma_t^2\right)dt + \zeta\sigma_t d\tilde{W}_t, \end{aligned} \tag{2.4.3}$$

where W and $\tilde{W}$ are standard Brownian motions, with $\mathbb{E}\{dW_t d\tilde{W}_t\} = \rho dt$, and Z_e is

independent of both W and $\tilde{W}$. Write the option price as

$$\begin{aligned} C(0,S) &= \int_{-\infty}^{\infty} \left(e^{\log(S+x)} - K\right)^+ f(x)dx \\ &= (e^{\cdot} - K)^+ * f(-\cdot)\,(\log(S)), \end{aligned}$$

where f denotes the p.d.f. of $\log(\frac{S_T}{S_0})$ and $*$ denotes the convolution operator. Denoting with $\mathcal{F}(g(x)) \equiv \int_{\mathbb{R}} e^{-i\omega x} g(x)\,dx$ the Fourier operator acting on the function g, we can then write the price of the European call as

$$C(0,S) = e^{\gamma \log(S)} \mathcal{F}^{-1}\left\{\mathcal{F}\left\{e^{-\gamma x}(Se^x - K)^+\right\}\Psi(\omega - i\gamma)\right\}. \tag{2.4.4}$$

where the introduction of the dampening factor $e^{-\gamma x}$ is necessary because the payoff is not integrable[3]. The same observations have been made in Lord et al. (2008), where (4.1.10) is implemented as part of a new pricing algorithm. Jackson et al. (2008) also derive the same formula by analyzing the associated pricing PIDE in Fourier space. One can then apply a Fast Fourier transform (FFT) algorithm to price according to (4.1.10). In addition, these methods can be adapted to price American options, as we will do in Section 4.4.

2.5 Pre-Earnings Announcement Implied Volatility Properties

The market observations in Figures 2.1-2.2 motivate us to analyze some characteristics of the pre-earnings announcement implied volatility. In Section 2.5.1, we provide upper and lower bounds for the IV under a class of models. In Section 2.5.2, we study some IV asymptotics with focus on small and large strikes.

2.5.1 Implied Volatility Bounds

For our analysis of the IV bounds of European options, we consider a general framework where the terminal stock price is written in the form

$$S_T = S_t e^{X_{t,T} + Z_e}, \tag{2.5.1}$$

[3]Notice that, in order for $\Psi(\omega - i\gamma)$ to be well-defined, we must also ensure that $\mathbb{E}^{\mathbb{Q}}\{S^\gamma\} < \infty$.

with S_t the stock price at time $t < T_e$. The martingale condition on S implies that $(X_{t,T})_{0\le t\le T}$ satisfies $\mathbb{E}\left\{e^{X_{t,T}}\right\} = e^{r(T-t)}$. The r.v. Z_e is a continuous mixture of Gaussian r.v.'s with p.d.f. $f_{Z_e}(y) = \int_{\mathbb{R}^+} \phi\left(y; -\frac{\hat{\sigma}^2}{2}, \hat{\sigma}\right) \mathbb{G}(d\hat{\sigma})$, where $\phi(\cdot; a, b)$ represents the p.d.f. of a Gaussian r.v. with mean a and variance b^2, and $\mathbb{G}(\cdot)$ is a measure over the space $\mathbb{R}^+$ with $\mathbb{G}[0,\infty) = 1$.

Note that we have not specified the distribution of $X_{t,T}$, therefore the base model can be very general. We have the following lower bound for the IV volatility function.

Proposition 2.5.1. *Suppose the terminal stock price S_T follows (2.5.1). Then, the implied volatility $I(t;K,T)$ admits the lower bound*

$$I(t;K,T) \ge \frac{\hat{\sigma}_{min}}{\sqrt{T-t}}, \quad t < T_e, \tag{2.5.2}$$

where $\hat{\sigma}_{min} := \inf\{\hat{\sigma} \in \mathbb{R}_+ : \mathbb{G}[0,\hat{\sigma}] > 0\}$. In addition, if $X_{t,T}$ is also distributed as a Gaussian mixture, $f_{X_{t,T}}(y) = \int_{\mathbb{R}^+} \phi\left(y; r(T-t) - \frac{\tilde{\sigma}^2}{2}, \tilde{\sigma}\right) \mathbb{H}(d\tilde{\sigma})$, then the lower bound improves to

$$I(t;K,T) \ge \sqrt{\frac{\tilde{\sigma}_{min}^2 + \hat{\sigma}_{min}^2}{T-t}}\ ,\ t < T_e,$$

where $\tilde{\sigma}_{min} := \inf\{\tilde{\sigma} \in \mathbb{R}_+ : \mathbb{H}[0,\tilde{\sigma}] > 0\}$.

The proof of Proposition 2.5.1 is provided in Appendix A.3. We note that $\hat{\sigma}_{min} \ge 0$, so the bound (2.5.2) is nontrivial only if $\hat{\sigma}_{min} > 0$. This means that the measure G has zero weight on Gaussian r.v.'s with variance smaller than $\hat{\sigma}_{min} > 0$. Such a condition is satisfied, for example, by any finite mixture of Gaussian r.v.

In addition, we obtain an upper bound for the implied volatility.

Proposition 2.5.2. *Suppose the terminal stock price S_T follows (2.5.1) and assume that both X_T and Z_e are distributed as continuous Gaussian mixtures,*

$$f_{Z_e}(y) = \int_{\mathbb{R}^+} \phi\left(y; -\frac{\hat{\sigma}^2}{2}, \hat{\sigma}\right) \mathbb{G}(d\hat{\sigma}), \tag{2.5.3}$$

$$f_{X_{t,T}}(y) = \int_{\mathbb{R}^+} \phi\left(y; r(T-t) - \frac{\tilde{\sigma}^2}{2}, \tilde{\sigma}\right) \mathbb{H}(d\tilde{\sigma}). \tag{2.5.4}$$

Then, the following upper bound for the implied volatility of a European ATM-forward call option, $K = e^{r(T-t)}S_t$, holds:

$$I\left(t; e^{r(T-t)}S_t, T\right) \le \sqrt{\int_{\mathbb{R}^+} \frac{\tilde{\sigma}^2}{T-t}\mathbb{H}(d\tilde{\sigma}) + \int_{\mathbb{R}^+} \frac{\hat{\sigma}^2}{T-t}\mathbb{G}(d\hat{\sigma})}\ ,\ t < T_e. \tag{2.5.5}$$

The proof of Proposition 2.5.2 is provided in Appendix A.3. Notable examples of models that satisfy conditions (2.5.4) include the extended Merton and Heston (when $\rho = 0$) models. However, we remark that Gaussian mixtures can also be used to approximate other distributions. Moreover, our bounds can serve as analytical benchmarks for the IV under different models. As an example, we derive the explicit expressions for the bounds (2.5.5) under the Heston model.

According to Propositions 2.5.1 and 2.5.2, the IV bounds under different models exhibit similar behaviors as time approaches the earnings announcement. Comparing the bounds to the IV function I in (2.3.4), it is not too surprising that the simple extended BS model was able to fit the observed ATM IV over time (see Figure 2.3).

Example 2.5.3. *Assume that S follows the Heston dynamics (2.4.3). In the case $\rho = 0$ it is known that, conditioned on the path of $(\sigma_u)_{t\leq u\leq T}$, $\int_t^T \sigma_u dW_u \sim N\left(0, \tilde{\sigma}^2\right)$, where $\tilde{\sigma}^2 \equiv \int_t^T \sigma_u^2 du$. From this we observe that $X_{t,T} \equiv \left(r - \frac{\tilde{\sigma}^2}{2(T-t)}\right)(T-t) + \int_t^T \sigma_u dW_u$ satisfies the second part of (2.5.4). In turn, direct computation yields that $\int_{\mathbb{R}^+} \frac{\tilde{\sigma}^2}{T-t}\mathbb{H}(d\tilde{\sigma}) = \vartheta + \frac{\sigma_t^2-\vartheta}{\nu(T-t)}\left(1-e^{-\nu(T-t)}\right)$. Therefore, for example, in the case of a Gaussian EA jump, the term $\int_{\mathbb{R}^+} \frac{\hat{\sigma}^2}{T-t}\mathbb{G}(d\hat{\sigma})$ is equal to $\frac{\sigma_e^2}{T-t}$ and the bound (2.5.5) reads*

$$I\left(t; e^{r(T-t)}S_t, T\right) \leq \sqrt{\vartheta + \frac{\sigma_t^2-\vartheta}{\nu(T-t)}\left(1-e^{-\nu(T-t)}\right) + \frac{\sigma_e^2}{T-t}}. \tag{2.5.6}$$

If we instead assume that the jump is distributed as a symmetric double-exponential, $Z_e \sim DE\left(\frac{1}{2}, \eta, \eta\right)$, then we use the fact that $Z_e \overset{d}{=} \sqrt{\frac{2}{\eta^2}}\epsilon Z$, where $\epsilon \sim Exp(1)$ and $Z \sim N(0,1)$ are independent. In fact, in that case, $\mathbb{G}(x) = \eta^2 x e^{-\frac{\eta^2 x^2}{2}}$, $\int_{\mathbb{R}^+} \frac{\hat{\sigma}^2}{T-t}\mathbb{G}(d\hat{\sigma}) = \frac{2}{\eta^2(T-t)}$, and the bound (2.5.5) reads

$$I\left(t; e^{r(T-t)}S_t, T\right) \leq \sqrt{\vartheta + \frac{\sigma_t^2-\vartheta}{\nu(T-t)}\left(1-e^{-\nu(T-t)}\right) + \frac{2}{\eta^2(T-t)}}. \tag{2.5.7}$$

In Figure 2.6 we plot the explicit bounds (2.5.6) and (2.5.7) from Example 2.5.3. As we can see, the upper bound is relatively close to the model IV curve and shares a very similar time dependence. In particular, when the EA jump is Gaussian (Figure 2.6, top), the bound is almost indistinguishable from the model IV. To see this, as $t \to T$, the lower and upper bounds ((2.5.2) and (2.5.6)) share a common leading term $\frac{\sigma_e^2}{T-t}$. In practical cases as in this

example, the term $\int_{\mathbb{R}^+} \frac{\tilde{\sigma}^2}{T-t}\mathbb{H}(d\tilde{\sigma}) \approx \sigma_t^2$ is typically at least one order of magnitude smaller than $\sigma_e^2/(T-t)$ since $T-t$ is very small and σ_e and σ_t are of the same order. Also, in Figure 2.6, we observe that the model IV with a non-zero ρ still admits a similar time behavior and are very close to the bounds (2.5.6) and (2.5.7) for the case $\rho = 0$. As a curious note, the coefficient $\frac{2}{\eta^2}$ of the leading term in (2.5.7) as $t \to T$, is exactly the variance of Z_e when $Z_e \sim DE(\frac{1}{2}, \eta, \eta)$, the same way that the coefficient σ_e^2 of the leading term in (2.5.6) is the variance of the Gaussian Z_e. Therefore, an interesting question is whether the rate of change of the IV is approximately proportional to the standard deviation of the EA jump, at least as time approaches the EA date (see also Figure 2.5).

To conclude, we recall that Propositions 2.5.1 and 2.5.2 also give us information about the term structure of the IV. Indeed, for models whose dynamics are time-homogeneous, we observe the relationship: $\frac{\partial I(t;K,T)}{\partial t} = -\frac{\partial I(t;K,T)}{\partial T}$. This implies that one should expect a decreasing term structure for options prior to the EA date.

2.5.2 Small and Large Strikes Asymptotics

We now analyze the asymptotics of the IV surface for small and large strikes for the extended Heston and Kou model. Our asymptotics follow from an adaptation of the results of Benaim and Friz (2008) (see also Benaim et al. (2012)). We state the results here and provide the proofs in Appendix A.4.

Proposition 2.5.4. *Let S satisfy the extended Heston dynamics (2.4.3) where Z_e is either:*

Case 1: normally distributed, $Z_e \sim N\left(0, \frac{\sigma_e^2}{2}\right)$; or

Case 2: double-exponentially distributed, $Z_e \sim DE(u, \eta_1, \eta_2)$.

Then for any fixed $t < T_e$, the implied volatility $I(t;K,T)$ satisfies

$$\frac{I^2(t;K,T)(T-t)}{\log\left(\frac{K}{S_t}\right)} \sim \xi(q^*), \text{ as } K \to 0, \tag{2.5.8}$$

$$\frac{I^2(t;K,T)(T-t)}{\log\left(\frac{K}{S_t}\right)} \sim \xi(r^*-1), \text{ as } K \to \infty, \tag{2.5.9}$$

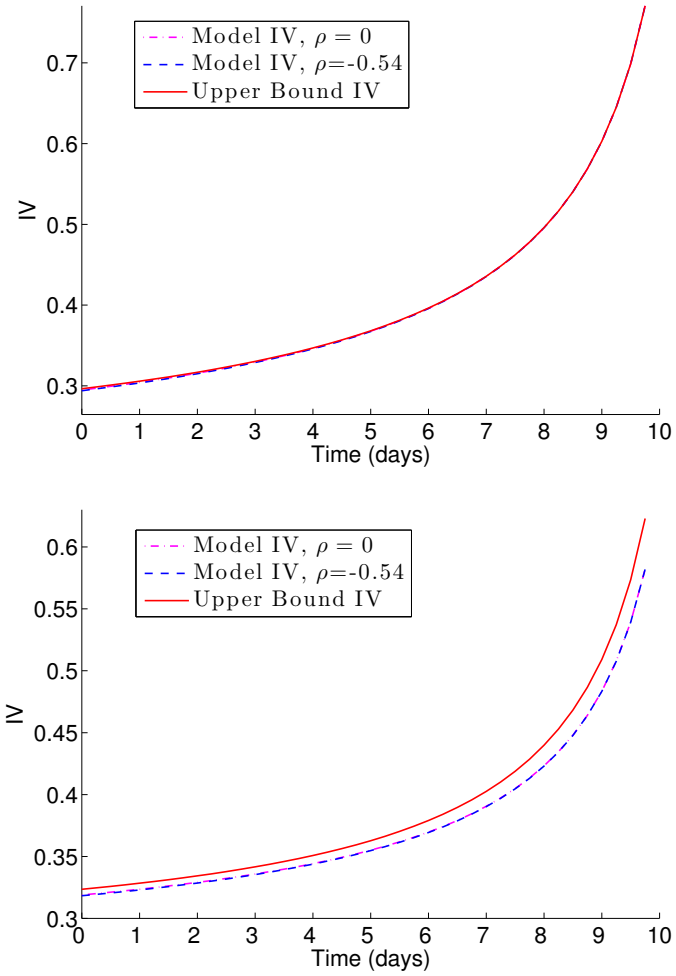

Figure 2.6: The model IV plotted against the upper bounds in (2.5.6) and (2.5.7) under the extended Heston model with a Gaussian EA jump (top) and DE EA jump (bottom) respectively. Parameters: $\nu = 4.04,\ \vartheta = 0.05,\ \sigma_0 = 1.01,\ \rho \in \{0, -0.54\},\ \zeta = 0.03,\ \sigma_e = .0473,\ u = 0.5,\ \eta_1 = \eta_2 = 40.$

where $\xi(x)$ *is defined by* $\xi(x) \equiv 2 - 4\left(\sqrt{x^2+x} - x\right)$ *and*

$$q^* = \begin{cases} p_- & \text{case 1,} \\ \min\{p_-, \eta_2\} & \text{case 2,} \end{cases}, \quad r^* = \begin{cases} p_+ & \text{case 1,} \\ \min\{p_+, \eta_1\} & \text{case 2,} \end{cases}$$

and $p_\pm$ *is the smallest positive solution to, respectively,*

$$\nu \mp \rho\zeta p_\pm + \sqrt{(\nu \mp \rho\zeta p_\pm)^2 + \zeta^2(\pm p_\pm - (p_\pm)^2)} \cdot \coth\left(\frac{(T-t)}{2}\sqrt{(\nu \mp \rho\zeta p_\pm)^2 + \zeta^2(\pm p - (p_\pm)^2)}\right) = 0.$$

Proposition 2.5.5. *Let* S *follow the extended Kou dynamics (2.4.1) where* Z_e *is either:*

Case 1: normally distributed, $Z_e \sim N\left(0, \frac{\sigma_e^2}{2}\right)$*; or*

Case 2: double-exponentially distributed, $Z_e \sim DE(u, \eta_1, \eta_2)$*.*

Then for any fixed $t < T_e$*, the implied volatility* $I(t; K, T)$ *satisfies*

$$\frac{I^2(t;K,T)(T-t)}{\log\left(\frac{K}{S_t}\right)} \sim \xi(q^*), \text{ as } K \to 0, \tag{2.5.10}$$

$$\frac{I^2(t;K,T)(T-t)}{\log\left(\frac{K}{S_t}\right)} \sim \xi(r^*-1), \text{ as } K \to \infty, \tag{2.5.11}$$

where $\xi(x) \equiv 2 - 4\left(\sqrt{x^2+x} - x\right)$ *and*

$$q^* = \begin{cases} \lambda_2 & \text{case 1,} \\ \min\{\lambda_2, \eta_2\} & \text{case 2,} \end{cases}, \quad r^* = \begin{cases} \lambda_1 & \text{case 1,} \\ \min\{\lambda_1, \eta_1\} & \text{case 2.} \end{cases}$$

First, we observe that if the EA jump is Gaussian, then it has no role in the IV asymptotics in strikes (see (2.5.8) and (2.5.10)). Hence, in either the Heston or Kou model, the large/small strikes asymptotics with and without the EA jump are in fact identical. On the other hand, if the tails of the EA jump are fatter than those of the base model, then the IV asymptotics are determined by the EA jump parameters. In such cases, the asymptotics are observed for less extreme strikes with short maturities, which is when the EA jump variance dominates. For longer maturities, however, the asymptotics hold for more extreme strikes. An intuitive explanation is that, as time-to-maturity increases, the EA jump variance is relatively low and the tails behavior is manifest only for extreme values.

In Figure 2.7, we show the IV asymptotics under the extended Kou (top) and Heston (bottom) models compared to the IV obtained by inverting the BS formula on option prices calculated via Fourier transform (see Section 2.4.2). We plot the asymptotic volatility function $I(t;K,T) = c + \sqrt{\log(K/S_t)\,\xi(\omega)}$ for fixed (t,T), where c is a constant chosen so that the asymptotics and the model IVs coincide at the most extreme strikes considered. In each particular case, ω is a constant set according to (2.5.10)-(2.5.11) (for the extended Kou model) and (2.5.8)-(2.5.9) (for the extended Heston model). In Figure 2.7 (top) the double-exponential EA jump tails dominates those of the daily jumps, as this generally holds in practice. In Figure 2.7 (bottom), the EA jump is Gaussian and thus does not affect the IV asymptotics from the base model.

2.6 Calibration and Parameter Estimators

In this section, we perform calibrations of the extended BS, Kou and Heston models to the observed market prices of options near an earnings announcement. This allows us to evaluate whether the model extensions improve the accuracy of the calibration compared to that of the base models. Calibration results can also be used to infer information about the distribution of the EA jump and, in one simple example, we compare the estimators obtained through calibration on IBM options data to estimates given by its historical distribution.

2.6.1 Model Calibration

In our calibration procedure, we consider a set of N vanilla calls and puts with observed market prices, $\hat{C}_i$, $i = 1, ..., N$. These options have different contractual features, such as strike, maturity, and option type. For a given model, the set of model parameters is denoted by Θ. In turn, the model price of option i is denoted by $C_i(\Theta)$. To calibrate a given model, we minimize the sum of squared errors (see e.g. Dennis (1977); Andersen and Andreasen (2000); Bates (1996); Cont and Tankov (2002)):

$$\min_{\Theta} \sum_{i=1}^{N} \left(C_i(\Theta) - \hat{C}_i \right)^2, \tag{2.6.1}$$

We use the best-bid and best-ask mid-point prices. Furthermore, we adapt a trust-region-reflective gradient-descent algorithm (Coleman and Li (1994); Coleman and Li (1996)),

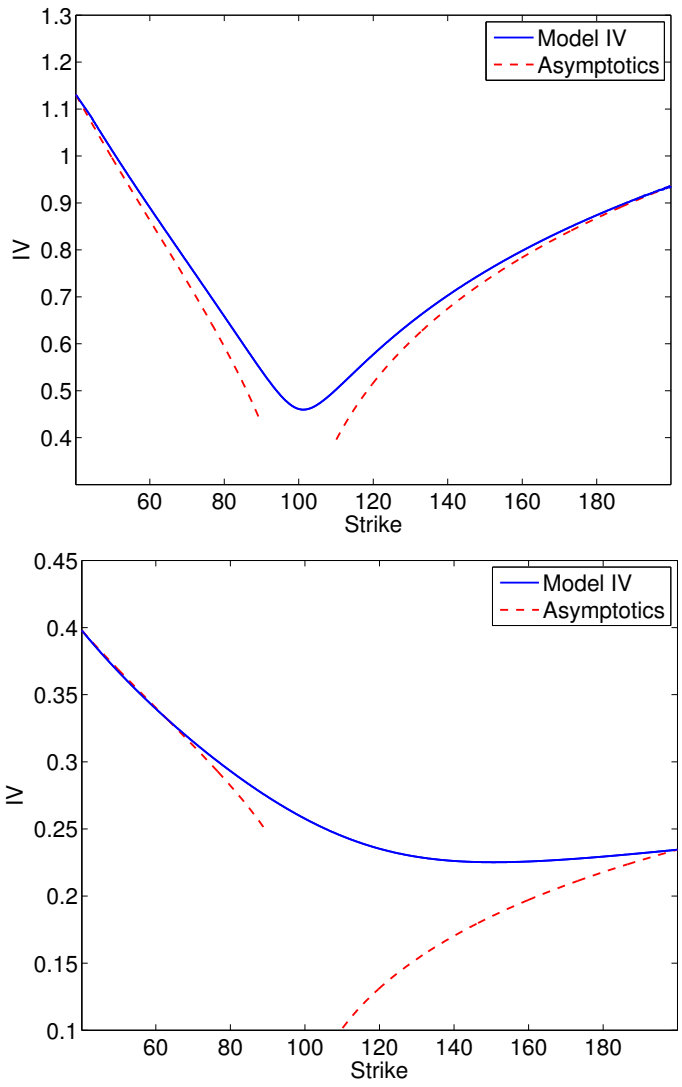

Figure 2.7: Top: The IV obtained from numerical option prices against the asymptotics (2.5.10)-(2.5.11) under the extended Kou model with a log-DE EA jump. Parameters: $S = 100,\ r = 0.02,\ T = \frac{4}{252},\ \kappa = 300,\ p = 0.5,\ \lambda_1 = \lambda_2 = 100,\ u = 0.5,\ \eta_1 = 30,\ \eta_2 = 25$. Bottom: The IV obtained from numerical option prices against the asymptotics (2.5.8)-(2.5.9) under the extended Heston model with a log-normal EA jump. Parameters: $S = 100,\ r = 0.02,\ T = 1,\ \nu = 2.7,\ \vartheta = 0.077,\ \sigma_0 = 0.7075,\ \rho = -0.54,\ \zeta = 0.073,\ \sigma_e = 0.04$.

starting from different initial points to guarantee a better exploration of the parameters space. While our numerical tests show the adopted method results in an effective calibration, we remark that there are many alternative, possibly more advanced, calibration procedures available (see e.g. Cont and Tankov (2002) and references therein).

The majority of equity options in the US are of the American type. While in Section 4.4 we will discuss the pricing of American options, the methods are generally too computationally-intensive to be practically used in conjunction with a gradient-descent method for calibration, especially as the number of options and parameters increase. Related studies typically circumvent this issue by simply assuming the American options are European-style (see e.g. Dubinsky and Johannes (2006); Broadie et al. (2009)). In contrast, our procedure begins by inverting the market prices of American puts and calls via a relatively fast American option pricer under the Black-Scholes model. This gives us the observed IVs. In turn, we apply the Black-Scholes European put/call pricing formula, with the volatility parameter being the observed IV, and derive the associated *European* put or call price. We then use the resulting prices as inputs to calibrate against the option prices generated from a model. In all our experiments, we obtain option price data, available up to August 2013, from the OptionMetrics Ivy database.

We now present an example using the extended BS, Kou and Heston models with different distributions for the EA jump. Our objective is to illustrate the calibrated IV surfaces under these models and compare them with the empirical IV surface. Recall from Figure 2.2 the empirical implied volatility surface of IBM on July 15, 2013. That is observed 2 days prior to the earnings announcement by IBM on July 17, 2013 after market. The closest options expiration date was Friday July 19, 2013. As noted earlier, the front month IVs are significantly higher than those for options with longer maturities. In Figure 2.8 we show the associated calibrated IV surfaces for the 3 base models and their extensions, resulting in a total of 9 calibrated models. Table 2.2 summarizes the calibrated parameters. In the original Black-Scholes model, the implied volatility surface is flat and takes a high value of 28.11%. As we incorporate the EA jump, under both Gaussian and DE distributions, the calibrated values of the stock price volatility σ are lower. More importantly, in every case, the base model is unable to generate the characteristic shape of the IV surface before

the EA. Between the extended Heston and Kou models, the IV surface generated from the Kou model tends to flatten more rapidly as maturity lengthens. Overall, the Heston model seems to be able to reproduce the IV surface more accurately, and the incorporation of a Gaussian EA jump seems to reproduce the IV surface better than with a DE EA jump in this example. We will further compare the two EA jump distributions in Section 2.6.3.

Black-Scholes	σ	σ_e	u	η_1	η_2
Base	28.11%	—	—	—	—
Gaussian jump	27.69%	7.11%	—	—	—
DE jump	21.42%	—	38.28%	23.03	6.3

Heston	ν	ϑ	ζ	ρ	σ_0^2	σ_e	u	η_1	η_2
Base	3.70	0.05	0.90	-0.51	0.05	—	—	—	—
Gaussian jump	4.04	0.05	1.01	-0.55	0.03	4.73%	—	—	—
DE jump	3.10	0.05	0.84	-0.54	0.03	—	42.06%	34.77	24.95

Kou	σ	κ	p	λ_1	λ_2	σ_e	u	η_1	η_2
Base	2.80%	232.3	46.85%	275.9	82.1	—	—	—	—
Gaussian jump	0.03%	193.6	51.17%	998.9	70.0	3.61%	—	—	—
DE jump	0.39%	85.1	79.46%	990.3	30.0	—	98.73%	32.9	2.0

Table 2.2: Summary of calibrated parameters based on the observed IV surface in Figure 2.2. The corresponding calibrated IV surfaces are displayed in Figure 2.8.

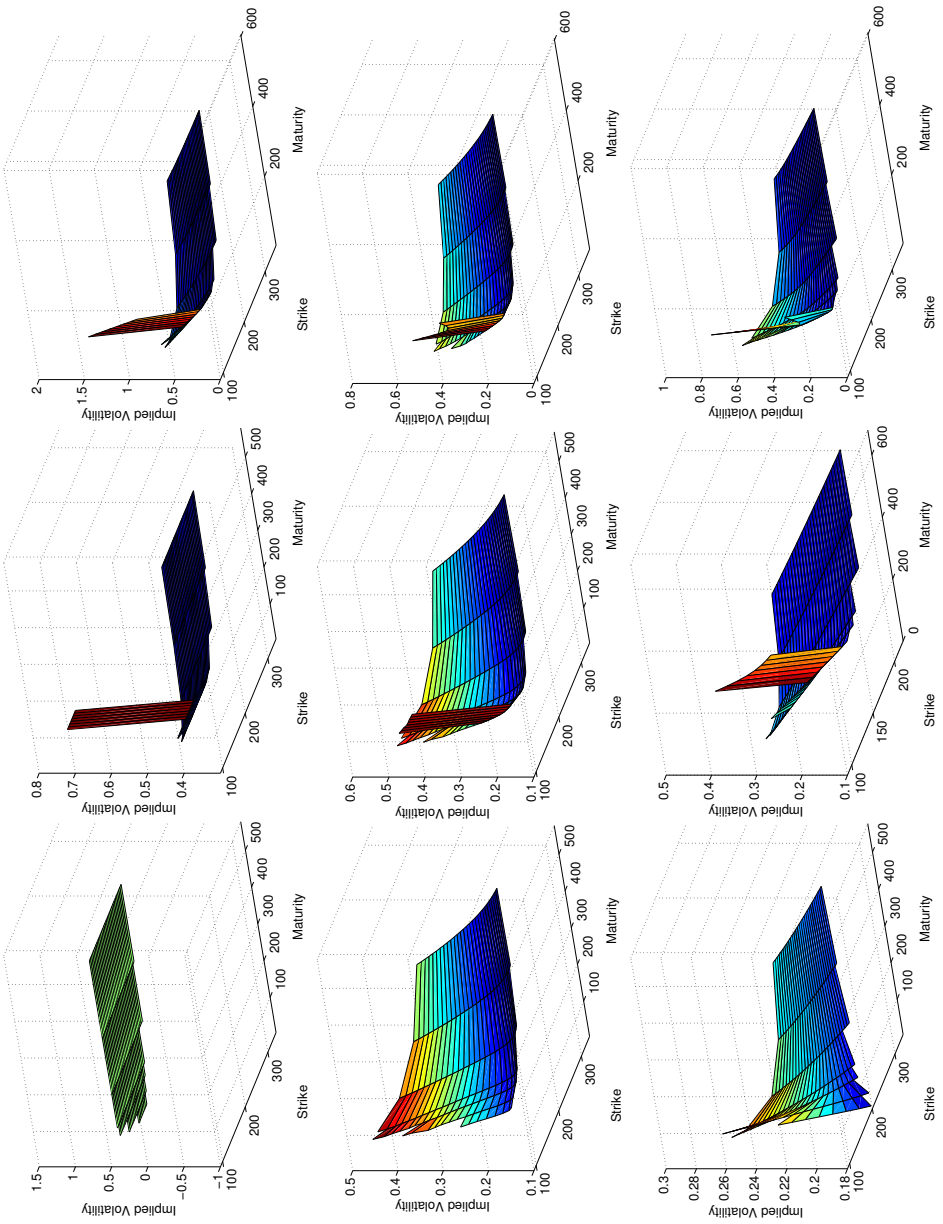

Figure 2.8: Calibrated surfaces for the Black-Scholes, Heston, and Kou models (1st, 2nd, 3rd rows respectively) without EA jump (left column), and with Gaussian (middle) and DE (right) EA jumps. The calibrated model parameters are listed in Table 2.2.

2.6.2 Analytic Estimators under the Extended BS Model

In the extended BS model (2.3.1), it is possible to derive analytical estimators for the models parameters (σ, σ_e), as discussed in Dubinsky and Johannes (2006). We apply these estimators to compare with the estimators obtained by calibrating other models (see Table 2.3). First, we consider the extended BS model where the EA jump Z_e is normally distributed. To calibrate this model, it suffices to use any pair of options of different maturities. Let $\sigma_{IV}(T_1)$, $\sigma_{IV}(T_2)$ represent the implied volatilities of two options with maturities T_1 and T_2, respectively. Then, applying (2.3.4), the model parameters (σ, σ_e) can be estimated by

$$\begin{aligned}\sigma^{TS} &= \sqrt{\frac{(T_1 - t)\,\sigma_{IV}^2(T_1) - (T_2 - t)\,\sigma_{IV}^2(T_2)}{T_1 - T_2}},\\ \sigma_e^{TS} &= \sqrt{\frac{\sigma_{IV}^2(T_1) - \sigma_{IV}^2(T_2)}{\frac{1}{T_1 - t} - \frac{1}{T_2 - t}}}.\end{aligned} \tag{2.6.2}$$

where the superscript TS indicates the relevance of the IV term structure to these estimators. In particular, we call σ_e^{TS} the *term structure estimator* of the jump volatility under the risk-neutral measure $\mathbb{Q}$. We stress that a set of two options with identical maturity would not allow us to estimate σ and σ_e separately, but only the aggregate value $\sigma^2 + \frac{\sigma_e^2}{T-t}$.

Alternatively, one can utilize option prices at different times for parameter estimation. In fact, given the implied volatilities σ_{IV,t_1} and σ_{IV,t_2} at times t_1 and t_2, with $t_1 < t_2 < T_e$, we apply (2.3.4) to get the following estimators:

$$\begin{aligned}\sigma^{ts} &= \sqrt{\frac{(T - t_1)\,\sigma_{IV,t_1}^2(T) - (T - t_2)\,\sigma_{IV,t_2}^2(T)}{t_2 - t_1}},\\ \sigma_e^{ts} &= \sqrt{\frac{\sigma_{IV,t_1}^2(T) - \sigma_{IV,t_2}^2(T)}{\frac{1}{T - t_1} - \frac{1}{T - t_2}}}.\end{aligned} \tag{2.6.3}$$

They are called the *time-series estimators* (see also Dubinsky and Johannes (2006)).

We observe from (2.6.2) that one must require that $\sigma_{IV}(T_1) > \sigma_{IV}(T_2)$ in order to obtain well-defined estimators. Similarly for σ^{ts} and σ_e^{ts} in (2.6.3), their definitions suggest that $\sigma_{IV,t_2} > \sigma_{IV,t_1}$ must hold. In our empirical tests, we find that, before an earnings announcement, $\sigma_{IV}(T_1) > \sigma_{IV}(T_2)$ always holds, but the condition $\sigma_{IV,t_1} > \sigma_{IV,t_2}$ is sometimes violated. Similar observations are also discussed in Dubinsky and Johannes (2006), who have also conducted a comprehensive empirical test using ATM options.

We emphasize that these analytical estimators are based on a specific extension of the BS model. Since market prices are not necessarily generated by this model, the analytical estimators and the calibrated parameters may not coincide. Moreover, these parameters depend on the choice of options whose IVs are inputs to the estimator formulas. On the other hand, the main advantage of these analytical estimators is that they can be computed instantly, and they are also used in practice (see e.g. Mehra et al. (2014)) and related studies.

2.6.3 Implied EA jump Distribution and Risk Premia

With the choice of a pricing model, our calibration procedure extracts the implied distribution of the EA jump. One useful application is to compare the risk-neutral and historical distributions of the EA jump. Their discrepancy will shed some light on the risk premium associated with the EA jump. As an example, let us consider the empirical EA jumps of the IBM stock starting from 1994. We assume that both risk-neutral and historical distributions are Gaussian, which is amenable for comparison since we only need to estimate a single parameter, i.e. the EA jump volatility. In Table 2.3, we report the estimate of EA jump volatility obtained by calibrating the Heston model extended with a Gaussian EA jump, σ_e^Q, and the empirical EA jump volatility, σ_e^P based on data from 1994 up to the given date. For comparison, we also list the EA jump volatility estimators according to (2.6.2). As we can see, for each given date, the ratio σ_e^P/σ_e^Q is very close to 1. This suggests that under the extended Heston model, the EA jump distributions share a similar standard deviation under both historical and risk-neutral measures. On the other hand, the ratio σ_e^P/σ_e^{TS} is smaller and less than 1 in this example, suggesting that the extended BS model would imply a higher EA jump volatility than the empirical one. In summary, the volatility σ_e^Q calibrated from the extended Heston model is smaller than the term structure EA jump volatility estimator σ_e^{TS} which is based on the extended BS model without stochastic volatility.

Date	σ_e^P	σ_e^Q	σ_e^P/σ_e^Q	σ_e^{TS}	σ_e^P/σ_e^{TS}
18-Jul-12	4.64%	4.68%	99.3%	5.22%	89.0%
16-Oct-12	4.62%	4.18%	110.5%	4.70%	98.4%
22-Jan-13	4.62%	4.58%	100.9%	5.71%	81.0%
18-Apr-13	4.61%	4.68%	98.5%	5.49%	84.1%
17-Jul-13	4.63%	4.61%	100.4%	5.76%	80.3%

Table 2.3: The implied and historical EA jump volatilities for IBM. For each date in the table, the historical EA jump volatility σ_e^P is estimated using price data from 1994 up to that date. The implied volatility σ_e^Q is calibrated from the extended Heston model.

2.7 American Options

While index options are typically of European style, most US equity options are American-style. In general, the American option pricing problem does not admit closed-form formulas, so we discuss a numerical method for computing the option price and exercise boundary. In addition, we apply the analytic results from the European case to approximate the American option price before an earnings announcement.

2.7.1 American Option Price and Exercising Boundary

We assume that the stock price evolves according to the extended Kou model with an EA jump defined in (2.4.1). The value of the American option is defined by

$$A(t,S) = \sup_{t\le\tau\le T} \mathbb{E}\left\{e^{-r(\tau-t)}(K-S_\tau)^+ | S_t = S\right\}, \quad t \le T, \tag{2.7.1}$$

where τ is a stopping time w.r.t. the filtration generated by S. By the dynamic programming principle, the option price can be written as (see, e.g. (Øksendal, 2003, Chap. 10))

$$A(t,S) = \sup_{t\le\tau\le T_e} \mathbb{E}\left\{e^{-r(\tau-t)}\left(1_{\{\tau<T_e\}}(K-S_\tau)^+ + 1_{\{\tau=T_e\}}A\left(T_e, S_{T_{e-}}e^{Z_e}\right)\right) | S_t = S\right\}. \tag{2.7.2}$$

Therefore, we see that for $t < T_e$ the problem is equivalent to pricing an American option under the Kou model but with "terminal" payoff $\mathbb{E}\left\{A\left(T_e, Se^{Z_e}\right) | S_{T_{e-}} = S\right\}$ at time T_e. Assume that $t < T_e < T$ and that Z_e admits the p.d.f. $g(z)$. The American put price can

then be written as

$$A(t,S) = D(t,S)\,1_{\{t<T_e\}} + \widetilde{D}(t,S)\,1_{\{t\geq T_e\}},$$

where D and $\widetilde{D}$ satisfy the linear complementarity problems (see Bensoussan and Lions (1984) and Cont and Voltchkova (2005)):

$$\begin{cases} \widetilde{D}(t,S) \geq (K-S)^+, & T_e \leq t < T,\ S \geq 0, \\ r\widetilde{D}(t,S) - \frac{\partial \widetilde{D}}{\partial t}(t,S) - \mathcal{L}\widetilde{D}(t,S) \geq 0, & T_e \leq t < T,\ S \geq 0, \\ \left(\widetilde{D}(t,S) - (K-S)^+\right)\left(r\widetilde{D}(t,S) - \frac{\partial \widetilde{D}}{\partial t}(t,S) - \mathcal{L}\widetilde{D}(t,S)\right) = 0, & T_e \leq t < T,\ S \geq 0, \\ \widetilde{D}(T,S) = (K-S)^+, & S \geq 0; \end{cases} \tag{2.7.3}$$

$$\begin{cases} D(t,S) \geq (K-S)^+, & 0 \leq t < T_e,\ S \geq 0, \\ rD(t,S) - \frac{\partial D}{\partial t}(t,S) - \mathcal{L}D(t,S) \geq 0, & 0 \leq t < T_e,\ S \geq 0, \\ \left(D(t,S) - (K-S)^+\right)\left(rD(t,S) - \frac{\partial D}{\partial t}(t,S) - \mathcal{L}D(t,S)\right) = 0, & 0 \leq t < T_e,\ S \geq 0, \\ D(T_e,S) = \int_{\mathbb{R}} \widetilde{D}(T_e, Se^z)\, g(z)\, dz, & S \geq 0. \end{cases} \tag{2.7.4}$$

We have denoted by $\mathcal{L}$ the infinitesimal generator of S under model (2.4.1):

$$\mathcal{L}V(S) \equiv \frac{\sigma^2 S^2}{2}\frac{\partial^2 V}{\partial S^2} + rS\frac{\partial V}{\partial S} + \kappa \int_{-\infty}^{\infty} \left(V(Se^y) - V(S)\right) f_J(y) dy, \tag{2.7.5}$$

and f_J is double exponential p.d.f.

It is worth noting that the integration at time T_e in (2.7.4) must be approximated with a sum because $\tilde{D}$ is not in closed form. The numerical computation of the integration may introduce computational errors, but it also adds to the computational burden since the sum is $\mathcal{O}\left(n^2\right)$, where n is the number of discretized stock price values. We remark that it is possible, for example, to reduce the complexity of the integration to $\mathcal{O}\left(n\log\left(n\right)\right)$ using an FFT algorithm. It is also worth noticing that when $T_e = T$, the complexity reduces to $\mathcal{O}\left(n\right)$ if closed form formulas are available for the European option (e.g. if the EA jump is Gaussian or double-exponential). Furthermore, the complexity reduces to $\mathcal{O}\left(n\right)$ when the announcement is imminent, i.e. $T_e = 0^+$. This motivates us to look for a closed-form approximation to the American option price based on these scenarios, as discussed in Sect.

2.7.2. It is useful to compare the American option prices under the same model but with different earnings announcement dates.

Proposition 2.7.1. *Let $A(t,S;u)$ denote the American option price as in (4.4.1) with $T_e = u$. Then, we have*

$$A(t,S;l) \leq A(t,S;u) \quad , \quad l \geq u > t. \tag{2.7.6}$$

The proof of Proposition 2.7.1 is provided in Appendix A.5. As a result of the relationship (2.7.6), the American option price is monotonically decreasing as the EA date T_e approaches maturity. Consequently, $A(t,S;t)$ and $A(t,S;T)$ become the upper and lower bounds, respectively, for the American option price $A(t,S;u)$, $t \leq u \leq T$. As an interesting comparison, the European option price is completely independent of the exact EA date as long as it is at or prior to maturity. In Figure 2.9 (center) we show the time-value[4] of an American put, with strike, maturity, and spot price fixed, over different announcement times T_e. Consistent with Proposition 2.7.1, the time-value of the American put is indeed monotonically decreasing in T_e.

To solve problems (2.7.3)-(2.7.4) we use the Fourier transform based method presented in Jackson et al. (2008). Unless $T_e = T$ or $T_e = 0^+$, we solve backward in time for $\tilde{D}$ in (2.7.3), perform the numerical integration and feed it as a terminal condition for problem (2.7.4) which is solved backward in time as well.

Figure 2.9 (top) shows the exercise boundary for different values of T_e under the Kou model with a DE EA jump, along other common parameters. Naturally, the scheduled announcement introduces a discontinuity in the exercising boundary. We mark the EA dates with three crosses. As expected, after the largest date T_e the three boundaries coincide. Interestingly, the exercise boundary is decreasing rapidly in time near T_e, which means that the option holder is more likely to wait until the earnings announcement, rather than exercising immediately. This can also be seen in terms of the option's time-value. In Figure 2.9 (bottom), we illustrate that the time-value of an American put, with both strike and

[4]The time-value of an American put is defined as $A - (K - S)^+$ where A is the put price, S is the spot price and K is the strike. With spot price S fixed, inequality (2.7.6) also holds for the corresponding time-values.

spot price fixed, is increasing as time approaches the EA date.

2.7.2 Analytical Approximations

One major method proposed by Barone-Adesi and Whaley (1987) to analytically approximate the price of an American option is to express the American option price in terms of an European option price plus a correction term. The correction term is determined as the solution of an approximation of the Black-Scholes equation, with the addition of elementary boundary condition. Kou and Wang (2004) present an analytical approximation to the American option price under the Kou model. Here we adapt the Barone-Adesi approximation and apply it to our extended Kou model. The details for our calculations are provided in Appendix A.6.

When $T_e = T$ the approximation is virtually identical to the original one. Let $P_E(t,S)$ denote the European put price (as in Proposition 2.4.1). The approximate price for the American put is similar to that of Kou and Wang (2004) and is given by

$$\tilde{A}(t,S) = \begin{cases} P_E(t,S) + \gamma_1 S^{-\beta_1} + \gamma_2 S^{-\beta_2} & , \ if \ S > \alpha(t), \\ (K-S)^+ & , \ if \ S \leq \alpha(t), \end{cases} \tag{2.7.7}$$

with the positive constants

$$\gamma_1 \equiv \frac{\alpha^{\beta_1}}{\beta_2 - \beta_1}\left(\beta_2 K - (1+\beta_2)(\alpha + P_E(t,\alpha)) + Ke^{-r(T-t)}q(\alpha(t))\right), \tag{2.7.8}$$

$$\gamma_2 \equiv \frac{\alpha^{\beta_2}}{\beta_1 - \beta_2}\left(\beta_1 K - (1+\beta_1)(\alpha + P_E(t,\alpha)) + Ke^{-r(T-t)}q(\alpha(t))\right), \tag{2.7.9}$$

where $q(s) \equiv \mathbb{Q}\{S_T \leq K | S_t = s\}$, and $\beta_{1,2}$, $0 < \beta_1 < \lambda_2 < \beta_2 < \infty$, are the two positive solutions to the equation

$$\frac{r}{1-e^{-r(T-t)}} = \beta\left(m\kappa - \frac{\sigma^2}{2} - r\right) + \frac{\sigma^2\beta^2}{2} + \kappa\left(p\frac{\lambda_1}{\lambda_1+\beta} + (1-p)\frac{\lambda_2}{\lambda_2-\beta} - 1\right). \tag{2.7.10}$$

Also, $\alpha(t) \in [0,K]$ is the solution to the equation

$$c_1 K - c_2(\alpha(t) + P_E(t,\alpha(t))) = (c_1 - c_2)Ke^{-r(T-t)}q(\alpha(t)), \tag{2.7.11}$$

with $c_1 = \beta_1\beta_2(1+\lambda_2)$ and $c_2 = \lambda_2(1+\beta_1)(1+\beta_2)$. The analytical expression for $P_E(t,S)$ and $q(s)$ can be directly obtained from Proposition 2.4.1. In contrast to the

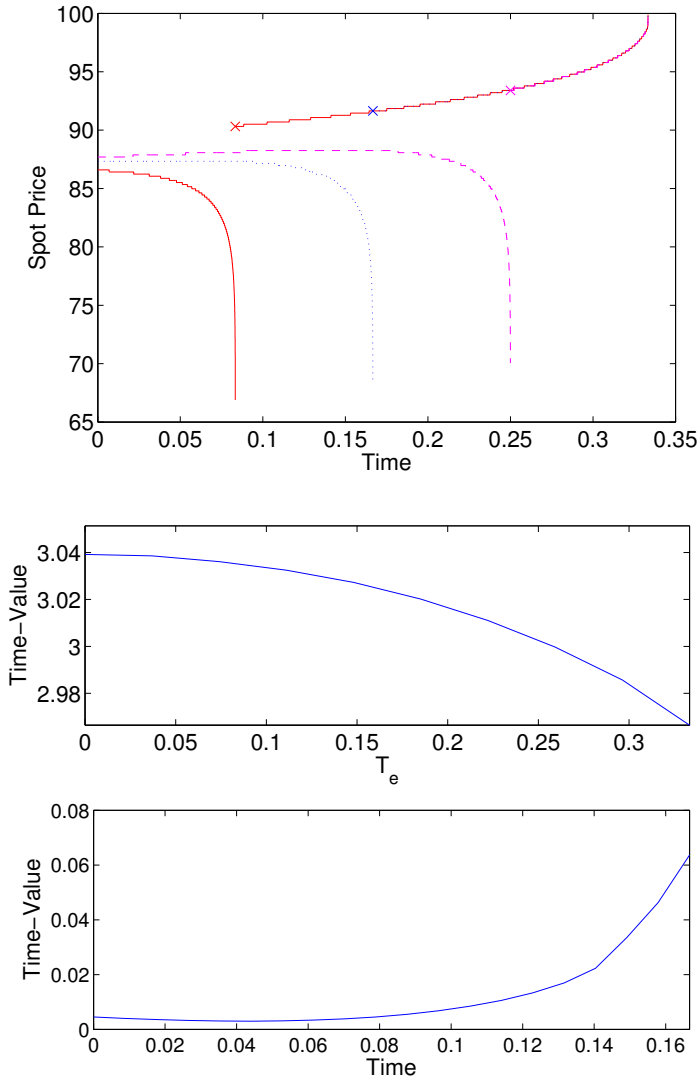

Figure 2.9: Top: The American put exercising boundary when T_e assumes different values, $T_e = 1, 2, 3$ months. Bottom: The time-value of a put (top) with spot and strike set at \$99.79 when T_e changes and the time-value of a put (bottom) with strike \$100 and spot \$87.33 when $T_e = 2$ months and time t changes. Parameters: $r = 0.02, T = 4$ months, $\sigma = 0.1, \kappa = 252, p = 0.5, \lambda_1 = 300, \lambda_2 = 300, u = 0.5, \eta_1 = 30, \eta_2 = 30$.

formula given in Kou and Wang (2004) (see equation (7) there), the calculation of $P_E(s,t)$, $q(\alpha(t))$, $\gamma_{1,2}$ and α accounts for the EA jump r.v. Z_e (see Appendix A.6).

When $t \leq T_e < T$, one could apply the same method used to derive the approximation above, writing the American option as $\tilde{A}(t,S) = \mathbb{E}\left\{e^{-r(T_e-t)}\tilde{A}(T_e, S_{T_e})\,|S_t = S\right\} + \epsilon(t,S)$. The functional form of ϵ would be identical, $\epsilon(t,S) = \gamma_1 S^{-\beta_1} + \gamma_2 S^{-\beta_2}$, because it is derived from the same PIDE (see Appendix A.6). The constants β_1 and β_2 are indeed solutions to equation (2.7.10), after adjusting the time parameters accordingly. In the case when the EA jump is imminent ($T_e = t^+$), we need to evaluate the expectation $\mathbb{E}\left\{\tilde{A}\left(t_+, Se^{Z_e}\right)\right\}$, where S is the stock price at time t. From (2.7.7), this amounts to computing

$$\int_{-\infty}^{+\infty} \Big(\Big(P_E(t_+, Se^z) + \gamma_1 e^{-\beta_1 z} S^{-\beta_1} + \gamma_2 e^{-\beta_2 z} S^{-\beta_2}\Big) 1_{\{Se^z > \alpha\}} + (K - Se^z) 1_{\{Se^z \leq \alpha\}}\Big) f_{Z_e}(z)\, dz \tag{2.7.12}$$

where α, $\gamma_{1,2}$, and $\beta_{1,2}$ are determined by (2.7.8)-(2.7.11). Notice that at time t there is no exercising boundary since $\tilde{A}(t,S) \geq (K-S)^+$ due to Jensen's inequality. In the extended Kou model with double-exponential EA jump, semi-closed formulas can be obtained in a similar fashion as in Proposition 2.4.1.

In Table 2.4, we present numerical results for the prices of American put options with different strikes and maturities under the extended Kou model. We compare the price computed via the Fourier transform method to that obtained with the analytical approximations (2.7.7) and (2.7.12). For different choices of model parameters, strikes and maturities, the approximations perform very well when $T_e \sim t$ or $T_e \sim T$. For the second set of parameters (last 6 columns), the EA jump has a greater impact on the options prices because the tails of the jump are fatter, and the volatility associated to the other part of the dynamics is lower. In this case, the difference between the "true" prices for different values of T_e increases, and so does the difference between the two approximations which might then not be suitable to approximate the options values for in-the-money options when T_e is not close to t or T.

K\T_e	$T-2$D	1.5M	3D	T	0	—	$T-2$D	1.5M	3D	T	0	—
	FST	FST	FST	BA_L	BA_H	EU	FST	FST	FST	BA_L	BA_H	EU
80	0.10	0.10	0.10	0.10	0.11	0.10	0.01	0.01	0.01	0.01	0.01	0.01
85	0.37	0.37	0.37	0.37	0.37	0.37	0.05	0.05	0.05	0.05	0.05	0.05
90	1.02	1.02	1.02	1.02	1.02	1.02	0.22	0.22	0.23	0.22	0.23	0.22
95	2.30	2.31	2.31	2.30	2.31	2.29	0.84	0.86	0.87	0.84	0.87	0.84
100	4.40	4.42	4.43	4.40	4.42	4.38	2.54	2.60	2.63	2.54	2.62	2.53
105	7.35	7.39	7.40	7.36	7.38	7.32	5.68	5.81	5.91	5.70	5.91	5.66
110	11.07	11.11	11.14	11.06	11.11	10.98	10.01	10.10	10.28	10.03	10.30	9.87
115	15.36	15.40	15.45	15.35	15.42	15.20	15.00	15.00	15.08	15.00	15.10	14.57
120	20.06	20.07	20.14	20.04	20.13	19.77	20.00	20.00	20.01	20.00	20.04	19.45

Table 2.4: American put prices under the extended Kou model with a DE EA jump. The column "FST" shows the prices calculated by a Fourier transform method for three different values of T_e with expiration date $T = 3$ months fixed. The extended Barone-Adesi approximations (2.7.7) and (2.7.12) are given under columns "BA_L" and "BA_U". Column "EU" shows the corresponding European put price (see (2.4.2)). The first 6 columns are calculated with model parameters: $S = 100, r = 0.02, \sigma = 0.2, \kappa = 252, p = 0.5, \lambda_1 = 300, \lambda_2 = 300, u = 0.5, \eta_1 = 30, \eta_2 = 30$. The last 6 columns with $S = 100, r = 0.02, \sigma = 0.07, \kappa = 200, p = 0.5, \lambda_1 = 350, \lambda_2 = 350, u = 0.5, \eta_1 = 25, \eta_2 = 25$.

Chapter 3

Leveraged ETFs: Admissible Leverage and Risk Horizon

> When you combine ignorance and leverage, you get some pretty interesting results.
>
> *Warren Buffett*

In this chapter, we provide a quantitative risk analysis of LETFs with an emphasis on the impact of leverage and investment horizon on the fund's returns. In Section 3.1, we present the empirical observations about value erosion and volatility drag present in LETFs returns that motivate our analysis. In Section 3.2, we introduce a simple set of dynamics for the reference index and its leverage counterparts that we will use for the rest of the chapter. In Section 3.3 and 3.4 we introduce the concepts of admissible leverage ratios and admissible risk horizon, respectively. That is, given a risk-horizon (resp. leverage ratio) we analyze what leverage ratios (resp. risk horizon) are consistent with a certain level of risk. In Section 3.5, we introduce and analyze the related concept of intra-horizon risk, or the probability of the LETF hitting a certain level given both a leverage ratio and a risk horizon. This leads us to evaluate a stop-loss/take-profit strategy for LETFs in Section 3.6. In particular, we determine the optimal take-profit given a stop-loss risk constraint. Lastly, in Section 3.7 we investigate the impact of volatility exposure on the returns of different LETF portfolios. The results of this chapter are adapted from Leung and Santoli (2012).

3.1 Empirical Returns of LETFs

In this section, we first compare the historical returns between the SPDR S&P 500 ETF (SPY) and a number of LETFs that also track S&P 500 with different leverage ratios. In Figure 3.1, we show the logarithmic returns of the ProShares Ultra S&P 500 ETF (SSO) with double long leverage and the ProShares UltraShort S&P 500 ETF (SDS) with double short leverage, against ± 2 multiples of the SPY returns. We consider 1-day, 14-day and 60-day rolling periods from September 29, 2010 to September 30, 2012.

In Figures 3.1(a) and 3.1(b), we observe that the returns fall along the 45 degree line. This reflects that for both SSO and SDS are able to replicate, on a daily basis, the relative multiple of the underlying ETF returns. However, when the holding period lengthens to 14 days and 60 days, returns discrepancies start to build (see Figures 3.1(c)–3.1(f)). In these cases, the LETF performance is often inferior to that of the underlying ETF, though the opposite could also happen, typically in a period with strong momentum. In general, a longer horizon also accumulates the erosion due to volatility drag. We shall investigate this more closely in subsequent sections.

In Figure 3.2, we present the same analysis between SPY and the triple-leveraged ETFs UPRO (3x) and SPXU (-3x). As we can see, the one-day returns are matched very closely, but longer horizons again lead to higher discrepancies in returns between the triple LETFs and the underlying. Comparing across leverage ratios, the underperformance over a 60-day period is more pronounced for the triple than the double leverage ratios (see Figures 3.1(e)-3.1(f) and 3.2(e)-3.2(f)). Finally, short LETFs tend fail to replicate the required returns more often than their long leveraged counterparts.

Although long and short LETFs are supposed to move in opposite directions daily by design, it is possible for both to have negative cumulative returns at the same point in time. Figure 3.3 shows the historical cumulative returns of SSO and SDS from December 2010 to November 2011. Over several time intervals in this period, both LETFs have negative cumulative returns. This coincides with the highly volatile period in the market during the second half of 2011. This result, though counterintuitive at first glance, is a natural consequence of the value erosion effect generated by daily tracking of leveraged returns, and is magnified during periods of high volatility.

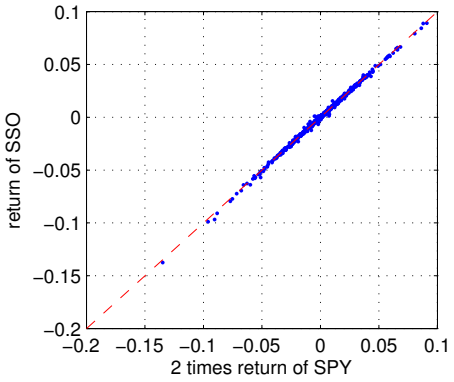

(a) SPY vs SSO: 1-day returns

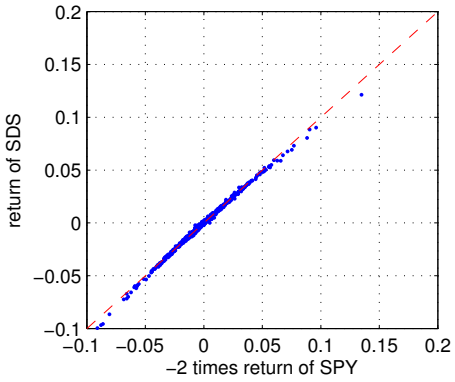

(b) SPY vs SDS: 1-day returns

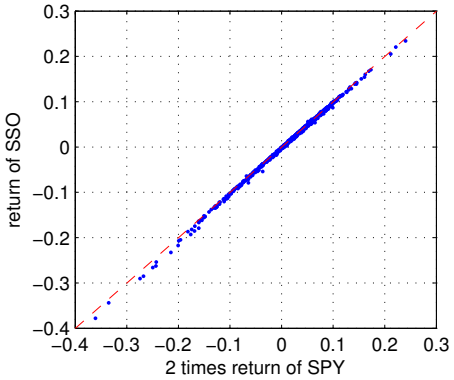

(c) SPY vs SSO: 2-week returns

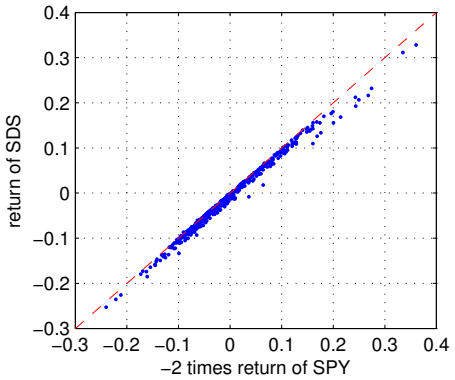

(d) SPY vs SDS: 2-week returns

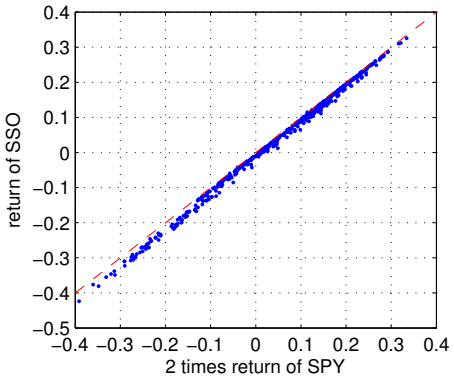

(e) SPY vs SSO: 2-month returns

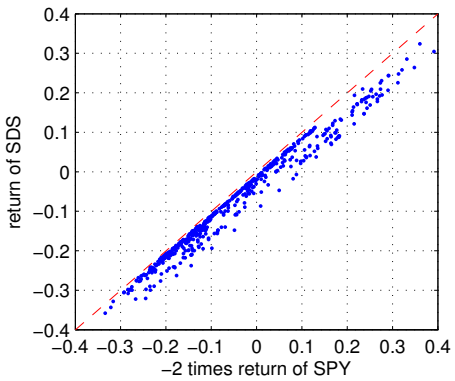

(f) SPY vs SDS: 2-month returns

Figure 3.1: 1-day (top), 2-week (center) and 2-month (bottom) returns of SPY against SSO (left) and SDS (right), in logarithmic scale. We considered 1-day, 2-week and 2-month rolling periods from September 29, 2010 to September 30, 2012.

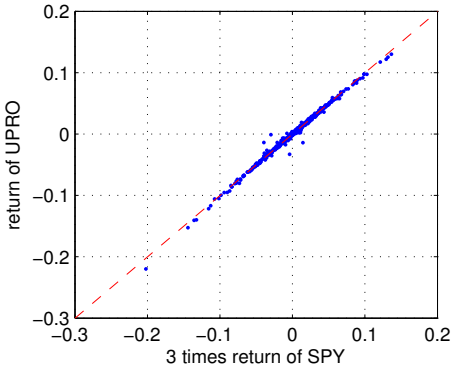

(a) SPY vs UPRO: 1-day returns

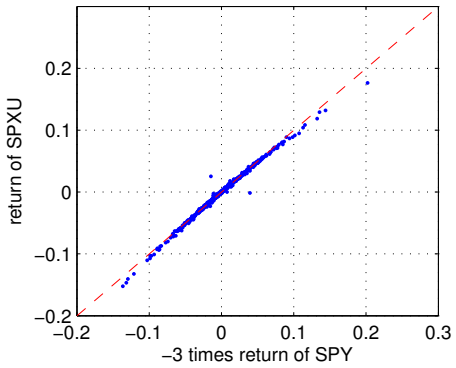

(b) SPY vs SPXU: 1-day returns

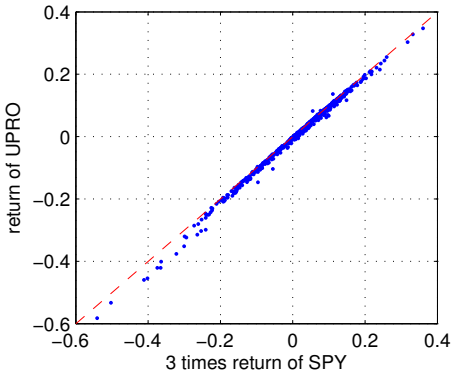

(c) SPY vs UPRO: 2-week returns

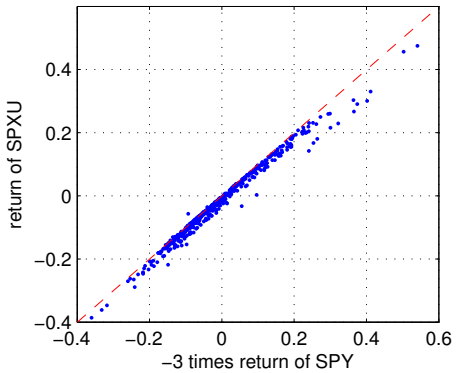

(d) SPY vs SPXU: 2-week returns

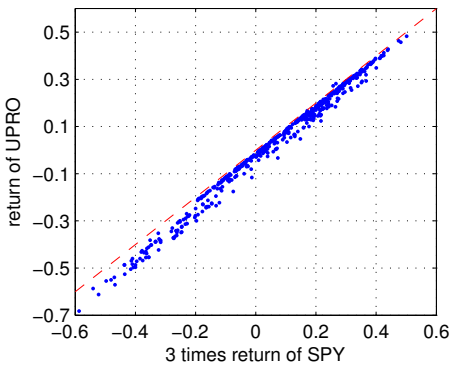

(e) SPY vs UPRO: 2-month returns

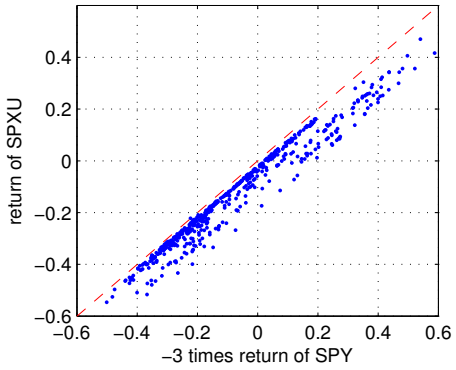

(f) SPY vs SPXU: 2-month returns

Figure 3.2: 1-day (top), 2-week (center) and 2-month (bottom) returns of SPY against UPRO (left) and SPXU (right), in logarithmic scale. We considered 1-day, 2-week and 2-month rolling periods from September 29, 2010 to September 30, 2012.

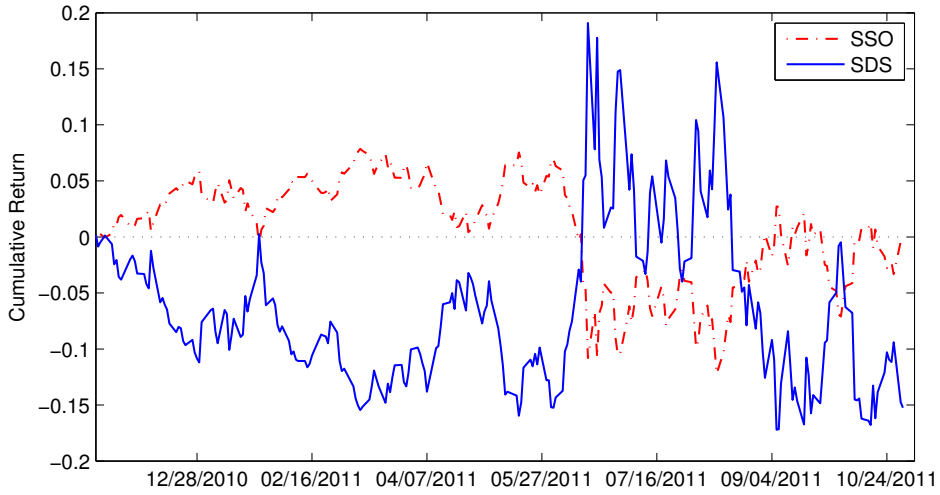

Figure 3.3: SSO and SDS cumulative returns from December 2010 to November 2011. Observe that both SSO and SDS can give negative returns (below the dotted line) simultaneously over several periods in time.

3.2 Price Dynamics of Leveraged ETFs

We model the evolution of the underlying index $(S_t)_{t\geq 0}$ by a geometric Brownian motion (GBM):

$$dS_t = S_t\,(\mu\,dt + \sigma\,dW_t),$$

where W is a standard Brownian motion under the historical measure $\mathbb{P}$. The parameter μ is the ex-dividend annualized growth rate and $\sigma > 0$ is the constant volatility. Based on the reference index S, a long leveraged ETF $(L_t)_{t\geq 0}$ with leverage ratio $\beta \geq 1$ is constructed by simultaneously investing the amount βL_t (β times the fund value) in the underlying S, and borrowing the amount $(\beta - 1)L_t$ at the interest rate $r \geq 0$. This is essentially a constant proportion trading strategy (see Haugh (2011)). As is typical for all ETFs, a small expense rate $f \geq 0$ is incurred. As a result, the β-LETF value evolves according to

$$dL_t = L_t\,\beta\,\frac{dS_t}{S_t} - L_t((\beta - 1)r + f)\,dt. \tag{3.2.1}$$

On the other hand, a leveraged fund with a negative leverage ratio $\beta \leq -1$ involves taking a short position of amount $|\beta L_t|$ in S and keeping $(1-\beta)L_t$ in the money market account. The fund value $(L_t)_{t\geq 0}$ also satisfies (3.2.1) with $\beta \leq -1$. For some short LETFs, it would be appropriate to incorporate the rate of borrowing $\lambda \geq 0$ for short selling S. This can be achieved by replacing μ with $\mu + \lambda$ in (3.2.1) with $\beta \leq -1$. See Avellaneda and Zhang (2010) for this approach. Theoretically, one can also construct constant proportion portfolios with $\beta \in (-1, 1)$, but we do not discuss this since, in practice, the most typical leverage ratios are $\beta = 2, 3$ (long) and $-2, -3$ (short).

For both long and short LETFs, we recognize from (3.2.1) that L is again a GBM:

$$L_t = L_0 \exp\left(\big(\beta\mu - (\beta-1)r - f - \frac{\beta^2\sigma^2}{2}\big)t + \beta\sigma W_t \right) \tag{3.2.2}$$

$$= L_0 \left(\frac{S_t}{S_0}\right)^{\beta} \exp\left(-\big((\beta-1)r + f + \frac{1}{2}\beta(\beta-1)\sigma^2\big)t \right). \tag{3.2.3}$$

Taking log on both sides, we express the log return of L in terms of that of S, namely,

$$\log\left(\frac{L_t}{L_0}\right) = \beta \log\left(\frac{S_t}{S_0}\right) - \left((\beta-1)r + f + \frac{1}{2}\beta(\beta-1)\sigma^2 \right) t. \tag{3.2.4}$$

In view of the second term, the long and short LETFs possess asymmetric return characteristics. Due to volatility exposure, for $|\beta| > 1$, there is an erosion in (log) return proportional to $\sigma^2 t$. Note that this effect is larger for a short LETF than its long leverage counterpart with the same leverage magnitude. In addition, the expense fee also leads to decay in return, as expected.

To motivate our analysis, we first look at the mean and standard deviation of the discounted relative return of LETFs:

$$\hat{r}(\beta) \equiv \mathbb{E}\left\{L_t/L_0 - 1\right\} = e^{(\beta(\mu-r)+r-f)T} - 1, \tag{3.2.5}$$

$$\hat{\sigma}(\beta) \equiv \mathrm{std}\left\{L_t/L_0 - 1\right\} = e^{(\beta(\mu-r)+r-f)T}\sqrt{e^{\beta^2\sigma^2 T} - 1}.$$

When selecting a LETF, a risk-sensitive investor may consider the ratio $\hat{r}(\beta)/\hat{\sigma}(\beta)$ which, loosely speaking, represents the unit of return that one gets for each unit of risk, or the mean-variance trade-off. To choose a range of leverage ratios, the investor can require that

$$\frac{\hat{r}(\beta)}{\hat{\sigma}(\beta)} \geq c\,, \tag{3.2.6}$$

where $c > 0$ is the mean-variance trade-off coefficient.

Figure 3.4 (top) shows the mean-variance frontier, along which the leverage ratio varies from 0 to 3. With a positive drift $\mu = 10\%$, negative leverage ratios yield inferior expected return for the same standard deviation, and thus, are not shown in this figure. The mark 'o' (resp. '$*$') locates the critical leverage ratio β^* satisfying (3.2.6) in equality with $c = 0.23$ (resp. $c = 0.25$). On the right hand side of the marks, the ratio $\hat{r}(\beta)/\hat{\sigma}(\beta)$ falls below the required level c, effectively preventing the investor from selecting the higher leverage ratios.

3.3 Admissible Leverage Ratios

In this section, we investigate the impact of leverage ratio on the risk associated with an LETF. Specifically, we define the *admissible leverage ratio* based on two risk measures, namely, value-at-risk (VaR) and conditional VaR.

3.3.1 VaR

Given a fixed investment horizon T, the probability that the LETF will suffer a relative loss greater than $z \in [0, 1]$, is given by

$$p(z, \beta, T) = \mathbb{P}\{1 - L_T/L_0 > z\} \tag{3.3.1}$$

$$= \Phi\left(\frac{\ln(1-z) - \psi(\beta)T}{|\beta|\sigma\sqrt{T}}\right), \tag{3.3.2}$$

where $\Phi(\cdot)$ is the normal c.d.f. and

$$\psi(\beta) = \beta(\mu - r) + r - f - \frac{\beta^2\sigma^2}{2}. \tag{3.3.3}$$

Note that $\psi(\beta)t$ is related to the log return difference between L and S in (3.2.4). The loss probability is illustrated in Figure 3.4 (bottom).

In view of the continuous distribution of L_T, we define the (relative) value-at-risk, VaR_α, at confidence level $\alpha \in (0, 1)$, via the equation

$$p(VaR_\alpha, \beta, T) = \alpha. \tag{3.3.4}$$

Intuitively, a larger VaR_α means a higher level of risk. For our analysis, $VaR_\alpha \equiv VaR_\alpha(\beta, T)$ is often viewed as a function of leverage ratio β and horizon T. Inverting the loss probability function in (3.3.4), we obtain an expression for VaR_α.

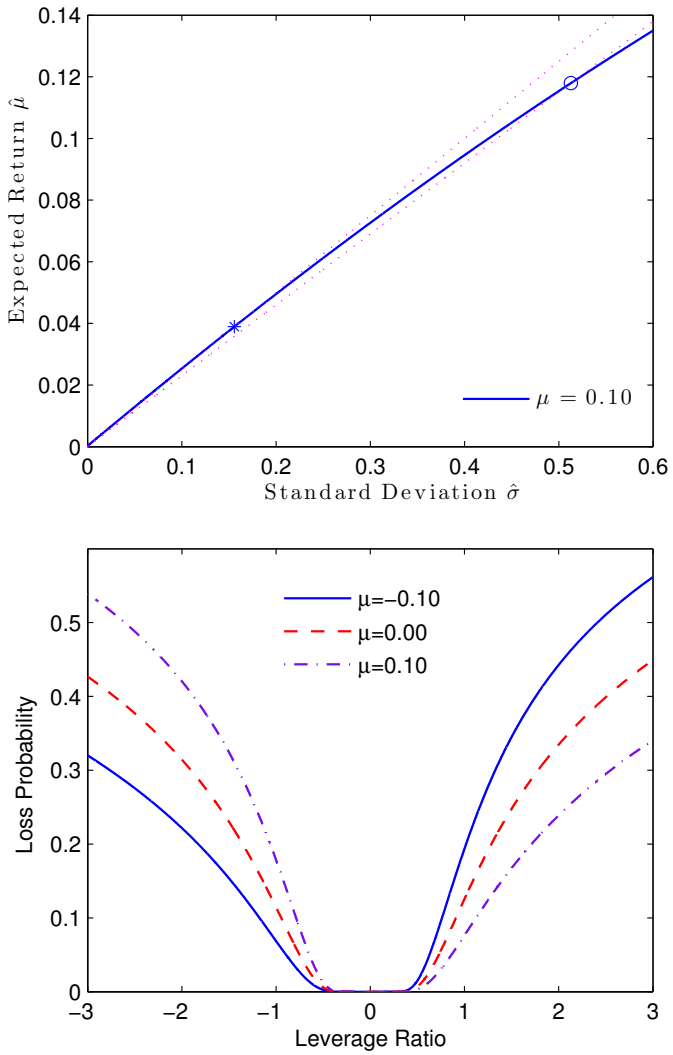

Figure 3.4: Top: The mean-variance frontier (solid), where each point corresponds to a different leverage ratio within $[0, 3]$. The mark 'o' (resp. '$*$') locates the critical leverage ratio β^* satisfying (3.2.6) in equality with $c = 0.23$ (resp. $c = 0.25$). Bottom: Loss probability increases drastically with higher leverage ratios. Parameters: $z = 20\%$, $r = 2\%, T = 0.5$, σ=25% and $f = 0.95\%$.

Proposition 3.3.1. *Given any investment horizon T and leverage ratio β, the (relative) value-at-risk of holding the LETF is given by*

$$VaR_\alpha(\beta\,,T) = 1 - \exp\left(\psi(\beta)T + |\beta|\sigma\sqrt{T}\,\Phi^{-1}(\alpha)\right). \tag{3.3.5}$$

with $\psi(\beta)$ defined in (3.3.3)*.*

To better understand the property of $VaR_\alpha(\beta, T)$, we differentiate w.r.t. β to get

$$\frac{\partial\, VaR_\alpha}{\partial\beta} = ((\mu - r - \beta\sigma^2)T + \text{sign}(\beta)\Phi^{-1}(\alpha)\sigma\sqrt{T})(VaR_\alpha - 1).$$

Note that this derivative is discontinuous at $\beta = 0$ and changes sign once. In practical applications, the term $\Phi^{-1}(\alpha)\sigma\sqrt{T}$ is negative, and therefore the jump in $\beta = 0$ is upward. Given these observations, either the derivative vanishes at some β^*, or the derivative is negative for $\beta < 0$ and positive for $\beta > 0$. To summarize, we define

$$\beta^* = \begin{cases} \frac{\mu-r}{\sigma^2} + \frac{\Phi^{-1}(\alpha)}{\sigma\sqrt{T}} & \text{if } \frac{\mu-r}{\sigma^2} + \frac{\Phi^{-1}(\alpha)}{\sigma\sqrt{T}} > 0, \\ \frac{\mu-r}{\sigma^2} - \frac{\Phi^{-1}(\alpha)}{\sigma\sqrt{T}} & \text{if } \frac{\mu-r}{\sigma^2} - \frac{\Phi^{-1}(\alpha)}{\sigma\sqrt{T}} < 0, \\ 0 & \text{otherwise,} \end{cases} \tag{3.3.6}$$

and conclude that $VaR_\alpha(\beta)$ is decreasing in β for $\beta \le \beta^*$ and increasing for $\beta \ge \beta^*$. This is illustrated in Figure 3.5. Also, note that β^* does not depend on the expense rate f and increases linearly with the excess return.

One way to describe an investor's risk tolerance is to consider the maximum VaR_α threshold $\bar{z}$ which leads to the inequality in β

$$VaR_\alpha(\beta, T) \le \bar{z}. \tag{3.3.7}$$

This will in turn exclude a range of leverage ratios β. Notice that at $\beta = 0$,

$$VaR_\alpha(0\,,T) = 1 - e^{(r-f)T},$$

which is typically a low (positive) point of VaR_α, as discussed above and shown in Figure 3.5. In Figure 3.5 (top), VaR_α is always increasing in $|\beta|$ and $\beta^* = 0$. Moreover, VaR_α is not symmetric in β: VaR_α tends to be lower for those leverage ratios β with the same sign as drift μ. In Figure 3.5 (bottom), we illustrate that, with a higher α, VaR_α reaches

its minimum at $\beta^* \neq 0$. Therefore, if risk tolerance is very low, or if the expense ratio is high, there might not exist any leverage ratio β for which the investor is willing to invest. Precisely, we have the following result.

Proposition 3.3.2. *The admissible range of leverage ratios based on criterion (3.3.7) is given by*

$$I^- \cup I^+,$$

where

$$I^{\pm} = \begin{cases} [l^{\pm}, u^{\pm}] & \text{if } \Delta^{\pm} \text{ is real,} \\ \emptyset & \text{otherwise,} \end{cases}$$

with

$$l_+ = \max\{0, \Gamma^+(\alpha) - \Delta^+(\alpha)\}, \quad u_+ = \max\{0,\, \Gamma^+(\alpha) + \Delta^+(\alpha)\,\}, \tag{3.3.8}$$

$$l_- = \min\{0,\, \Gamma^-(\alpha) - \Delta^-(\alpha)\,\}, \quad u_- = \min\{0,\, \Gamma^-(\alpha) + \Delta^-(\alpha)\,\}, \tag{3.3.9}$$

and

$$\Gamma^{\pm}(\alpha) = \frac{1}{\sigma^2 T}\left((\mu - r)T \pm \Phi^{-1}(\alpha)\sigma\sqrt{T}\right),$$
$$\Delta^{\pm}(\alpha) = \frac{1}{\sigma^2 T}\sqrt{((\mu - r)T \pm \Phi^{-1}(\alpha)\sigma\sqrt{T})^2 - 2\sigma^2 T((f - r)T + \ln(1 - \bar{z}))}.$$

Using Proposition 3.3.2, we can precisely identify the interval of acceptable leverage ratios. To visualize this, we look at Figure 3.5 (top) and consider the leverage ratios whose value-at-risk is lower than a given level. For instance, setting the risk tolerance level $\bar{z} = 0.5$, the leverage ratios 2 and -2 are admissible but 3 and -3 are excluded. In Figure 3.5 (bottom), setting $\bar{z} = 0.25$, the admissible leverage ratio interval for $\mu = -18\%$ is $[l^-, u^-] \cup [l^+, u^+] = [-2.99, 1.21]$, so $\beta = -3$ is excluded. On the other hand, with $\mu = 18\%$, the admissible interval is $[-1.26, 2.76]$, so $\beta = 3$ is excluded. The concept of admissible leverage ratio provides a simple recipe for identifying LETFs that are too risky according to a given risk measure.

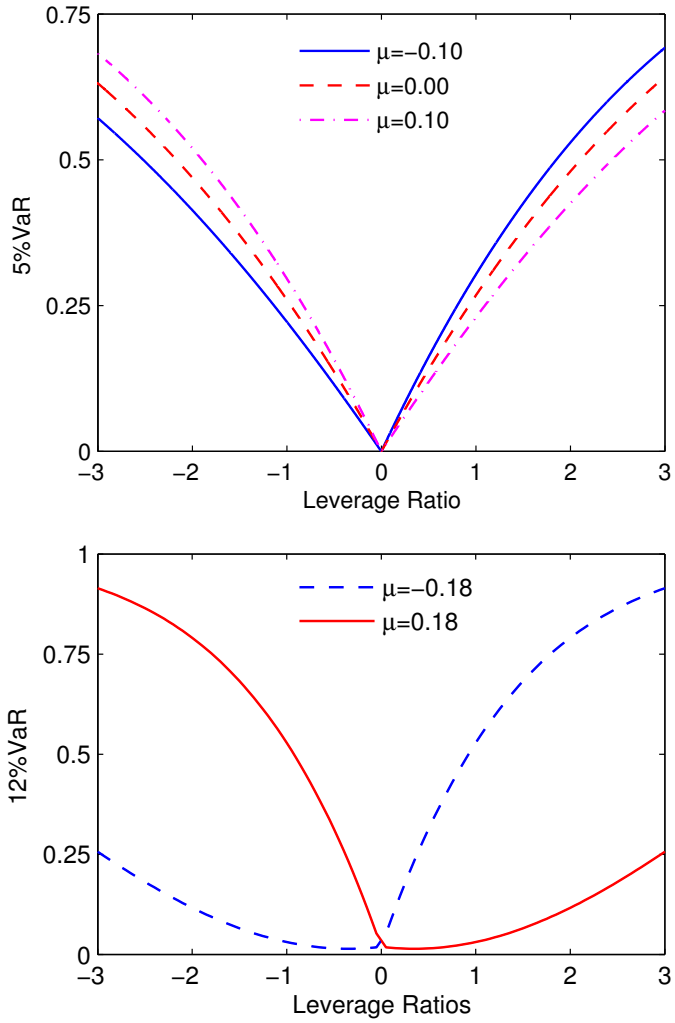

Figure 3.5: Top: VaR_α is lowest at $\beta = 0$, and increases as the absolute value of leverage ratio $|\beta|$ increases. Parameters: $r = 2\%, T = 0.5$, σ=25% and $f = 0.95\%$. Bottom: VaR_α achieves a minimum at a non-zero leverage, i.e. $\beta^* \neq 0$ (see (3.3.6)). Parameters: $r = 0\%, T = 2$, σ=20% and $f = 0.95\%$.

3.3.2 CVaR

In addition to value-at-risk, we define the conditional value-at-risk $CVaR_\alpha$ at confidence level α as

$$CVaR_\alpha(\beta, T) := \mathbb{E}\left\{1 - \frac{L_T}{L_0} \,|\, 1 - \frac{L_T}{L_0} > VaR_\alpha(\beta, T)\right\}.$$

Proposition 3.3.3. *Given any investment horizon T and leverage ratio β, the conditional value-at-risk for the LETF is given by*

$$CVaR_\alpha(\beta, T) = 1 - e^{(\beta(\mu-r)+r-f)T}\frac{\Phi(\Phi^{-1}(\alpha) - |\beta|\sigma\sqrt{T})}{\alpha}. \tag{3.3.10}$$

The $CVaR_\alpha(\beta)$ is decreasing in β for $\beta \le \beta^{**}$ and increasing for $\beta \ge \beta^{**}$, with the critical leverage β^{**} satisfying

$$\frac{\mu - r}{\sigma\sqrt{T}}\Phi(\Phi^{-1}(\alpha) - |\beta^{**}|\sigma\sqrt{T}) = \text{sign}(\beta^{**})\phi(\Phi^{-1}(\alpha) - |\beta^{**}|\sigma\sqrt{T}). \tag{3.3.11}$$

Proof. For any $\beta \in \mathbb{R}$, the expected (relative) shortfall is given by

$$\mathbb{E}\left\{\frac{L_0 - L_T}{L_0} \,\middle|\, \frac{L_0 - L_T}{L_0} > z\right\} = 1 - e^{(\beta(\mu-r)+r-f)T}\,\frac{\Phi(d_z - |\beta|\sigma\sqrt{T})}{\Phi(d_z)}, \tag{3.3.12}$$

where

$$d_z := \frac{\ln(1-z) - \psi(\beta)T}{|\beta|\sigma\sqrt{T}}.$$

Setting $z = VaR_\alpha$ gives $CVaR_\alpha$ in (3.3.10). Next, we compute the derivative

$$\frac{\partial CVaR_\alpha}{\partial \beta} = \frac{e^{(\beta(\mu-r)+r-f)T}}{\alpha}\Big((r-\mu)\Phi(\Phi^{-1}(\alpha) - |\beta|\sigma\sqrt{T}) + \text{sign}(\beta)\sigma\sqrt{T}\phi(\Phi^{-1}(\alpha) - |\beta|\sigma\sqrt{T})\Big).$$

The sign of the derivative depends on the term in the bracket, and equating this to zero yields the critical value β^{**} in (3.3.11). □

3.4 Admissible Risk Horizon

The risk analysis in the previous section sheds light on the choice of leverage ratios. Alternatively, the investor can control risk exposure by appropriately selecting the investment

horizon. For risk management purposes, it is important to determine the maximum investment horizon τ such that the risk measure stays under some threshold $C \in (0,1)$. This idea leads us to study the *admissible risk horizon* induced by a risk measure.

First, let us consider the value-at-risk $VaR_\alpha(\beta,\tau)$ for a β-LETF and horizon τ. The admissible risk horizon $ARH_\alpha(\beta,C)$ is defined by:

$$ARH_\alpha(\beta,C) = \inf\left\{\tau \geq 0 \,:\, VaR_\alpha\left(\beta,\tau\right) = C\right\}, \tag{3.4.1}$$

and we set $ARH_\alpha(\beta,C) = +\infty$ if the equation $VaR_\alpha\left(\beta,\tau\right) = C$ has no positive root (in τ). Herein, we impose an upper bound of 0.5 on α so that $\Phi(\alpha) < 0$. Using formula (3.3.5), we invert (3.4.1) to get an explicit expression for $ARH_\alpha(\beta,C)$.

Proposition 3.4.1. *Denote $b = |\beta|\,\sigma\Phi^{-1}(\alpha)$. If $b^2/4 \geq -\psi(\beta)\ln(1-C)$, then the admissible risk horizon for the β-LETF with VaR_α limited at C is given by*

$$ARH_\alpha(\beta,C) = \left(\frac{-b/2 - \sqrt{b^2/4 + \psi(\beta)\ln(1-C)}}{\psi(\beta)}\right)^2. \tag{3.4.2}$$

If $b^2/4 < -\psi(\beta)\ln(1-C)$, then $ARH_\alpha(\beta,C) = +\infty$.

To gain some insight on the conditions in Proposition 3.4.1, we first recall that $VaR_\alpha(\beta\,,T) = 1 - \exp\left(\psi(\beta)T + |\beta|\sigma\sqrt{T}\,\Phi^{-1}(\alpha)\right)$. If, given a certain β, $\psi(\beta) > 0$, then VaR_α is convex and eventually decreasing in T, and its maximum can potentially lie below the threshold C. In fact, whether this happens or not is determined by the condition $b^2/4 < -\psi(\beta)\ln(1-C)$. In reality, we tend to have $\psi(\beta) > 0$ when β is small or when $\text{sign}(\beta)\mu$ is large. The latter means that the investment has a high rate of return, so intuitively VaR_α can stay low.

On the other hand, when when $b^2/4 > -\psi(\beta)\ln(1-C)$ and $\psi(\beta) > 0$, the equation $VaR_\alpha\left(\beta,\tau\right) = C$ admits two positive roots and (3.4.2) selects only the smallest root, according to equation (3.4.1).

In contrast, if $\psi(\beta) < 0$, then VaR_α is increasing in T. Consequently, the equation $VaR_\alpha\left(\beta,\tau\right) = C$ always admits a unique strictly positive solution (note that $VaR_\alpha\left(\beta,0\right) = 0$).

Figure 3.6 illustrates how ARH_α varies for different values of β and μ. As we can see, the admissible risk horizon increases as $|\beta|$ decreases. For any fixed positive leverage ratio,

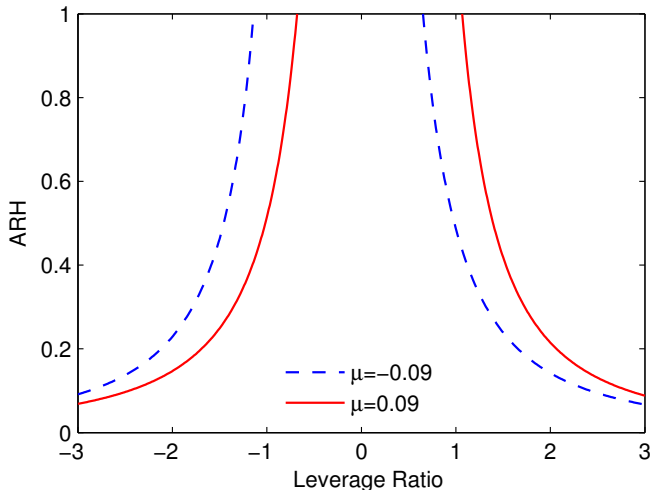

Figure 3.6: The admissible risk horizon tends to decrease as leverage ratio deviates from zero. Parameters: $C = 0.25, r = 1\%, \alpha = 5\%, \sigma$=25% and $f = 0.95\%$.

the admissible risk horizon tends to increase with drift μ. In addition, it is also preferable to choose a leverage ratio, say $\hat{\beta}$, with the same sign as that of μ, since the corresponding admissible risk horizon is greater than that of $-\hat{\beta}$.

Similarly, one can define an admissible risk horizon based on other risk measures. For instance, the admissible risk horizon $\widehat{ARH}_\alpha(\beta, C)$ based on the conditional value-at-risk is determined from the equation:

$$\widehat{ARH}_\alpha(\beta, C) = \inf\left\{\tau \geq 0 \,:\, CVaR_\alpha\left(\beta, \tau\right) = C\right\}. \tag{3.4.3}$$

In this case an analytical solution is not available. Nevertheless, one can easily find the zero(s) of the function $g(\tau) := CVaR_\alpha(\beta, \tau) - C$.

3.5 Intra-Horizon Risk

Both VaR and CVaR concern the loss distribution at a fixed future date, even though the LETF value may experience large losses at intermediate times. In reality, investors may monitor the asset price movement and impose a stop-loss level to limit downside risk. This motivates us to model a stochastic holding period until the LETF falls to a certain threshold.

We define the first passage time that the LETF, starting at L_0, reaches to a lower level ℓL_0:

$$\tau_\ell = \inf\{\, t \geq 0 \,:\, L_t \leq \ell L_0 \,\}, \qquad \ell \in (0,1).$$

With this, we define the intra-horizon loss probability

$$\underline{p}(\ell, \beta, T) = \mathbb{P}\{\tau_\ell \leq T\}.$$

This probability is related to the minimum of L over $[0,T]$, denoted by $\underline{L}_T = \min_{0\leq t\leq T} L_t$, and admits an explicit expression:

$$\begin{aligned}\underline{p}(\ell, \beta, T) &= \mathbb{P}\{\underline{L}_T \leq \ell L_0\} \\ &= \Phi\left(\frac{\ln(\ell) - \psi(\beta)T}{|\beta|\,\sigma\sqrt{T}}\right) + \ell^{2\psi(\beta)/(\beta\sigma)^2}\,\Phi\left(\frac{\ln(\ell) + \psi(\beta)T}{|\beta|\,\sigma\sqrt{T}}\right), \end{aligned} \tag{3.5.1}$$

where $\psi(\beta)$ is defined in (3.3.3).

Figure 3.7 (top) shows how $\underline{p}(\ell, \beta)$ varies with respect to β for three different threshold levels. As ℓ or β increases, the intra-horizon loss probability $\underline{p}(\ell, \beta)$ increases. In addition, for any pair of leverage ratios with the same absolute value, $\underline{p}(\ell, \beta)$ is lower for the positive leverage ratio.

Given any loss level ℓL_0, it is useful to know whether an LETF will reach it in the long run. This amounts to determining whether the probability $\mathbb{P}\{\tau_\ell < \infty\}$ is equal to or strictly less than 1. Taking $T \uparrow \infty$ in (3.5.1), direct computation shows that, when $\psi(\beta) \leq 0$, we have $\mathbb{P}\{\tau_\ell < \infty\} = 1$. In other words, to ensure $\mathbb{P}\{\tau_\ell < T\} < 1$, one has to restrict the leverage choice so that $\psi(\beta) > 0$.

To understand the condition in terms of leverage ratio β, we recall from (3.3.3) that $\psi(\beta)$ is not always of constant sign, and is quadratic in leverage ratio β. In particular, for large $|\beta|$, the volatility σ will have a dominant negative impact. If $f \leq r$, then we have $\psi(\beta) > 0$ over the interval of leverage ratios:

$$\beta \in \left(\frac{\mu - r - \sqrt{(\mu-r)^2 + 2\sigma^2(r-f)}}{\sigma^2}, \frac{\mu - r + \sqrt{(\mu-r)^2 + 2\sigma^2(r-f)}}{\sigma^2}\right).$$

Note that the width of the leverage interval is proportional to the excess return $\mu - r$, and inversely proportional to volatility. On the other hand, if $f > r$, then the above interval

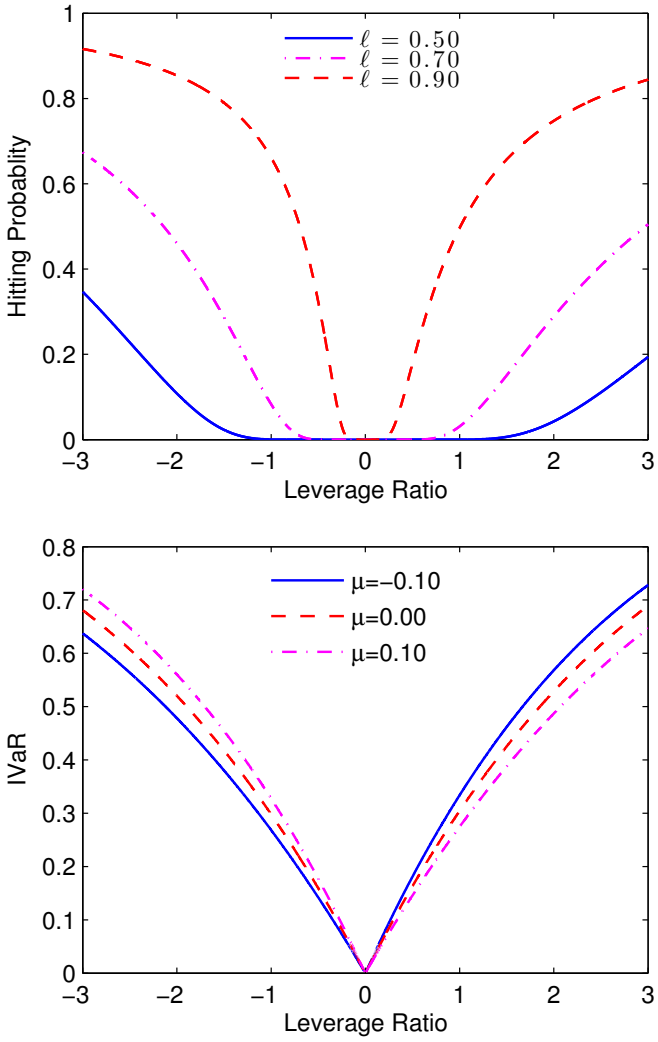

Figure 3.7: Top: Probability of hitting a lower level ℓ for different leverage ratios in [-3, 3], with $\mu = 10\%$. Bottom: Intra-horizon VaR vs leverage ratios, with $\alpha = 5\%$. Common parameters for both plots: $r = 2\%$, $T = 0.5$, $\sigma = 25\%$ and $f = 0.95\%$.

holds if and only if $(\mu - r)^2 \geq 2\sigma^2(f - r)$. Otherwise, we have $\psi(\beta) \leq 0$ and the interval of leverage ratio does not exist. In this case, the hitting time τ_ℓ is finite almost surely.

The intra-horizon loss probability leads us to define the *intra-horizon* value-at-risk, denoted by $IVaR_\alpha$, via the equation

$$\underline{p}\big(1 - IVaR_\alpha, \beta, T\big) = \alpha. \tag{3.5.2}$$

This is a modification of value-at-risk, and it incorporates the possibility that the LETF *ever* falls below a lower level. Due to the complicated form of equation (3.5.1), this risk metric does not admit an explicit formula. Nevertheless, the numerical solution for $IVaR_\alpha$ in (3.5.2) involves a straightforward and instant root finding.

In Figure 3.7 (bottom), we illustrate how $IVaR_\alpha$ varies with respect to β for different values of μ. Similar to VaR_α, $IVaR_\alpha$ also increases as leverage ratio deviates from 0. Notice that with common parameters, we have $IVaR_\alpha(\beta, T) > VaR_\alpha(\beta, T)$. This can be inferred from the definitions (3.3.4) and (3.5.2), along with the fact that $\underline{p}(1 - z, \beta, T) > p(z, \beta, T)$ (see (3.3.2) and (3.5.1)).

Proposition 3.5.1. *The intra-horizon value-at-risk admits the partial derivative*

$$\frac{\partial IVaR_\alpha}{\partial \beta} = \frac{(1 - IVaR_\alpha)\,|\beta|\,\sigma\frac{\partial p}{\partial \beta}}{\frac{1}{\sqrt{T}}\phi(\hat{d}_-) + \frac{2\psi(\beta)}{|\beta|\sigma}(1 - IVaR_\alpha)^{2\psi(\beta)/(\beta\sigma)^2}\Phi(\hat{d}_+) + \frac{(1-IVaR_\alpha)^{2\psi(\beta)/(\beta\sigma)^2}}{\sqrt{T}}\phi(\hat{d}_+)}, \tag{3.5.3}$$

where

$$\hat{d}_\pm := \frac{\ln(1 - IVaR_\alpha) \pm \psi(\beta)T}{|\beta|\,\sigma\sqrt{T}}.$$

We can deduce from (3.5.3) that the derivative would take the same sign as $\frac{\partial \underline{p}(z,\beta)}{\partial \beta}$, unless the drift term $\psi(\beta)$ is so negative that the denominator also becomes negative.

3.6 Stop-Loss Exit

The intra-horizon risk measure motivates a stop-loss exit strategy in order to limit downside risk during the investment horizon. Incorporating a stop-loss level ℓL_0, we denote $\mathcal{R}_T =$

$\frac{L_{T\wedge\tau_\ell}}{L_0}$ and express the expected relative value as

$$\mathbb{E}\left\{\mathcal{R}_T\right\} = \ell\,\mathbb{P}\{\tau_\ell < T\} + \mathbb{E}\left\{\frac{L_T}{L_0}1_{\{\tau_\ell>T\}}\right\}. \tag{3.6.1}$$

The first term is given by

$$\ell\mathbb{P}\{\tau_\ell < T\} = \ell\left[\Phi\left(\frac{\ln(\ell)-\psi(\beta)T}{|\beta|\sigma\sqrt{T}}\right) + \ell^{2\psi(\beta)/(\beta\sigma)^2}\Phi\left(\frac{\ln(\ell)+\psi(\beta)T}{|\beta|\sigma\sqrt{T}}\right)\right].$$

For the second term, we apply standard calculations to get

$$\begin{aligned}\mathbb{E}\left\{\frac{L_T}{L_0}1_{\{\tau_\ell>T\}}\right\} = e^{(\psi(\beta)+\frac{\beta^2\sigma^2}{2})T}\Bigg[&\Phi\left(|\beta|\sigma\sqrt{T}+\frac{\psi(\beta)\sqrt{T}}{|\beta|\sigma}-\frac{\ln(\ell)}{|\beta|\sigma\sqrt{T}}\right)\\ &-\ell^{2\psi(\beta)/(\beta\sigma)^2+2}\Phi\left(|\beta|\sigma\sqrt{T}+\frac{\psi(\beta)\sqrt{T}}{|\beta|\sigma}+\frac{\ln(\ell)}{|\beta|\sigma\sqrt{T}}\right)\Bigg].\end{aligned} \tag{3.6.2}$$

Moreover, the variance of the expected relative value with a stop-loss exit also admits a closed-form formula. Precisely, the variance is given by $\mathrm{var}\{\mathcal{R}_T\} = \mathbb{E}\{\mathcal{R}_T^2\} - (\mathbb{E}\{\mathcal{R}_T\})^2$, with $\mathbb{E}\{\mathcal{R}_T\}$ from (3.6.1) and

$$\begin{aligned}\mathbb{E}\{\mathcal{R}_T^2\} &= \frac{1}{L_0^2}\mathbb{E}\left\{\ell^2 1_{\{\tau_\ell<T\}} + L_T^2 1_{\{\tau_\ell>T\}}\right\}\\ &= \ell^2\left[\Phi\left(\frac{\ln(\ell)-\psi(\beta)T}{|\beta|\sigma\sqrt{T}}\right) + \ell^{2\psi(\beta)/(\beta\sigma)^2}\Phi\left(\frac{\ln(\ell)+\psi(\beta)T}{|\beta|\sigma\sqrt{T}}\right)\right] + e^{2T(\psi(\beta)+\beta^2\sigma^2)}\cdot\\ &\left[\Phi\left(2|\beta|\sigma\sqrt{T}+\frac{\psi(\beta)\sqrt{T}}{|\beta|\sigma}-\frac{\ln(\ell)}{|\beta|\sigma\sqrt{T}}\right) -\right.\\ &\left.\ell^{2\psi(\beta)/(\beta\sigma)^2+4}\Phi\left(2|\beta|\sigma\sqrt{T}+\frac{\psi(\beta)\sqrt{T}}{|\beta|\sigma}+\frac{\ln(\ell)}{|\beta|\sigma\sqrt{T}}\right)\right].\end{aligned}$$

Next, suppose the investor seeks to take profit when the asset reaches a sufficiently high level. Then, it is useful to compute the probability that LETF will fall to the stop-loss level before reaching the take-profit level. To fix ideas, we denote τ_ℓ (resp. τ_h) as the time for the LETF to hit a lower level $\ell\,L_0$ (resp. upper level hL_0), with $\ell \le 1 \le h$.

Proposition 3.6.1. *The probability that a β-LETF to reach a lower level ℓL_0 before a higher level hL_0 is given by*

$$\mathbb{P}\{\tau_\ell < \tau_h\} = \frac{1-h^{-2\psi(\beta)/(\beta\sigma)^2}}{\ell^{-2\psi(\beta)/(\beta\sigma)^2}-h^{-2\psi(\beta)/(\beta\sigma)^2}}. \tag{3.6.3}$$

The explicit loss probability formula (3.6.3) can be used to quantify the risk of holding an LETF with a take-profit/stop-loss strategy. A risk-sensitive investor may want to bound it by $q \in (0,1)$, namely,

$$\mathbb{P}\{\tau_\ell < \tau_h\} \leq q. \tag{3.6.4}$$

Let us think of the loss probability bound in (3.6.4) as exogenously specified. The investor selects the maximum admissible take-profit level h_{max} in terms of stop-loss level ℓ and probability bound q. From (3.6.3), we observe that $\mathbb{P}\{\tau_\ell < \tau_h\}$ monotonically increases with h, and arrive at two cases:

- Case 1: $\psi(\beta) > 0$ and $q \geq \ell^{2\psi(\beta)/(\beta\sigma)^2}$. As $h \to \infty$, $\mathbb{P}\{\tau_\ell < \tau_h\}$ is bounded by $\ell^{2\psi(\beta)/(\beta\sigma)^2} \leq 1$. If $q \geq \ell^{2\psi(\beta)/(\beta\sigma)^2}$, then the take-profit level can be arbitrarily high by the investor, i.e. $h_{max} = \infty$.

- Case 2: $\psi(\beta) > 0$ and $q < \ell^{2\psi(\beta)/(\beta\sigma)^2}$, or $\psi(\beta) < 0$. From (3.6.3), $h = 1 \Rightarrow \mathbb{P}\{\tau_\ell < \tau_h\} = 0$. By monotonicity, there exists a finite upper level $h_{max} \in [1, \infty)$. By rearranging the inequality (3.6.4) , we obtain the maximum admissible take-profit level

$$h_{max} = \left(\frac{1 - \ell^{-2\psi(\beta)/(\beta\sigma)^2} q}{1 - q} \right)^{-\frac{\beta^2\sigma^2}{2\psi(\beta)}}. \tag{3.6.5}$$

From this result, we also infer that h_{max} decreases with ℓ and increases with q.

3.7 LETF Portfolios and Volatility Exposure

LETFs can be used in combination to construct various portfolios. Some strategies are designed based on the anticipated tracking errors or value erosion of LETFs. On the other hand, we have seen that volatility exposure will diminish LETF returns. Hence, in this section, we discuss how the performance of some example strategies depends volatility exposure.

For our analysis, the underlying index S is assumed to follow a general diffusion price dynamics:

$$dS_t = S_t \left(\mu \, dt + \sigma_t \, dW_t \right),$$

where $(\sigma_t)_{t\geq 0}$ is the stochastic volatility process. Then, for both long and short LETFs, the LETF value is given by

$$L_t = L_0 \left(\frac{S_t}{S_0}\right)^{\beta} \exp\left(\left(-(\beta-1)r - f\right)t - \frac{1}{2}\beta(\beta-1)V_t\right), \tag{3.7.1}$$

where $V_t = \int_0^t \sigma_u^2\, du$ is the realized variance of S up to time t.

3.7.1 Short $\pm\beta$ LETFs

Due to volatility drag, both long and short leveraged ETFs tend to lose value over time. Based on this observation, some investors consider taking short positions in LETFs with both positive and negative leverage ratios. Specifically, let $\beta > 1$ and consider a portfolio that shorts one dollar of a (positively) β-LETF and simultaneously shorts one dollar of the $-\beta$-LETF. The two dollars received form short-selling the LETFs is assumed to earn at the risk-free rate $r \geq 0$. Without loss of generality, we take $S_0 = 1$. The portfolio value at time t can be expressed in terms of the ETF value S_t and its realized variance V_t:

$$\begin{aligned}\mathcal{E}(S_t, V_t) = &-S_t^{\beta} \exp\left(-\left(r\left(\beta-1\right)+f\right)t - \frac{\beta(\beta-1)}{2}V_t\right)\\ &- S_t^{-\beta} \exp\left(\left(r\left(\beta+1\right)-f\right)t - \frac{\beta(\beta+1)}{2}V_t\right) + 2e^{rt}, \quad \beta > 1.\end{aligned} \tag{3.7.2}$$

Note that the portfolio value can be both positive and negative. While we have chosen to short both $\pm\beta$-LETFs with identical absolute leverage ratio values, it is straightforward to construct a similar portfolio by shorting LETFs with completely different leverage ratios.

At any fixed $t \geq 0$, we determine the set of non-negative portfolio values:

$$\mathcal{S}_\beta = \{(s, v) \in \mathbb{R}_+^2 \,:\, \mathcal{E}(s, v) \geq 0\},$$

where

$$\mathcal{E}(s, v) = -s^{\beta} e^{-(r(\beta-1)+f)t - \frac{\beta(\beta-1)}{2}v} - s^{-\beta} e^{(r(\beta+1)-f)t - \frac{\beta(\beta+1)}{2}v} + 2e^{rt}.$$

In other words, we seek to determine all the pairs of ETF value s and realized variance v such that the portfolio value is non-negative. Interestingly, we do not need to specify the parameters μ and σ in order to study the value of $\mathcal{E}(s, v)$. Instead, we look at the ETF value s and realized variance v.

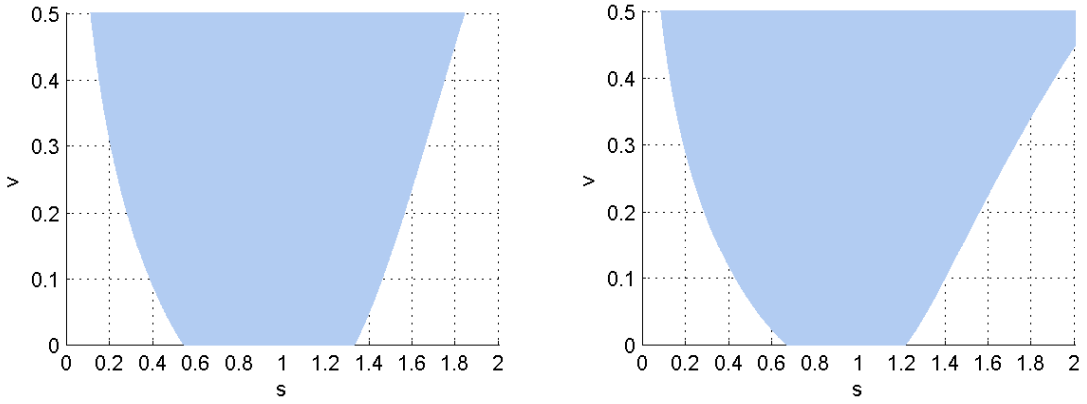

(a) $\beta = 2$ (b) $\beta = 3$

Figure 3.8: The shaded region indicates where the portfolio value is non-negative. For a high realized variance v, the region tends to be larger for $\beta = 3$ (right) than for $\beta = 2$ (left). Parameters: $T = 1, r = 1\%$, and $f = 0.95\%$.

Intuitively, when the future ETF value S_T deviates from 1, that means the ETF has experienced a large directional movement. If the realized variance V_T is large, then there is a lot of fluctuation in the ETF evolution. In order to visualize their effects on the profitability of the investment strategy, we illustrate in Figure 3.8 the set $\mathcal{S}_\beta$ for $\beta = 2$ and 3. When S_T is close to its initial value, the portfolio has a non-negative value. This is because the expense ratio and volatility drag will erode the values of both $\pm\beta$-LETFs, and the portfolio is taking a short position on them. Also, for any level of S_T, the portfolio benefits from increasing realized variance due to volatility drag. In other words, the short $\pm\beta$-LETF strategy works best when there is high realized variance but no strong trend in the underlying. However, it should be noted that a large directional movement in S can result in losses. This is evident from Figure 3.8, where the portfolio value is negative as long as s is sufficiently far away from 1, at any level of realized variance. In fact, for the double short strategy, the potential loss is unbounded.

3.7.2 β-LETF vs $\beta \times$ ETF

Next, we consider a strategy that is based on the difference between a β-LETF and β multiples of the underlying ETF, for any $|\beta| > 1$. The portfolio involves investing one dollar

in a β-LETF (i.e. $1/L_0$ shares) and simultaneously shorting β dollars of the underlying ETF. Again, we assume $S_0 = 1$ without loss of generality. The resulting portfolio value is

$$\mathcal{E}(S_t, V_t) = S_t^\beta \exp\left(-\left(r\left(\beta-1\right)+f\right)t - \frac{\beta(\beta-1)}{2}V_t\right) - \beta S_t - (1-\beta)e^{rt}, \quad \beta \in \mathbb{R}\backslash[-1,1]. \tag{3.7.3}$$

This is also discussed by Avellaneda and Zhang (2010) who solved for the break-even level of S_t with realized variance V_t held fixed for double LETFs. Here, we study the set

$$\mathcal{S}_\beta = \{(s,v) \in \mathbb{R}_+^2 \,:\, \mathcal{E}(s,v) \geq 0\},$$

where

$$\mathcal{E}(s,v) = s^\beta e^{-(r(\beta-1)+f)t - \frac{\beta(\beta-1)}{2}v} - \beta s - (1-\beta)e^{rt}.$$

In Figure 3.9, we show the region with non-negative portfolio value. In contrast to the short $\pm\beta$-LETFs strategy, the portfolio value here is different for $\beta = 2$ vs $\beta = -2$ (see Figures 3.9(a) and 3.9(c)), or $\beta = 3$ vs $\beta = -3$ (see Figures 3.9(b) and 3.9(d)). For all choices of leverage ratios, this strategy is not profitable when the underlying does not move in either direction. When the realized variance is high, then a larger directional movement is required to break even. Comparing across leverage ratios, the strategy corresponding to $\beta = 2$ generates a larger profitable region for large s and a smaller profitable region for small s, as compared to the case with $\beta = 3$. For inverse LETFs, the strategy with $\beta = -2$ generates a larger profitable region for $s < 1$ but a smaller profitable region for $s > 1$, as compared to the case with $\beta = -3$. Finally, we can reverse the regions simply by taking the opposite position to that in (3.7.3), i.e. shorting the β-LETF and buying the underlying ETF.

3.8 Conclusion

In view of the increasing popularity of ETFs and their leverage counterparts, it is important to better understand and rigorously quantify the risk involved. This paper studies LETFs under various risk measures, and points out the interaction between leverage ratio and investment horizon. Our study offers some guidance on risk control and proper selection of LETFs and associated strategies.

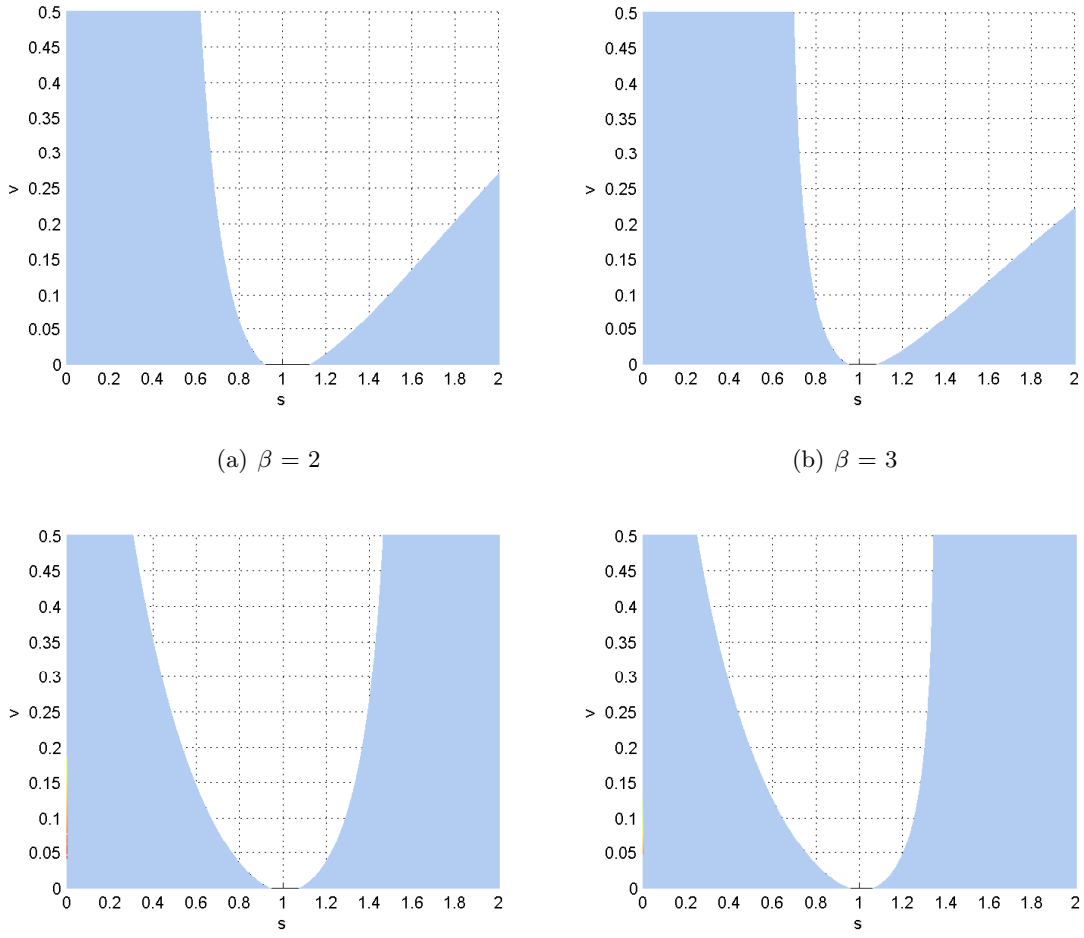

(a) $\beta = 2$ (b) $\beta = 3$

(c) β = -2 (d) β = -3

Figure 3.9: The shaded region indicates where the portfolio value is non-negative. Parameters: $T = 1, r = 1\%$, and $f = 0.95\%$.

There are a number of directions for future research. While the current paper looks at examples of equity ETFs, exchange-traded products are also available for other asset classes such as commodities, volatility, real estate, etc. Furthermore, there are options written on LETFs. Since different LETFs share similar sources of randomness, one major concern is the price consistency of LETF options across different leverage ratios (see Ahn et al. (2013) and Leung and Sircar (2015)). From the investor's perspective, it is also important to consider the optimal timing to buy or sell options on ETFs (see, e.g. Leung and Ludkovski (2011)). Moreover, models that capture the connection between ETFs and the broader financial market would be very useful. Advances in these directions would be important not only for individual and institutional investors, but also for regulators.

Chapter 4

Pricing Options on LETFs

> La mathématique est l'art de donner le même nom à des choses différentes.
>
> *Henri Poincaré*

In this chapter, we study the pricing problem for options written on LETFs and investigate the effects of leverage. We discuss a no-arbitrage valuation methodology that yields consistent prices among LETF options with the same reference index. In Section 4.1, a stochastic volatility pricing model is introduced and the consistent pricing of LETFs options under this framework is discussed. In Section 4.2, we calibrate the model to market data and discuss the empirical findings. In Section 4.3, we incorporate random jumps in the dynamics of the reference index and propose a pricing algorithm based on transform methods that allows for general choices of the jump size distribution. Our algorithm is compared to existing pricing methods through some numerical examples. Finally, further applications, including American-style LETF options and discrete rebalancing, are discussed in Section 4.4.

Since LETF options are relatively new to the market, there is little literature on the valuation of these options. In their theses, Russell (2009) analyzes LETF implied volatilities under the CEV model, and Zhang (2010) provides numerical results for pricing LETF options assuming the reference index follows the Heston model. Ahn et al. (2013) present an approximate pricing method to compute LETF option prices with Heston stochastic volatility along with Gaussian jumps for the underlying. On the other hand, Deng et al.

(2013) discuss the patterns of empirical LETF implied volatilities, and compare with the simulated implied volatilities from the Heston model. Leung et al. (2014) and Leung and Sircar (2015) apply asymptotic techniques to derive an approximation for both the LETF option price and implied volatility under, respectively, the multiscale stochastic volatility and local-stochastic volatility frameworks. They discuss two related concepts of *moneyness scaling* that are useful for implied volatility comparison across leverage ratios.

4.1 Pricing Under Stochastic Volatility

We consider a stochastic volatility model for the reference index S. Under a given risk-neutral pricing measure $\mathbb{Q}$, we assume that S follows the Heston dynamics:

$$\frac{dS_t}{S_t} = r dt + \sigma_t \, dW_t^{\mathbb{Q}}, \tag{4.1.1}$$

$$d\sigma_t^2 = \kappa \left(\vartheta - \sigma_t^2\right) dt + \zeta \sigma_t \, d\hat{W}_t^{\mathbb{Q}}. \tag{4.1.2}$$

Here, $W^{\mathbb{Q}}$ and $\hat{W}^{\mathbb{Q}}$ are two standard $\mathbb{Q}$-Brownian motions with instantaneous correlation ρ, and σ^2 is a Cox-Ingersoll-Ross (CIR) process (Cox et al. (1985)).

The corresponding leveraged ETF is constructed by a constant proportion portfolio strategy with leverage ratio β. Assuming continuous rebalancing, the price process L of the LETF is given by

$$\frac{dL_t}{L_t} = \beta \frac{dS_t}{S_t} + (1-\beta) \, r dt \tag{4.1.3}$$

$$= r dt + |\beta| \sigma_t \, d\tilde{W}_t^{\mathbb{Q}}, \tag{4.1.4}$$

where we have denoted $\tilde{W}^{\mathbb{Q}} := \text{sign}(\beta) W^{\mathbb{Q}}$. From (4.1.4), we observe that the risk-neutral LETF price also satisfies the Heston model, though with different parameters. Precisely, the LETF's stochastic volatility has been scaled, $\sigma_{L,t} \equiv |\beta| \sigma_t$, and follows a re-parametrized CIR dynamics

$$d\sigma_{L,t}^2 = \kappa \left(\beta^2 \vartheta - \sigma_{L,t}^2\right) + |\beta| \zeta \sigma_{L,t} d\hat{W}_t^{\mathbb{Q}}. \tag{4.1.5}$$

This also means that the instantaneous correlation between $\tilde{W}^{\mathbb{Q}}$ and $\hat{W}^{\mathbb{Q}}$ is $\rho_L = \text{sign}(\beta)\rho$. To summarize, if one assigns the reference index to a Heston model with the set of parame-

SV Model	Reference Index Volatility Dynamics	LETF Induced Volatility Dynamics
Heston	$d\sigma_t^2 = \kappa\left(\vartheta - \sigma_t^2\right)dt + \zeta\sigma_t\, d\hat{W}_t^{\mathbb{Q}}$	$d\sigma_{L,t}^2 = \kappa\left(\beta^2\vartheta - \sigma_{L,t}^2\right)dt + \lvert\beta\rvert\zeta\sigma_{L,t}\, d\hat{W}_t^{\mathbb{Q}}$
Stein-Stein	$d\sigma_t = \kappa\left(\vartheta - \sigma_t\right)dt + \zeta\, d\hat{W}_t^{\mathbb{Q}}$	$d\sigma_{L,t} = \kappa\left(\lvert\beta\rvert\vartheta - \sigma_{L,t}\right)dt + \lvert\beta\rvert\zeta\, d\hat{W}_t^{\mathbb{Q}}$
Geometric	$d\sigma_t = \kappa\sigma_t dt + \zeta\sigma_t\, d\hat{W}_t^{\mathbb{Q}}$	$d\sigma_{L,t} = \kappa\sigma_{L,t}dt + \zeta\sigma_{L,t}\, d\hat{W}_t^{\mathbb{Q}}$
3/2	$d\sigma_t^2 = \kappa\left(\sigma_t^2 - \vartheta\sigma_t^4\right)dt + \zeta\sigma_t^3\, d\hat{W}_t^{\mathbb{Q}}$	$d\sigma_{L,t}^2 = \kappa\left(\sigma_{L,t}^2 - \dfrac{\vartheta}{\beta^2}\sigma_{L,t}^4\right)dt + \dfrac{\zeta}{\lvert\beta\rvert}\sigma_{L,t}\, d\hat{W}_t^{\mathbb{Q}}$

Table 4.1: A short list of popular stochastic volatility models and the induced LETF dynamics, where we have defined $\sigma_{L,t} = |\beta|\sigma_t$.

ters $(\sigma_0, \kappa, \theta, \zeta, \rho)$, then the β-leveraged ETF also follows the Heston model with parameters

$$\left(|\beta|\sigma_0, \kappa, \beta^2\theta, |\beta|\zeta, \text{sign}(\beta)\rho\right). \tag{4.1.6}$$

As a result, we see that the leverage ratio effectively magnifies the stochastic variance long-run mean θ by a factor of β^2, and the volatility level σ_0 and the volatility of volatility ζ by a factor of $|\beta|$, though the speed of mean reversion remains the same.

Remark 4.1.1. *More generally, assume that S follows the dynamics*

$$\frac{dS_t}{S_t} = rdt + \sigma_t dW_t^{\mathbb{Q}}, \tag{4.1.7}$$

where the volatility $\{\sigma_t\}_{t\geq 0}$ is a stochastic process. Then, the LETF value follows

$$\frac{dL_t}{L_t} = rdt + \sigma_{L,t}d\tilde{W}_t^{\mathbb{Q}}, \tag{4.1.8}$$

where, as before, $\sigma_{L,t} = |\beta|\sigma_t$. A natural question is whether both S and L belong to the same model but with different parameters. In fact, well known stochastic volatility models such as the Heston, Stein-Stein, Geometric and 3/2 models satisfy this property. In Table 4.1 we summarize the ETF/LETF dynamics for this set of stochastic volatility models. A common feature of these models is that the volatility process does not explicitly depend on S, but is a function of another diffusion process. In contrast, the CEV and SABR models do not satisfy this property and S and L do not belong to the same model (see Leung and Sircar (2015)).

The no-arbitrage price of a European call written on the LETF L with strike K and maturity T is given by the risk-neutral expectation:

$$C\left(L\right) = \mathbb{E}^{\mathbb{Q}}\left\{e^{-rT}\left(L_T - K\right)^+ | L_0 = L, \sigma_0 = \sigma\right\}.$$

Since the LETF follows the Heston model, whose characteristic function is known analytically, it is easy to price European options on leveraged ETFs making use of available transform methods. For example, the methods of Carr and Madan (1999), Lee (2004), and Lord et al. (2008), among others, can be used to price European options. For our computations, we first denote by

$$\Psi_L(\omega) \equiv \mathbb{E}^{\mathbb{Q}} \left\{ e^{i\omega \log \frac{L_T}{L_0}} | \sigma_0 = \sigma \right\}$$

the characteristic function associated with the terminal LETF price. Applying the model parameters according to (4.1.6) Ψ_L reads[1]

$$\begin{aligned} \psi_L(\omega) = & \frac{\kappa\theta}{\zeta^2} \left((\kappa - \rho\beta\zeta\omega i - d)\, t - 2\log\left(\frac{1 - ge^{-dt}}{1-g} \right) \right) \\ & + \frac{\kappa - \rho\beta\zeta\omega i - d}{\zeta^2} \frac{1 - e^{-dt}}{1 - ge^{-dt}} \sigma^2, \end{aligned} \tag{4.1.9}$$

with

$$g = \frac{\kappa - \rho\beta\zeta\omega i - d}{\kappa - \rho\beta\zeta\omega i + d}, \quad \text{and} \quad d = \sqrt{(\kappa - \rho\beta\zeta\omega i)^2 + (\beta\zeta)^2 (\omega i + \omega^2)}.$$

We can then write the option price as

$$C(L) = \int_{-\infty}^{\infty} \left(e^{\log(L) + x} - K \right)^+ f(x) dx = (e^{\cdot} - K)^+ * f(-\cdot)\, (\log(L)),$$

where f denotes the probability distribution function (p.d.f.) of $\log(\frac{L_T}{L_0})$ and $*$ denotes the convolution operator. Denoting with $\mathcal{F}(g(x)) \equiv \int_{\mathbb{R}} e^{-i\omega x} g(x)\, dx$ the Fourier operator acting on the function g, we can then write the price of the European call as

$$C(L) = e^{\gamma \log(L)} \mathcal{F}^{-1} \left(\mathcal{F} \left(e^{-\gamma x} \left(L e^x - K \right)^+ \right) \Psi(\omega - i\gamma) \right), \tag{4.1.10}$$

where the introduction of the dampening factor $e^{-\gamma x}$ is necessary because the payoff is not integrable[2]. We can then apply an FFT algorithm to efficiently calculate the option price according to (4.1.10).

[1] See del Baño Rollin et al. (2009) for a summary of results on the Heston characteristic function.

[2] Notice that, in order for $\Psi(\omega - i\gamma)$ to be well-defined, we must also ensure that $\mathbb{E}^{\mathbb{Q}}\{S^{\gamma}\} < \infty$.

4.2 Model Calibration and Consistency

We now discuss the procedure to calibrate the Heston model to the market prices of unleveraged and leveraged ETF options. As is standard, given a set of market options prices C_i, $i = 1, ..., N$, we obtain the respective implied volatilities (IVs), $\sigma_{IV,i}$, by inverting the Black-Scholes price formula. In essence, our calibration problem involves solving the minimization problem

$$\min_{\Theta} \sum_{i=1}^{N} \omega_i |\sigma_{IV,i} - \hat{\sigma}_{IV,i}|^2 , \tag{4.2.1}$$

where $\hat{\sigma}_{IV,i}$ is the implied volatility computed based on the Heston model option price with parameters $\Theta \equiv \{\sigma_0, \kappa, \vartheta, \zeta, \rho\}$. The weights ω's will be chosen according to the liquidity of the options (see Section 4.2.1 below).

LETF options share the common source of risk due to the same reference index S. Moreover, recall that if the reference index S admits the Heston dynamics, then all the β- LETFs also follow a re-parametrized Heston model according to (4.1.6). This gives rise to the question of whether the parameters obtained from calibrating to one LETF options market are comparable with those from other LETF options markets. In other words, are the Heston model parameters $(\sigma_0, \kappa, \theta, \zeta, \rho)$ stable across leverage ratios? Our calibration results will shed light on this issue.

4.2.1 Data Preparation

Before presenting the calibration results, let us briefly discuss the data preparation and calibration procedures. We obtain the option price data from the OptionMetrics IVY database. To enhance the calibration accuracy and efficiency, we first filter the data as follows:[3]

1. We eliminate the entries with

   - no IV values;
   - bid quotes less than \$0.5;
   - strikes for which only a call or a put is available but not both;

[3]Our filtering criteria are adapted from Figlewski (2010) and Chapter 5.3 of Fouque et al. (2011).

- extreme moneyness, i.e. $M < 0.85$ or $M > 1.15$ for $M := K/S$.

2. Moreover, for each pair of strike and maturity (K, T), we interpolate the IVs of the associated put and call to obtain a unique value. In particular, for any given strike K, denoted by $\sigma_{IV,P}$ and $\sigma_{IV,C}$ respectively for the put and call, we set the final IV value σ_{IV} by convex combination, namely,

$$\sigma_{IV} = w\sigma_{IV,P} + (1-w)\sigma_{IV,C}, \tag{4.2.2}$$

with the assigned weight $w := (1.15S - K)/(0.3S)$. In other words, the parameter w weights the implied volatility of out-of-the-money options more.

In addition, we also weigh the IVs according to the liquidity of the options. Specifically, we choose ω_i to be inversely proportional to the (relative) bid-ask spread,

$$\omega_i = c\frac{b_i + a_i}{2|a_i - b_i|}, \tag{4.2.3}$$

where b_i and a_i denote the bid and ask prices of option i, respectively and where

$$c = \frac{N}{\sum_{i=1}^{N} \frac{b_i+a_i}{2|a_i-b_i|}}$$

is a normalizing constant so that $\sum_{i=1}^{N} \omega_i = N$. As a consequence of our choice, less liquid options will be considered less relevant during the calibration procedure.

In Figure 4.1, we plot the ω weights for the SPY and UPRO ETF options on June 25, 2013. In the top panel we show the weights for each ETF separately, i.e. where the normalizing constant c is calculated for the two set of options. Therefore, the proportionality to the bid-ask spread is valid only between omega values of options on the same ETF and not between options on different ETFs. This picture illustrates the different liquidity across srikes and maturities for each ETF market. As we can see, the weights are higher for options close to the ATM strike for both ETFs, and for shorter maturities as well. In the bottom panel, we calculate the ω weights for the same ETFs but where the normalizing constant is calculated on the union of the two sets. This way, it is possible to compare the liquidity of options on the two ETFs and these weights could be used to calibrate a model on the collection of options on both ETFs. It is not surprising then that the ω weights for UPRO

appear to be much lower than those for SPY due to the presence of wider bid-ask spreads on the less liquid UPRO options. For the same reason then, when calibrating a model on the entire collection of data on both ETFs one might want to use the ω weights showed in the top panel. Otherwise, because of the discrepancy in liquidity, the results would be affected only by the most liquid ETF's data.

4.2.2 Calibration Results

In Figures 4.2 and 4.3 we show the observed, cleaned IVs for the selected ETFs on the S&P 500 index on Tuesday, June 25, 2013. For the SPY ETF, we have the following maturities, listed as calendar days to expiration: 24, 52, 87, 115, 178, 206, 269, 360. For other ETFs (besides SH), we have a subset of these maturity dates. We calibrate the Heston model repetitively by (approximately) solving problem (4.2.1) using options on each different ETF—that is, with different leverage ratios. Notice that for each ETF the ω weights in (4.2.1) are calculated according to (4.2.3) using options on that particular ETF. To price the options we adopt the approach introduced in Section 4.1 and to perform the calibration we adapt a trust-region-reflective gradient-descent algorithm (Coleman and Li (1994); Coleman and Li (1996)), starting from different initial points to guarantee a better exploration of the parameters space. While our numerical tests show the adopted method results in an effective calibration, we remark that there are many alternative, possibly more advanced, calibration procedures available (see e.g. Cont and Tankov (2002) and references therein).

The results of the calibration are reported in Table 4.2 and Figure 4.4. Notice that for each ETF, the Heston model parameters reported in Table 4.2 are with respect to the reference, unleveraged index consistently with the transformation (4.1.6). This way the models are directly comparable to each other. The mean, relative cross-calibration error, $\epsilon_{j,k}$, is calculated separately for each pair of ETFs (denoted by the tuple (j,k)), and is defined as the arithmetic mean of the relative error computed on each option on ETF j when using the calibration parameters obtained for ETF k:

$$\epsilon_{j,k} \equiv \frac{1}{N_j} \sum_{i=1}^{N_j} \frac{|\sigma_{IV,i} - \hat{\sigma}_{IV,i}(\Theta_k)|}{\sigma_{IV,i}}, \tag{4.2.4}$$

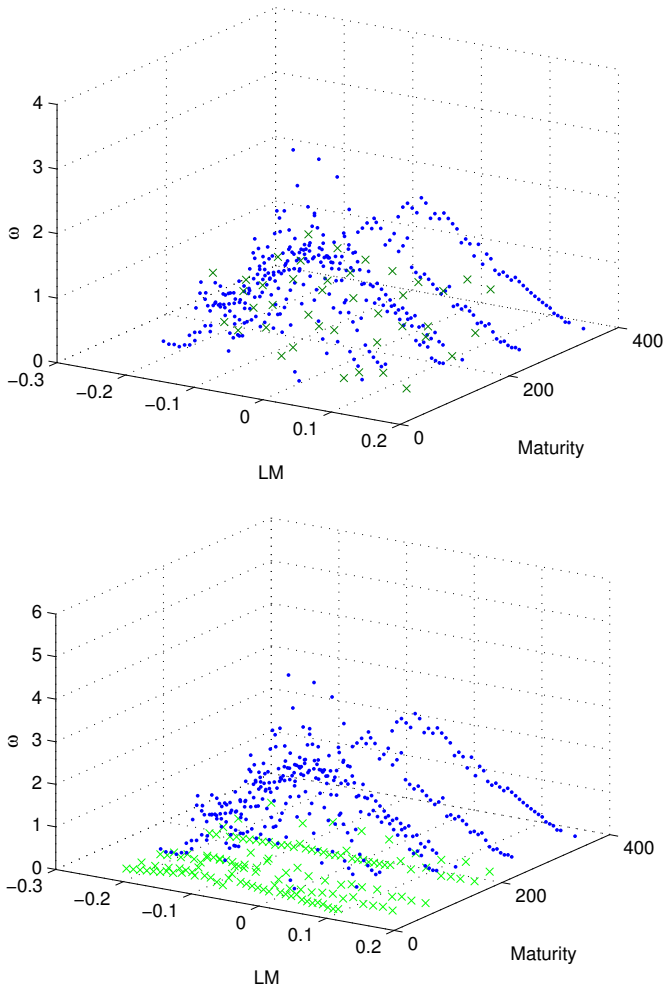

Figure 4.1: The weights, ω, obtained from the bid-ask spreads on the SPY (dots) and UPRO (crosses) options on June 25, 2013. In the top panel the normalizing constant in (4.2.3) is computed for the SPY and URPO ETFs separately. In the bottom panel the normalizing constant is the same, allowing a direct comparison of liquidity between SPY and UPRO options.

ETF	β	σ_0^2	κ	θ	ρ	ζ
SPY	1	0.032	3.1	0.052	-0.75	0.89
SSO	2	0.031	2.2	0.056	-0.77	0.85
UPRO	3	0.031	2.3	0.057	-0.84	0.82
SH	-1	0.033	4.4	0.035	-0.93	0.55
SDS	-2	0.032	8.9	0.036	-0.84	0.93
SPXU	-3	0.033	10	0.033	-0.85	0.85

Table 4.2: Parameters obtained by approximately solving (4.2.1) under the Heston model for each ETF on data obtained for Tuesday, June 25, 2013. See Figures 4.2, 4.3 for the observed IVs.

where the sum is over the N_j options available for ETF_j and where we have denoted with $\hat{\sigma}_{IV,i}(\Theta_k)$ the model IV obtained for option i of ETF j when applying the parameters obtained through calibration for ETF k, Θ_k.

Although the parameters do not exactly match, they are often comparable to each other. In addition, we notice that the greatest error difference is between long and short ETFs, particularly with respect to the parameter κ. For example, as we can see from Figure 4.4, when we calibrate the model using SPY options data, we obtain an error of around 1% on the same SPY options, and of about 2% for the SSO and UPRO ETFs, while the error is around 3.5% and 4% for the SDS and SPXU ETFs, respectively. Overall, we can see that, for each line, the points relative to the long ETFs are closer to each other than to those relative to the short ETFs, and vice versa.

Motivated by the observations above, we then perform two separate calibrations, one on long and one on short ETFs. The results of these calibrations are listed in Table 4.3 and Figures 4.5, 4.7, 4.9. In particular, 4.7, in each plot, we superimpose the calibrated IVs obtained by solving problem (4.2.1) on the long ETFs options on the observed IVs. Similarly, in Figure 4.9 we show those obtained by calibrating on the short ETFs options. Once again, the results show the difference between the two classes of ETFs. A calibration that aims to reduce the error on one class will produce a somewhat higher error on the other. From Figure 4.7 we can observe that the model calibrated on the long ETFs data seem to

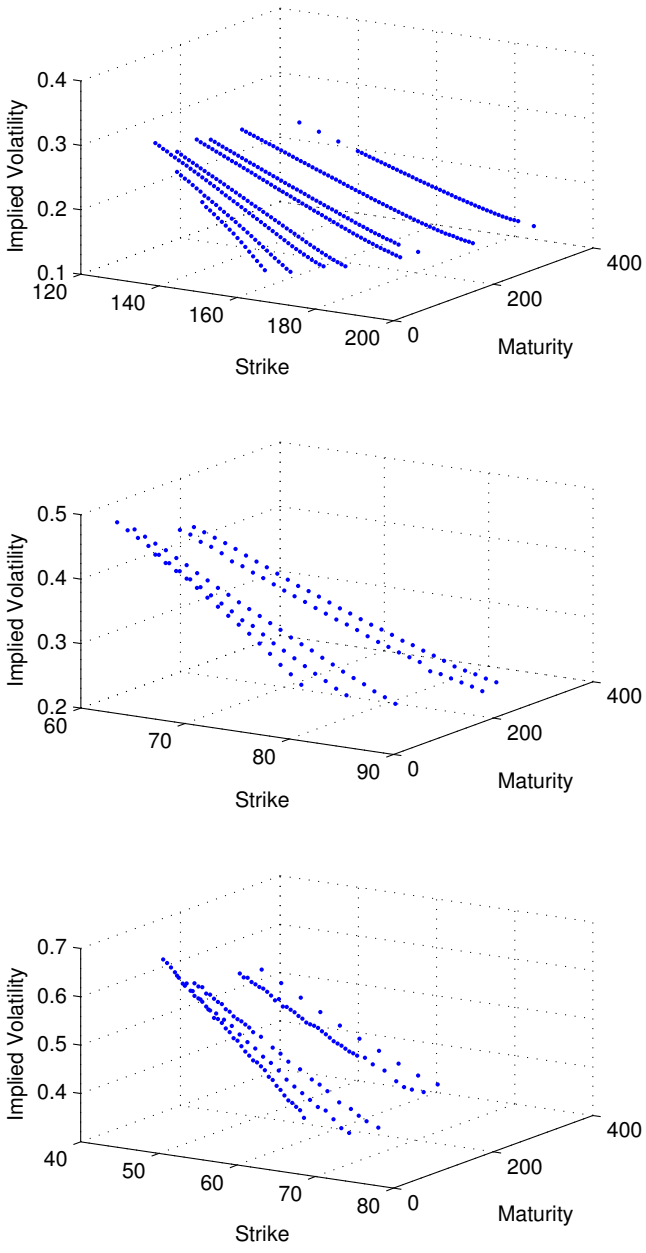

Figure 4.2: The observed, cleaned IVs for the selected ETFs on Tuesday, June 25, 2013. In order, from top to bottom, we have the SPY, SSO and UPRO IV surfaces.

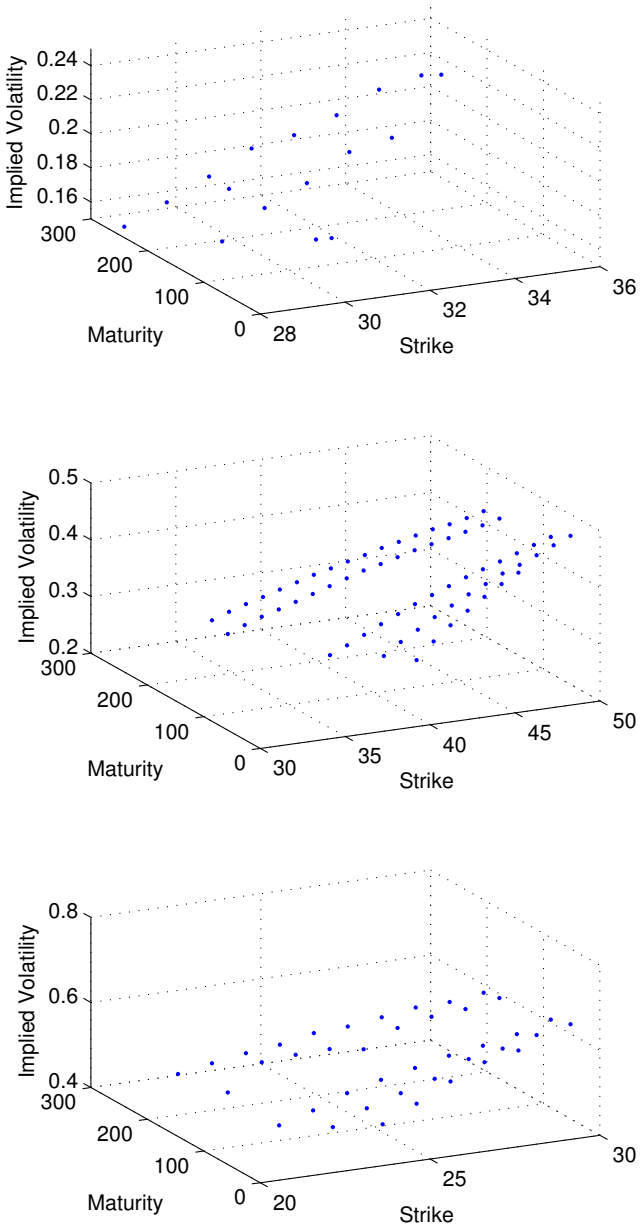

Figure 4.3: The observed, cleaned IVs for the selected ETFs on Tuesday, June 25, 2013. In order, from top to bottom, we have the SH, SDS and SPXU IV surfaces.

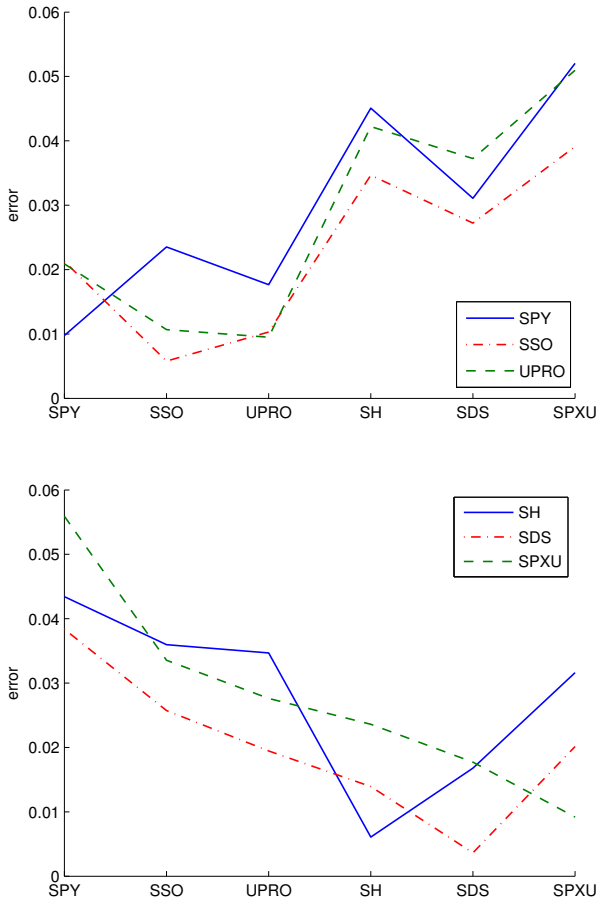

Figure 4.4: The cross calibration errors calculated according to (4.2.4) when the model parameters are as in Table 4.2. The top (bottom) panel reports the cross calibration errors using the parameters obtained for each of the long (short) ETFs.

ETF	σ_0^2	κ	θ	ρ	ζ
Long	0.031	2.7	0.054	-0.79	0.86
Short	0.033	9.5	0.035	-0.79	1.01

Table 4.3: The obtained calibrated parameters when solving (4.2.1) for the aggregate long ($\beta > 0$) and short ($\beta < 0$) LETF IVs on June, 25, 2013. Compare with Table 4.2.

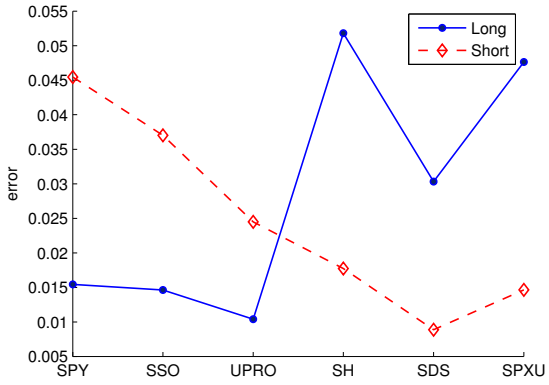

Figure 4.5: The cross calibration errors computed according to (4.2.4) when the model parameters are as in Table 4.3 and the calibration has been performed on aggregate long ($\beta > 0$) and short ($\beta < 0$) ETF option data.

overprice options with positive moneyness on the short ETFs while slightly underpricing those with negative moneyness. Interestingly, the same observation holds when we reverse the role of the long and short ETFs, as exemplified in Figure 4.9.

4.3 Incorporating Jumps with Stochastic Volatility

We now extend the dynamics (4.1.1) by incorporating jumps in the reference index. In particular, we assume that the reference ETF S follows

$$\begin{aligned} \log\frac{S_t}{S_0} &= \mu t + X_t + \sum_{i=1}^{N_t} Z_i, \\ X_t &= \int_0^t \sigma_s dW_s^{\mathbb{Q}} - \int_0^t \frac{\sigma_s^2}{2} ds, \\ d\sigma_s^2 &= \kappa\left(\vartheta - \sigma_s^2\right) ds + \zeta\sigma_s d\hat{W}_s^{\mathbb{Q}}, \end{aligned} \tag{4.3.1}$$

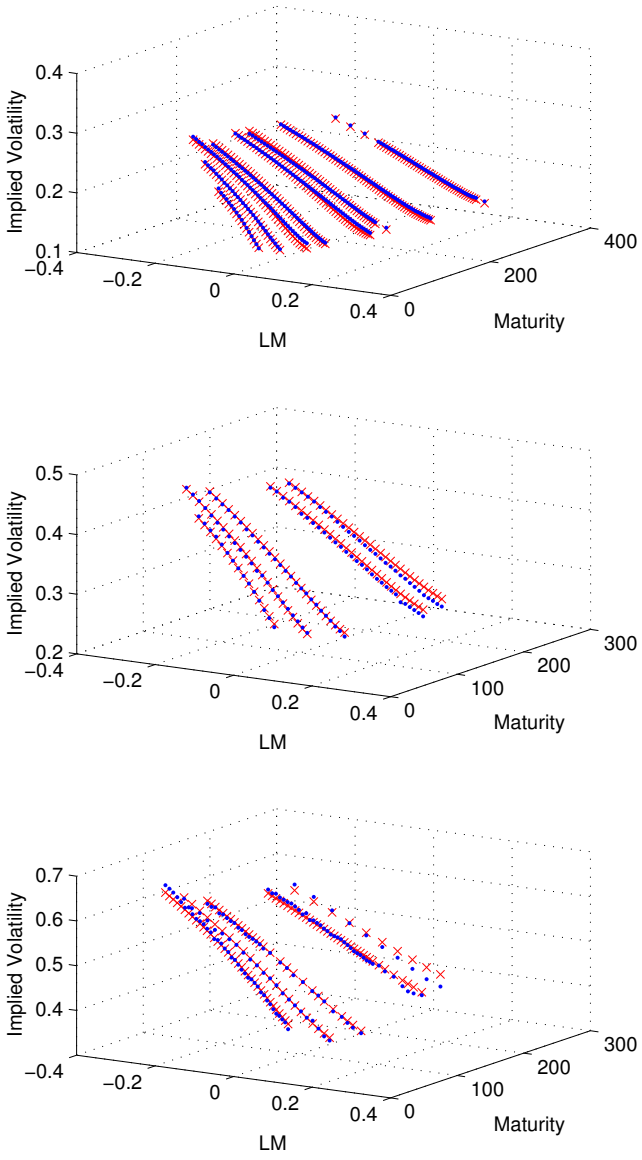

Figure 4.6: The IV surfaces for long ETFs when the model parameters are calibrated on long ETFs options data, see Table 4.3. The dotted points represent observed IVs while the crossed ones represent calibrated IVs.

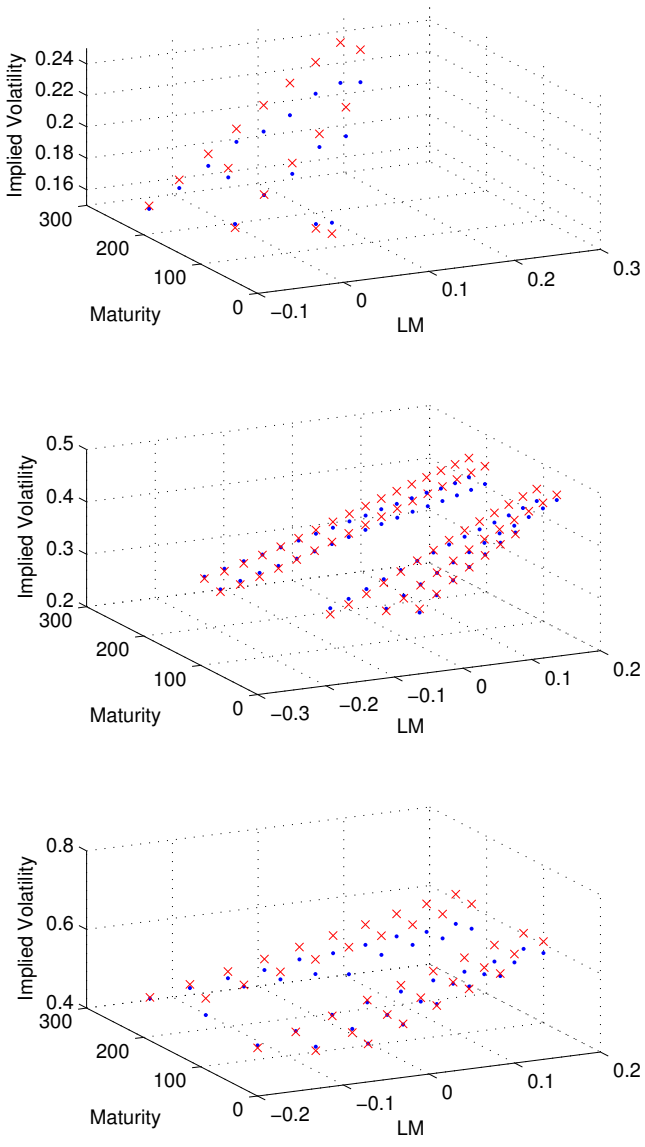

Figure 4.7: The IV surfaces for short ETFs when the model parameters are calibrated on long ETFs options data, see Table 4.3. The dotted points represent observed IVs while the crossed ones represent calibrated IVs.

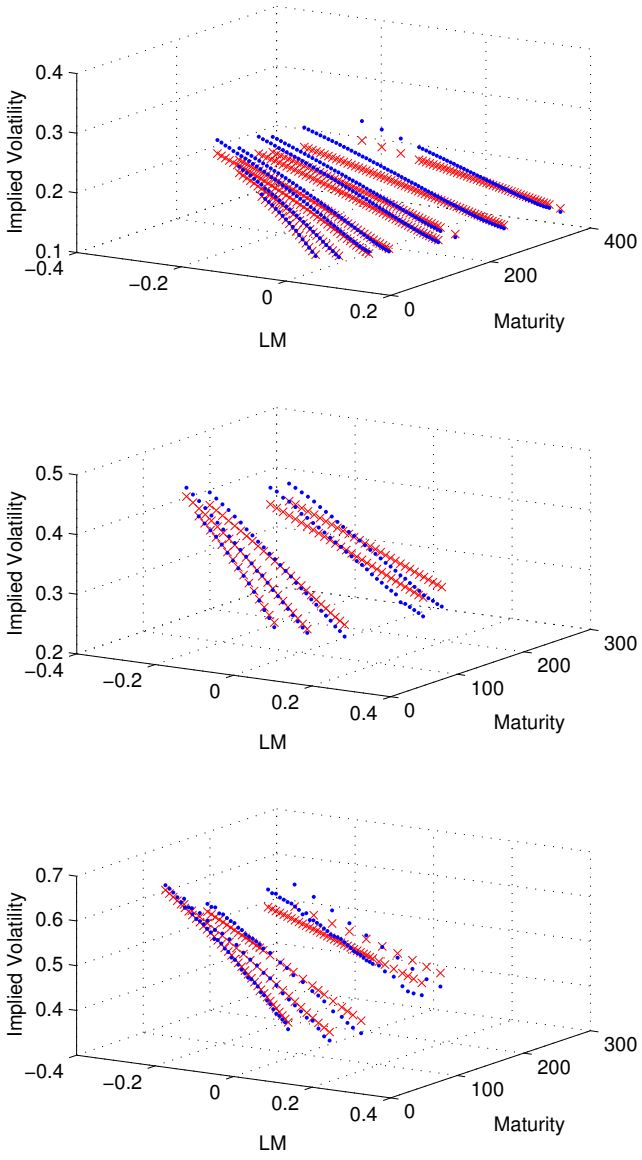

Figure 4.8: The IV surfaces for long ETFs when the model parameters are calibrated on short ETFs options data, see Table 4.3. The dotted points represent observed IVs while the crossed ones represent calibrated IVs.

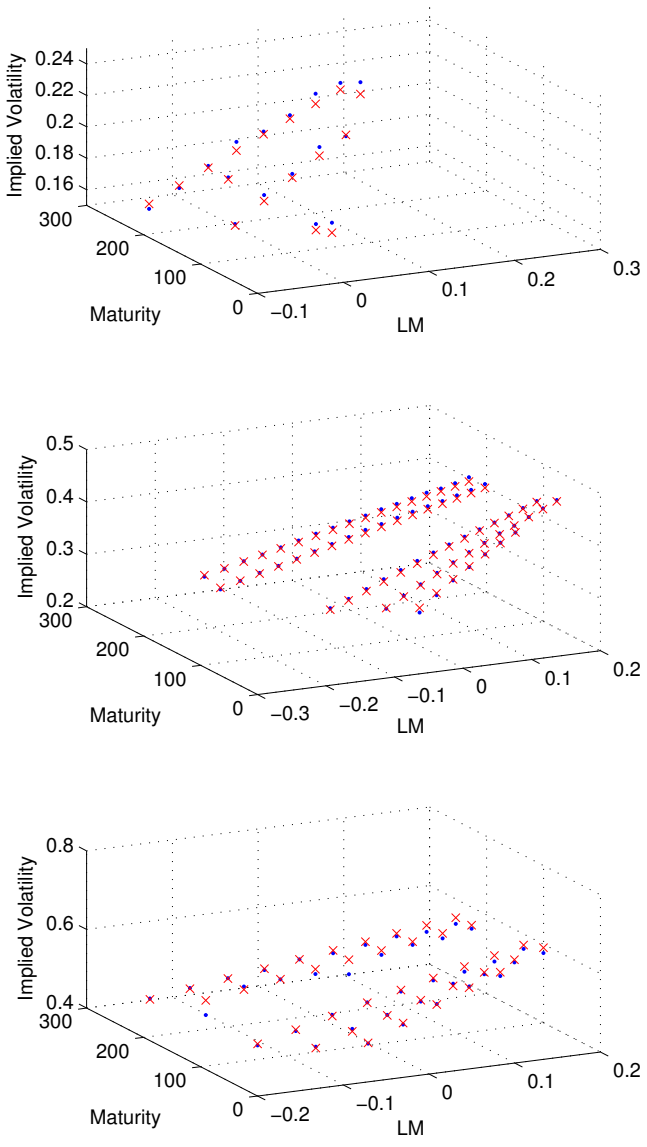

Figure 4.9: The IV surfaces for short ETFs when the model parameters are calibrated on short ETFs options data, see Table 4.3. The dotted points represent observed IVs while the crossed ones represent calibrated IVs.

where $W^{\mathbb{Q}}$, $\hat{W}^{\mathbb{Q}}$ are two $\mathbb{Q}$-Brownian motions with instantaneous correlation $\rho \in (-1, 1)$. N is a Poisson process with intensity λ. The random jump sizes $(Z_i)_{i=1,2,...}$ are independent, identically distributed random variables whose distribution satisfies $\mathbb{E}^{\mathbb{Q}}\left\{e^Z\right\} < \infty$. In addition, N and the jumps $(Z_i)_{i=1,2,...}$ are assumed to be independent of each other and of the processes $W^{\mathbb{Q}}$ and $\hat{W}^{\mathbb{Q}}$. Finally, we set $\mu = rt - \lambda mt$, where $m \equiv \mathbb{E}^{\mathbb{Q}}\left\{e^Z - 1\right\}$, so that the reference price $e^{-rt}S$ is a $\mathbb{Q}$-martingale. The stochastic volatility jump-diffusion model is related to those in the literature, including the SVJ (Bates (1996)), Merton (1976), Kou (2002), Variance Gamma (Madan and Unal (1998)) and CGMY (Carr et al. (2002)) models.

Recall that the LETF is designed to yield a multiple of the daily returns of the underlying. In principle, it is possible for the fund to experience a loss greater than 100%. However, protected by the principle of limited liability, the LETF value can never be negative. In practice, some LETF providers design the fund so that the daily returns are capped both downward and upward[4]. If we assume a continuous rebalancing frequency and LETF returns capped from below and above at the levels l and h, respectively, then the dynamics of L read:

$$L_t = L_0 e^{\left(\mu_L t + X_{L,t}\right)} \prod_{i=1}^{N_t} \left(1 + Y_{L,i}\right), \tag{4.3.2}$$

$$X_{L,t} = \int_0^t \beta \sigma_s dW_s^{\mathbb{Q}} - \int_0^t \frac{\beta^2 \sigma_s^2}{2} ds,$$

$$Y_{L,i} \equiv \min\left\{\max\left\{\beta\left(e^{Z_i} - 1\right), l\right\}, h\right\}, \tag{4.3.3}$$

[4]For example, according to the summary prospectus of the Direxion Daily S&P 500 Bull 3x Shares: "Gain Limitation Risk: If the Funds underlying index moves more than 33% on a given trading day in a direction adverse to the Fund, you would lose all of your money. Rafferty will attempt to position the Funds portfolio to ensure that the Fund does not lose more than 90% of its NAV on a given day. The cost of such downside protection will be limitations on the Funds gains. As a consequence, the Funds portfolio may not be responsive to Index gains beyond 30% in a given day. For example, if the Index were to gain 35%, the Fund might be limited to a daily gain of 90% rather than 105%, which is 300% of the Index gain of 35%." This suggests a two-sided cap on the jump sizes. Source: http://www.direxioninvestments.com/products/direxion-daily-sp-500-bull-3x-etf.

with $l \geq -1$, $h \in [0, +\infty]$, and where

$$\mu_L \equiv r - \lambda m_L, \tag{4.3.4}$$

$$m_L \equiv \mathbb{E}^{\mathbb{Q}}\{Y_L\}. \tag{4.3.5}$$

As in Section 4.1, the continuous part, $e^{X_{L,t}}$ follows a Heston process with stochastic volatility $\sigma_{L,t} \equiv |\beta|\sigma_t$ (see equation (4.1.5)). On the other hand, the jump distribution of $e^Z - 1$ will generally differ from that of Y_L. This might thus introduce another layer of complexity in the pricing of options written on L.

4.3.1 Pricing via the Characteristic Function

Again, we are interested in pricing the European call option given by the risk-neutral expectation

$$C(L) = \mathbb{E}^{\mathbb{Q}}\left\{e^{-rT}(L_T - K)^+ | L_0 = L, \sigma_0 = \sigma\right\}.$$

In order to use the results of Section 4.1 and formula (4.1.10) to price the option, we need to calculate $\Psi_L(\omega) \equiv \mathbb{E}^{\mathbb{Q}}\left\{e^{i\omega \log \frac{L_T}{L_0}} | \sigma_0 = \sigma\right\}$. However, $\log(L_T)$ is not well-defined in this case because the price L_T can actually reach zero with positive probability. To overcome this, we write

$$C(L) = p\mathbb{E}^{\mathbb{Q}}\left\{e^{-rT}(L_T - K)^+ | L_T > 0, L_0 = L, \sigma_0 = \sigma\right\}, \tag{4.3.6}$$

where

$$p \equiv \mathbb{Q}\{L_T > 0 | L_0 = L\} = e^{-\lambda T \mathbb{Q}\{Y_L \leq -1\}}. \tag{4.3.7}$$

As a result, we can price the call option using (4.1.10) if we are able to obtain $\tilde{\Psi}_L(\omega) \equiv \mathbb{E}^{\mathbb{Q}}\left\{e^{i\omega \log \frac{L_T}{L_0}} | L_T > 0, \sigma_0 = \sigma\right\}$. Notice that, in order to use the Fourier transform method (4.1.10), we also need to verify that $\mathbb{E}\{\log(L_T) | L_T > 0\} < \infty$. We analyze the validity of this condition at the end of this section.

Next, we show how to compute $\tilde{\Psi}_L$. We start by observing that the characteristic function of $\log \frac{S_T}{S_0}$ reads

$$\mathbb{E}^{\mathbb{Q}}\left\{e^{i\omega \log \frac{S_T}{S_0}} | \sigma_0 = \sigma\right\} = e^{i\omega\mu T + \psi_X(\omega) + \lambda T\left(e^{\psi_Z(\omega)} - 1\right)}, \tag{4.3.8}$$

where $\psi_X(\omega) \equiv \log\mathbb{E}^{\mathbb{Q}}\left\{e^{i\omega X_T}|\sigma_0 = \sigma\right\}$ and $\psi_Z(\omega) \equiv \log\mathbb{E}^{\mathbb{Q}}\left\{e^{i\omega Z}\right\}$. In particular, $\psi_X(\omega)$ is the characteristic exponent of the Heston model, see equation (4.1.9). On the other hand, the characteristic exponent of Z depends on the particular choice of the jump distribution. For example, when Z is distributed as a double-exponential random variable, $Z \sim DE(u, \eta_1, \eta_2)$, the characteristic exponent will read $\psi_Z(\omega) = u\frac{\eta_1}{\eta_1 - i\omega} + (1-u)\frac{\eta_2}{\eta_2 + i\omega}$.

To continue, notice that $\{L_T > 0\} = \{Y_{L,i} > -1\ , i = 1, ..., N_T\}$. Therefore, we can write

$$\tilde{\Psi}_L(\omega) = \mathbb{E}^{\mathbb{Q}}\left\{e^{i\omega\left(\mu_L T + X_{L,T} + \sum_{i=1}^{N_T} Z_{L,i}\right)}|L_T > 0, L_0 = L, \sigma_0 = \sigma\right\}, \tag{4.3.9}$$

where

$$Z_{L,i} \equiv \begin{cases} \log\left(1 + Y_{L,i}\right), & Y_{L,i} > -1, \\ 0, & Y_{L,i} = -1. \end{cases} \tag{4.3.10}$$

Therefore, $\tilde{\Psi}_L$ reads

$$\tilde{\Psi}_L\left(\omega\right) = e^{i\omega\mu_L T + \psi_{X_L}(\omega) + \lambda T\left(e^{\psi_{Z_L}(\omega)} - 1\right)}, \tag{4.3.11}$$

where $\psi_{X_L}(\omega) \equiv \log\mathbb{E}^{\mathbb{Q}}\left\{e^{i\omega X_{L,T}}|\sigma_0 = \sigma\right\}$ and $\psi_{Z_L}(\omega) \equiv \log\mathbb{E}^{\mathbb{Q}}\left\{e^{i\omega Z_L}|Y_{L,i} > -1\right\}$. We derived the analytic expression for $\psi_{X_L}(\omega)$ in Section 4.1, see equation (4.1.9). However, an explicit expression for ψ_{Z_L} is not easily obtained. Ahn et al. (2013), who use a different transform method, analyze the special case when Z is Gaussian and circumvent the aforesaid issue by finding an analytic, approximate expression for ψ_{Z_L}. In contrast, because of the choice of the pricing formula (4.1.10), we are able to calculate the values of ψ_{Z_L} numerically as shown below, introducing no approximation error and providing a method that can be used for virtually any distribution of the jump Z.

Recall that Z_L is a function of Z, see (4.3.10) and (4.3.2). Therefore, if the p.d.f. of Z is known, we can easily obtain the analytic expression for the p.d.f. of Z_L. The desired values of the characteristic function $e^{\psi_{Z_L}}$ can then be easily computed via an FFT algorithm and plugged into (4.3.11) in order to obtain Ψ_L and price the option according to (4.1.10). If the p.d.f. of Z is not available but its characteristic function is, one further step can be added in order to first obtain the p.d.f. from its c.f. via FFT. Importantly, in this case, because of the transformation (4.3.3) we would need to make use of a non-uniform FFT algorithm. The numerical results for this method are presented in the next section.

Finally, we need to prove that, given $L_T > 0$, $\log(L_T)$ is L_1-integrable. We showed with (4.3.11) that $\tilde{\Psi}_L$ can be obtained from the characteristic functions of X_L and Z_L. The results on the the log-spot under the Heston model are well known (see, for example, del Baño Rollin et al. (2009)) and we do not discuss them. On the other hand, under the assumption that Z is integrable, we show that Z_L is integrable, too. For simplicity, we assume that Z admits the p.d.f. $f_Z(x)$, and that the returns of the leveraged ETF L are not capped, i.e. $l = -1$ and $h = \infty$. Given $Y_{L,i} > -1$, we can then write $Z_L = \log\left(\beta\left(e^{Z_i} - 1\right) + 1\right)$. As a result, the p.d.f. of $Z_L | Y_{L,i} > -1$ can be written as

$$f_{Z_{L|Y_{L,i}>-1}}(x) = c\frac{\text{sign}(\beta)e^x}{e^x + \beta - 1} f_Z\left(g^{-1}(x)\right), \tag{4.3.12}$$

with

$$x \in \mathbb{R} \text{ if } \beta > 0, -\infty < x < \log(1-\beta) \text{ if } \beta < 0,$$

and where $g(x) \equiv \log(\beta(e^x - 1) + 1)$ and $g^{-1}(x) = \log\left(\frac{e^x + \beta - 1}{\beta}\right)$. c is a normalizing constant. Therefore, we see that for very small values of x,

$$f_{Z_L}(x) \approx c\frac{\text{sign}(\beta)e^x}{\beta - 1} f_Z\left(\log(\frac{\beta - 1}{\beta})\right) \quad , \quad x \ll 0, \tag{4.3.13}$$

while, for very big values of x (which is possible only when $\beta > 0$),

$$f_{Z_L}(x) \approx c f_Z(x - \log\beta) \quad , \quad x \gg 0. \tag{4.3.14}$$

Therefore, the integrability of Z is sufficient to guarantee the integrability of Z_L.

β	M_S	M_L	SV				SVJ				error	
			FT_{AHJ}	MC_{AHJ}	FT_{LS}	MC_{LS}	FT_{AHJ}	MC_{AHJ}	FT_{LS}	MC_{LS}	FT_{AHJ}	FT_{LS}
1	0.9	0.9	33.66	33.66	33.66	33.66	33.66	33.66	33.66	33.66	0.00	0.00
1	1	1	20.10	20.1	20.10	20.10	20.05	20.05	20.05	20.05	0.00	0.00
1	1.1	1.1	11.23	11.23	11.23	11.23	11.22	11.23	11.22	11.22	0.00	0.00
2	0.75	0.5	60.66	60.74	60.66	60.66	61.41	61.51	61.44	61.44	-0.03	0.00
2	1	1	37.78	37.87	37.78	37.78	38.41	38.43	38.37	38.37	0.04	0.00
2	1.25	1.5	24.11	24.18	24.11	24.11	24.52	24.45	24.41	24.41	0.11	0.00
3	0.75	0.25	81.82	81.98	81.82	81.82	83.08	83.25	83.07	83.07	0.01	0.00
3	1	1	52.77	53.09	52.77	52.77	53.98	54.07	53.87	53.87	0.11	0.00
3	1.25	1.75	37.30	37.6	37.30	37.30	37.91	37.84	37.69	37.69	0.22	0.00
-1	0.75	1.25	14.14	14.15	14.14	14.14	13.87	13.93	13.90	13.90	-0.03	0.00
-1	1	1	21.15	21.19	21.15	21.15	21.03	21.16	21.10	21.10	-0.07	0.00
-1	1.25	0.75	32.73	32.79	32.72	32.72	33.01	33.24	33.16	33.16	-0.15	0.00
-2	0.75	1.5	31.88	32.09	31.88	31.88	30.92	31.29	31.01	31.02	-0.10	-0.01
-2	1	1	41.68	41.95	41.68	41.68	41.13	41.6	41.26	41.27	-0.14	-0.01
-2	1.25	0.5	60.02	60.25	60.02	60.02	60.56	61.09	60.76	60.77	-0.21	-0.01
-3	0.75	1.75	50.72	51.48	50.72	50.72	48.47	49.43	48.46	48.74	-0.27	-0.28
-3	1	1	60.17	60.88	60.17	60.17	58.57	59.56	58.59	58.87	-0.30	-0.28
-3	1.25	0.25	81.46	81.74	81.46	81.46	81.82	82.59	81.89	82.17	-0.35	-0.29

Table 4.4: LETF option prices calculated according to model (4.3.2) with a Gaussian jump, $Z \sim N(\mu_Z, \sigma_Z)$. Our prices are calculated according to a simple Euler MC scheme (MC_{LS}) and the Fourier transform (FT_{LS}) method presented in Section 4.1. For comparison, the prices from Ahn et al. (2013) (pg.18) are also reported. The errors are calculated as the difference between the respective Fourier transform prices and our MC prices. Parameters: $r = .01, \kappa = .65, \zeta = .7895, \theta = .3969, \sigma_0^2 = .3969, \rho = .7571, \lambda = 2.1895, \mu = .0105, \sigma_Z = .2791$.

4.3.2 Numerical Results

In Table 4.4, we present LETF option prices computed via formula (4.1.10) and via a standard Monte Carlo algorithm with an Euler scheme applied to the SVJ process. For comparison, in the same table, we also report the prices[5] obtained by Ahn et al. (2013)(AHJ) for the same case and we discuss the differences below.

As we can observe from Table 4.4, the error between our prices obtained via formula (4.1.10) and via the Monte Carlo method are in good agreement. Beside the case of negatively leveraged ETF, the error is virtually zero. On the other hand, we notice that AHJ prices, which are also calculated via a transform and Monte Carlo method, differ from ours. We stand to explain the differences as follows:

- In their Monte Carlo implementation, AHJ opt to simulate a process where the LETF is rebalanced daily while the dynamics and transform method adopted assume continuous rebalancing.

- In their Fourier transform implementation, AHJ approximate the analytic form of the c.f. Ψ_L and use this when applying the Carr and Madan (1999) algorithm to obtain prices. Instead, we opt to calculate the c.f. of Ψ_L numerically, without introducing further approximations, and easily deploy it thank to the use of a different formula for pricing, based on the transform of a convolution, namely expression (4.1.10).

In Table 4.4, the pricing errors from both methods are very small and therefore negligible for practical applications. Nevertheless, our method has some advantages because 1) it does not introduce any approximation and is in principle more accurate, with the only error in pricing being attributed to the discretization of the Fourier integral; and 2) it is more general because it can accommodate a variety of models and jump distributions for the underlying.

Next, we discuss other features of the model (4.3.2) by analyzing numerical results obtained through the implementation of (4.3.11). In Figure 4.10, we show the IV surfaces for a particular instance of the SVJ model when $\rho \neq 0$. It is evident that, in this model, prices for long and short LETFs with the same absolute leverage ratio are not equal. In

[5]See pages 14-18 of their paper.

contrast, under the BS framework with continuous rebalancing, prices of similar options on LETFs with opposite leverage ratios are equal. This is a result of the fact that the LETFs dynamics under BS admit marginal distributions that are symmetric in the leverage parameter β. However, this property does not hold for many other models. In particular, under the Heston model, marginals are not symmetric because the parameter ρ_L satisfies $\rho_L(\beta) = -\rho_L(-\beta)$. In fact, all other model parameters are symmetric in β and prices are symmetric when $\rho = \rho_L = 0$. In particular, this means that, while for a long LETF out-of-the-money (OTM) puts have higher IV than OTM calls, for a short LETF the contrary is true. This is rather intuitive if one thinks that an OTM put on a long LETF is a bet on the price of the underlying going downward, similarly to the bet expressed by an OTM call on the short LETF.

Figure 4.11 illustrates how the IV smiles are affected by the choice of different caps and floors for the LETF returns. In both the left and right plots, we observe that prices are monotonically increasing with the absolute value of the threshold l or h. This is somewhat intuitive if one realizes that capping returns lowers the variance of the stock price which, altogether with the requirement that the stock price be a martingale, reduces the averaged payoff or option price.

Finally, in Figure 4.12 we show the jump distribution Z_L under the SVJ model for different values of β and σ when $l = -1$ and $h = \infty$. We notice that the leveraged ETFs seem to have a fatter left tail and a thinner right one, when compared to the non-leveraged underlying. We can quantify this observation by recalling the form of the p.d.f. of Z_L obtained in (4.3.12). As shown in (4.3.13), the left tail follows that of an exponential random variable. Therefore, for example when Z is Gaussian, the left tail of Z_L is significantly fatter, see Figure 4.12. Furthermore, even if the left tail is truncated, when $l > -1$, one might still observe, as seen in Figure 4.12, that the likelihood of "extreme" (for practical applications) negative values for Z_L is significantly higher than that of Z. On the other hand, when $\beta > 0$ and $h = \infty$, the right tail is not truncated and we have the asymptotic (4.3.14). Therefore, the right tail follows the same functional form as that of Z, when it is not truncated. Nevertheless, as it appears in Figure 4.12, because of the form of (4.3.12) the likelihood of "extreme" positive values for Z_L might be significantly lower than that of Z.

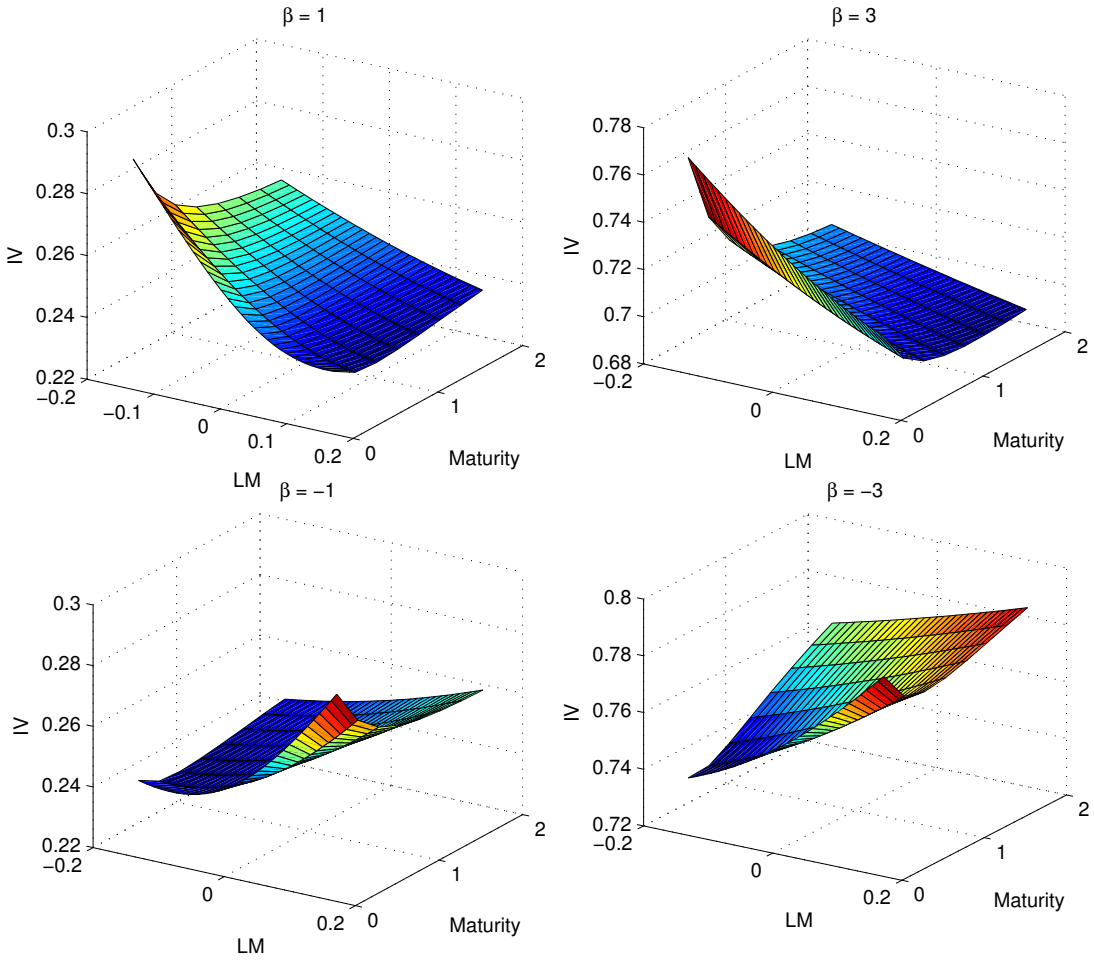

Figure 4.10: The IV surfaces against log-moneyness (LM) and maturity under the SVJ model and for different values of β. Parameters: $r = .02, \sigma_0^2 = .05\kappa = 2, \vartheta = .05, \rho = -.45, \zeta = .8, \lambda = 20, \mu = 0, \sigma = .03$).

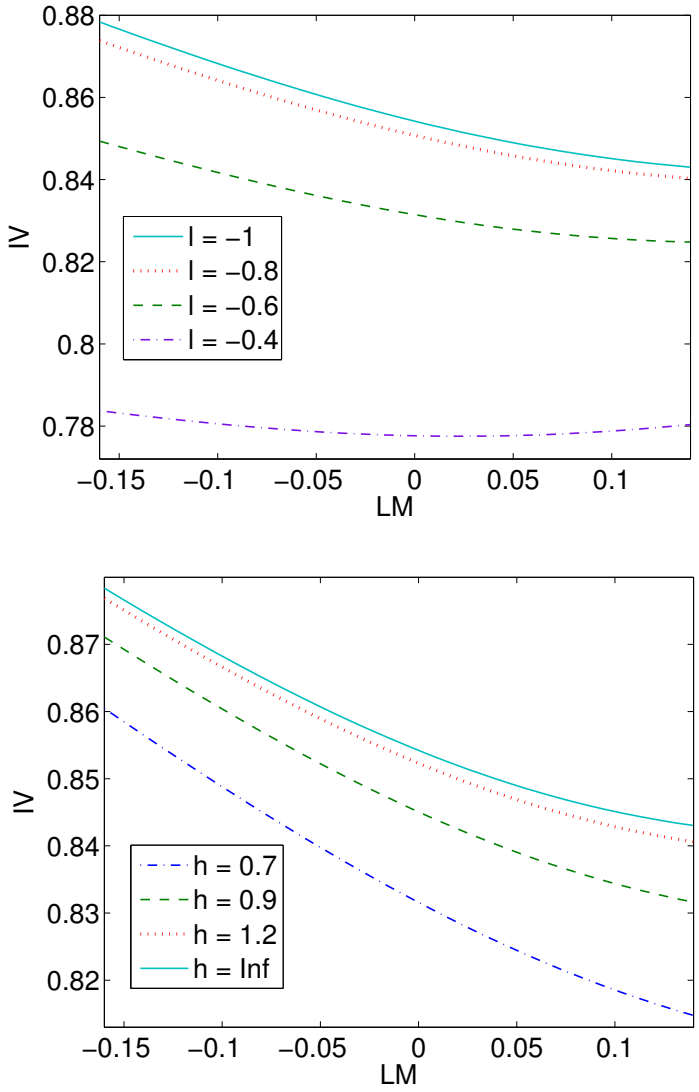

Figure 4.11: The IVs for a 3x leveraged ETF as the floor (l, top) and cap (h, bottom) thresholds vary. Model parameters: $r = .02, \sigma_0^2 = .011, \kappa = 2, \vartheta = .04, \rho = -.53, \zeta = .515, \lambda = 4, \mu = 0, \sigma = .13$).

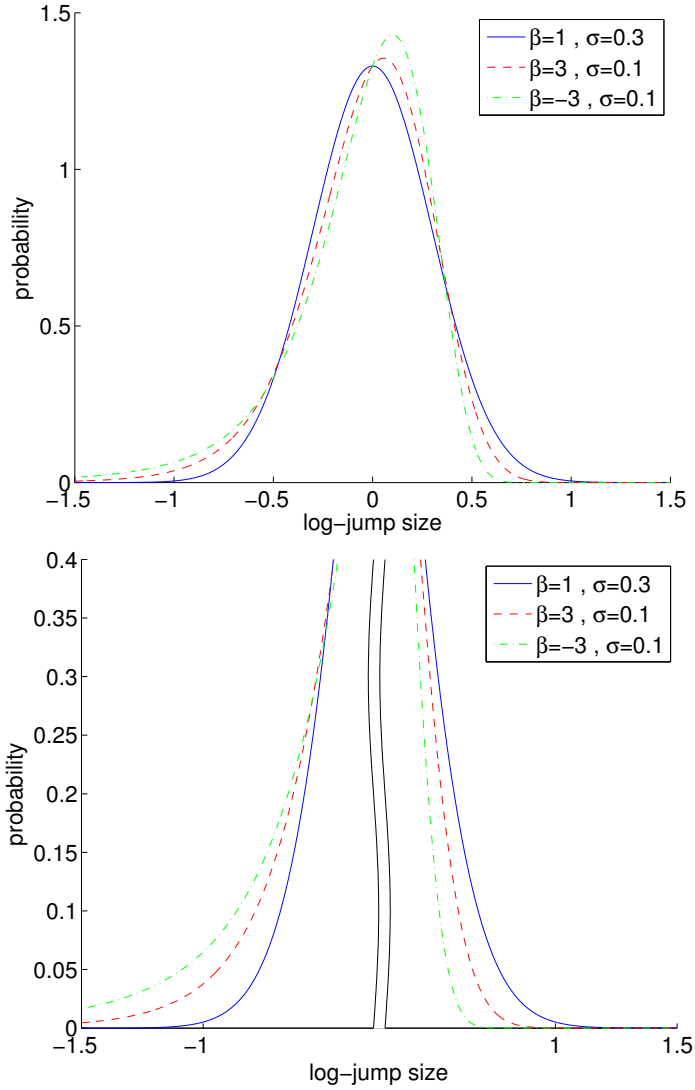

Figure 4.12: The reference and leveraged jump distributions (top) and their tails (bottom) when Z is Gaussian, with $\mu = 0$, and for different values of β and σ.

4.4 Other Applications

4.4.1 American Option Price and Exercising Boundary

While index options are typically of the European style, most LETF options are American-style. In general, the American option pricing problem does not admit closed-form formulas, so we discuss a numerical method for computing the option price and exercise boundary.

Assuming that the underlying follows the dynamics (4.3.2), the value of the American put option is defined by

$$A\left(L;\sigma\right)=\sup_{0\leq\tau\leq T}\mathbb{E}^{\mathbb{Q}}\left\{e^{-r\tau}\left(K-L_{\tau}\right)^{+}|L_{0}=L,\sigma_{0}=\sigma\right\}, \tag{4.4.1}$$

where τ is a stopping time w.r.t. the filtration generated by (L,σ). In order to approximate the American option price, we set a dynamic program for the Bermudan put option with exercise time τ_i, $i=1,...,D$. The price of the Bermudan option at time τ_i, say $B_i(L,\sigma)$ is equal to

$$B_{i}(L;\sigma)=\max\left\{\mathbb{E}^{\mathbb{Q}}\left\{e^{-r\delta\tau_{i+1}}B_{i+1}(L_{\tau_{i+1}};\sigma)|L_{\tau_{i}}=L\right\},\left(K-L\right)^{+}\right\}, \tag{4.4.2}$$

where $\delta\tau_{i+1}=\tau_{i+1}-\tau_i$. Then, if the p.d.f. of $L_{\tau_{i+1}}|L_{\tau_i}$ (or its Fourier transform) is easy to obtain, we can use a pricing methodology similar to that applied in Section 4.3.1. This is the case for the Black-Scholes, Merton and Kou dynamics as well as for the more general class of Lévy processes. On the other hand, the implementation for stochastic volatility models like Heston is computationally challenging (see, for example, Fang and Oosterlee (2011)).

To proceed, we thus assume that the underlying follows the dynamics 4.3.2 with a constant volatility σ. Recall that $\log\left(L_t\right)$ is not well defined, because the LETF price L_t can hit zero when $l=-1$. In order to use a Fourier transform method, we need to consider this outcome at each step, extending the approach taken in Section 4.3 for the European option. We start by writing

$$\begin{aligned}B_{i}\left(L\right)=&\max\Big\{e^{-r\delta\tau_{i+1}}\Big(p_{i}\mathbb{E}^{\mathbb{Q}}\left\{B_{i+1}(L_{\tau_{i+1}})|L_{\tau_{i+1}}>0,L_{\tau_{i}}=L\right\}\\&+(1-p_{i})B_{i+1}(0)\Big),\left(K-L\right)^{+}\Big\},\end{aligned} \tag{4.4.3}$$

where

$$p_i \equiv \mathbb{Q}\left\{L_{\tau_{i+1}} > 0 | L_{\tau_i} = L\right\} = e^{-\lambda\delta\tau_{i+1}\mathbb{Q}\{Y_L \leq -1\}},$$

and where we have dropped the parameter σ which is now constant. Adopting a notation analogous to Section 4.3 (compare with (4.3.11)),

$$\tilde{\Psi}_{L,i}(\omega) \equiv \mathbb{E}^{\mathbb{Q}}\left\{e^{i\omega\log\frac{L_{\tau_{i+1}}}{L_{\tau_i}}} | L_{\tau_{i+1}} > 0\right\} = e^{\delta\tau_{i+1}\left(i\omega\mu_L + \frac{\sigma^2\omega^2}{2} + \lambda\left(e^{\psi Z_L(\omega)} - 1\right)\right)}. \tag{4.4.4}$$

We can then write:

$$\begin{aligned} B_i(L) = \max\Big\{ & e^{-r\delta\tau_{i+1}}\left(p_i\mathcal{F}^{-1}\left(\mathcal{F}\left(e^{\gamma(L-x)}B_{i+1}(Le^x)\right)(\omega)\tilde{\Psi}_{L,i}(\omega - i\gamma)\right)\right. \\ & \left. + (1-p_i)B_{i+1}(0)\right), (K-L)^+ \Big\}. \end{aligned} \tag{4.4.5}$$

In Figure 4.13, we show the exercise boundary for an American put option under the Merton model. The boundary appears monotonically increasing in time and it is lower for higher (absolute) leverage ratios. Like in the case of the Heston model, the prices for the options with opposite leverage ratio are not identical. In this case, the discrepancy is due to the asymmetry of the distribution of $e^{Z_L} - 1 = \min\left\{\max\left\{\beta\left(e^Z - 1\right), l\right\}, h\right\}$ with respect to the parameter β. In Figure 4.14, we also plot the IV smile calculated inverting the BS formula for an American put under the same model and observe a similar behavior. For instance, the deep in-the-money put option on the 2x LETF appears more expensive than that put on the -2x LETF.

4.4.2 Discrete Rebalancing

Although we obtained the LETF dynamics (4.3.2) assuming continuous rebalancing, in practice the rebalancing period often is one trading day. We want to investigate how the rebalancing frequency affects option prices. Let δ be the length of the rebalancing period and let $t_i \equiv i\delta$, $i = 0, ..., M$, $t_{M+1} \equiv t$, where $M \equiv \sup\{n \in \mathbb{N} : n\delta < t\}$. Then the LETF

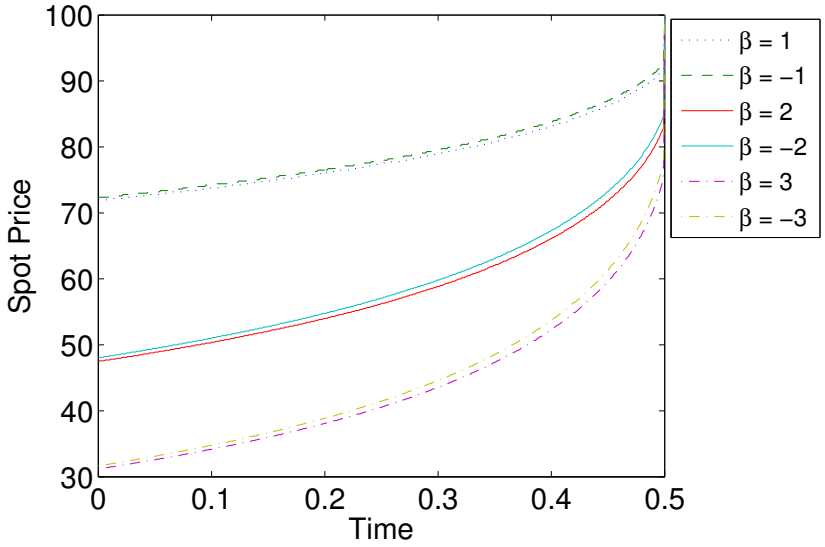

Figure 4.13: The exercise boundary for an American put option under the Merton model calculated according to (4.4.5) with parameters: $K = 100, r = .02, \sigma = .15, \lambda = 20, a = 0, b = .05$.

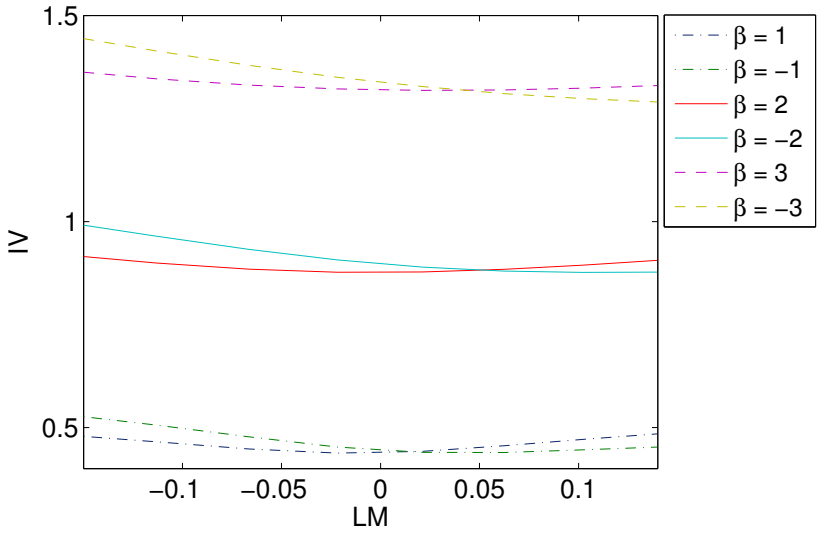

Figure 4.14: The IV for an American option under the Merton model calculated according to (4.4.5) with parameters: $S = 100, r = .02, T = .5, \sigma = .15, \lambda = 20, a = 0, b = .05$.

dynamics at time t read

$$\begin{aligned}\frac{L_t}{L_0} &= c\prod_{i=1}^{M+1}\min\left\{\max\left\{\beta\frac{S_{t_i}}{S_{t_{i-1}}}-(1-\beta)\,e^{r(t_i-t_{i-1})},1+l\right\},1+h\right\}\\ &= c\prod_{i=1}^{M+1}\min\left\{\max\left\{\beta e^{\mu(t_i-t_{i-1})+(X_{t_i}-X_{t_{i-1}})+\left(\sum_{i=1}^{N_{t_i}}Z_i-\sum_{i=1}^{N_{t_{i-1}}}Z_i\right)}\right.\right.\\ &\quad\left.\left.-(1-\beta)\,e^{r(t_i-t_{i-1})},1+l\right\},1+h\right\},\end{aligned}\tag{4.4.6}$$

where the constant c is implicitly defined by setting $\mathbb{E}^{\mathbb{Q}}\left\{\frac{L_t}{L_0}|\sigma_0=\sigma\right\}=1$. In order to price the option, we would like to obtain the c.f. of the factors in (4.4.6) or, even better, of their product. However, in general, the calculation of the c.f. of the factors in (4.4.6) is far from trivial or computationally efficient, especially in the presence of stochastic volatility (see, for example, Fang and Oosterlee (2011)). If we limit ourselves to a few dynamics for which we have the analytic expression for the p.d.f. of $\log\frac{S_{t_i}}{S_{t_{i-1}}}$, we can use the approach introduced in Section 4.1. Examples for which the p.d.f. is known include the Merton and Kou dynamics. In these cases, as the factors in (4.4.6) are i.i.d., one can also compute the price in a single step (this is not possible, for example, under the Heston model). In Figure 4.15, we show the IV smile for options prices under the Black-Scholes, Merton and Heston models when we vary the rebalancing frequency. We use a Monte Carlo approach for the Heston dynamics and the aforesaid transform methods for the remaining two models. We observe larger differences in prices between models with low rebalancing frequency while the differences for models with $M=252$ (daily) and $M=2016$ (four times per day) drop significantly. In all of our examples the relative difference—the ratio between the difference in IV and its level—was less than 15 basis points. As expected, in all the examples the IV seems to converge to the that of the continuous case. For example, in the Black-Scholes case, as we increase the frequency the IV approaches a constant line, $\sigma_{IV}(K)=60\%$, which is indeed the IV of the 3x LETF when the volatility of the reference index is 20%.

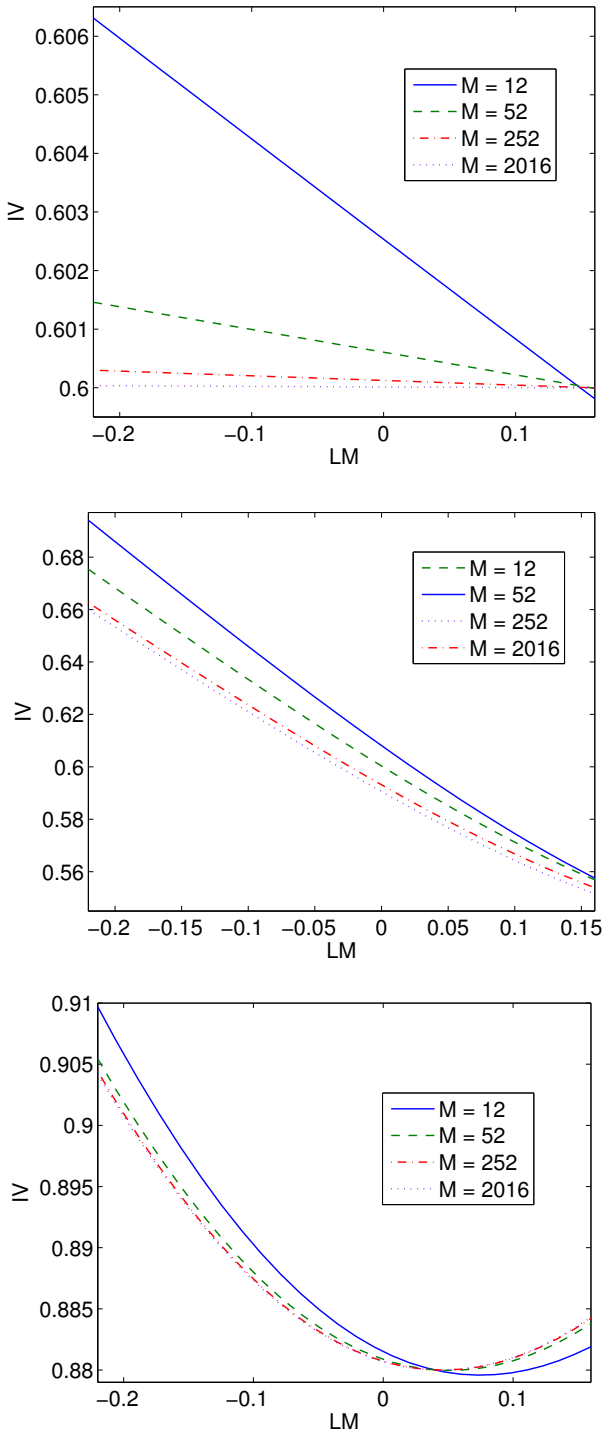

Figure 4.15: The IV smile when we apply discrete rebalancing at different frequencies M, calculated according to the dynamics (4.4.6). Parameters: $S = 100, r = 0.02, T = .5$ (common), $\sigma = 0.2$ (BS, top), $\sigma_0^2 = .054, \kappa = 2, \theta = .05, \rho = -.5, \zeta = .8$ (Heston, middle), $\sigma = .2, \lambda = 20, \mu_J = 0, \sigma_J = .03$ (Merton, bottom).

Bibliography

Ahn, A., Haugh, M., and Jain, A. (2013). Consistent pricing of options on leveraged ETFs. *SSRN Preprint*.

Andersen, L. and Andreasen, J. (2000). Jump diffusion models: volatility smile fitting and numerical methods for pricing. *Review of Derivatives Research*, 4:231–262.

Avellaneda, M. and Zhang, S. (2010). Path-dependence of leveraged ETF returns. *SIAM Journal of Financial Mathematics*, 1:586–603.

Barone-Adesi, G. and Whaley, R. (1987). Efficient analytic approximation of American option values. *The Journal of Finance*, 17(2):301–320.

Barth, M., Johnson, T., and So, E. C. (2011). Dynamics of earnings announcement news: Evidence from option prices. *Working paper*.

Bates, D. (1996). Jumps and stochastic volatility: The exchange rate processes implicit in Deutschemark options. *Review of Financial Studies*, 9(1):69–107.

Benaim, S. and Friz, P. (2008). Smile asymptotics II: models with known moment generating functions. *Journal of Applied Probability*, 45 (1):1–291.

Benaim, S., Friz, P., and Lee, R. (2012). On the Black-Scholes implied volatility at extreme strikes. In Cont, R., editor, *Frontiers in Quantitative Finance: Volatility and Credit Risk Modeling*, pages 19–45. Wiley & Sons.

Bensoussan, A. and Lions, J. (1984). *Impulse control and quasivariational inequalities*. Wiley & Sons.

Billings, M. and Jennings, R. (2011). The option markets anticipation of information content in earnings announcements. *Review of Accounting Studies Conference Version*, 16:587–619.

Black, F. and Scholes, M. (1973). The pricing of options and corporate liabilities. *Journal of Political Economy*, 81:637–654.

Broadie, M., Chernov, M., and Johannes, M. (2009). Understanding index option returns. *Review of Financial Studies*, 22(11):4493–4529.

Carr, P., Geman, H., Madan, D., and Yor, M. (2002). The fine structure of asset returns: An empirical investigation. *Journal of Business*, 75(2):305–332.

Carr, P. and Madan, D. (1999). Option pricing and the fast Fourier transform. *Journal of Computational Finance*, 2:61–73.

Chatrah, A., Christie-David, R., and Lee, K. (2009). How potent are news reversals?: Evidence from the futures markets. *Journal of Futures Market*, 29:42–73.

Cheng, M. and Madhavan, A. (2009). The dynamics of leveraged and inverse exchange traded funds. *Journal Of Investment Management*, 4.

Chordia, T. and Shivakumar, L. (2006). Earnings and price momentum. *Journal of Financial Economics*, 80(3):627–656.

Coleman, T. and Li, Y. (1994). On the convergence of reflective Newton methods for large-scale nonlinear minimization subject to bounds. *Mathematical Programming*, 67, 2:189–224.

Coleman, T. and Li, Y. (1996). An interior, trust region approach for nonlinear minimization subject to bounds. *SIAM Journal on Optimization*, 6:418–445.

Cont, R. and Tankov, P. (2002). Calibration of jump-diffusion option-pricing models: a robust non-parametric approach. *Working paper*.

Cont, R. and Voltchkova, E. (2005). A finite difference scheme for option pricing in jump diffusions and exponential Lévy models. *SIAM Journal on Numerical Analysis*, 43:1596–1626.

Cox, J., Ingersoll, J., and Ross, S. (1985). A theory of the term structure of interest rates. *Econometrica*, 53:38517407.

del Baño Rollin, S., Ferreiro-Castilla, A., and Utzet, F. (2009). A new look at the Heston characteristic function. Preprint.

Deng, G., Dulaney, T., McCann, C., and Yan, M. (2013). Crooked volatility smiles. *Journal of Derivatives and Hedge Funds*, 19(4):278–294.

Dennis, J. (1977). Nonlinear least-squares. In Jacobs, D., editor, *State of the Art in Numerical Analysis*, pages 269–312. Academic Press.

Donders, M. and Vorst, T. (1996). The impact of firm specific news on IVs. *Journal of Banking and Finance*, 20:1447–1461.

Dubinsky, A. and Johannes, M. (2006). Fundamental uncertainty, earning announcements and equity options. Working paper.

Duffie, D., Pan, J., and Singleton, K. J. (2000). Transform analysis and asset pricing for affine jump-diffusions. *Econometrica*, 68(6):1343–1376.

Fang, F. and Oosterlee, C. W. (2011). A Fourier-based valuation method for Bermudan and barrier options under Heston's model. *SIAM Journal on Financial Mathematics*, 2(1):439–463.

Figlewski, S. (2010). Estimating the implied risk neutral density for the U.S. market portfolio. In M. Watson, T. B. and Russell, J., editors, *Volatility and Time Series Econometrics: Essays in Honor of Robert Engle*. Oxford University Press.

Fouque, J.-P., Papanicolaou, G., Sircar, R., and Sølna, K. (2011). *Multiscale Stochastic Volatility for Equity, Interest Rate, and Credit Derivatives*. Cambridge University Press.

Haugh, M. (2011). A note on constant proportion trading strategies. *Operations Research Letters*, 39:172–179.

Heston, S. (1993). A closed-form solution for options with stochastic volatility with applications to bond and currency options. *Rev. Financ. Stud.*, 6(2):327–343.

Isakov, D. and Perignon, C. (2001). Evolution of market uncertainty around earnings announcements. *Journal of Banking and Finance*, 25:1769–1788.

Jackson, K., Jaimungal, S., and Surkov, V. (2008). Fourier space time-stepping for option pricing with Lévy models. *Journal of Computational Finance*, 12(2):1–29.

Kou, S. (2002). A jump-diffusion model for option pricing. *Management Science*, 48:1086–1101.

Kou, S. G. and Wang, H. (2004). Option pricing under a double exponential jump diffusion model. *Management Science*, 50(9):1178–1192.

Lee, R. (2004). Option pricing by transform methods: extensions, unification, and error control. *Journal of Computational Finance*, 7:51–86.

Lee, S. and Mykland, P. (2008). Jumps in financial markets: A new nonparametric test and jump dynamics. *Review of Financial Studies*, 21(6):2535–2563.

Leung, T., Lorig, M., and Pascucci, A. (2014). Leverage ETF implied volatilities from ETF dynamics. *Working Paper*.

Leung, T. and Ludkovski, M. (2011). Optimal timing to purchase options. *SIAM Journal on Financial Mathematics*, 2(1):768–793.

Leung, T. and Santoli, M. (2012). Leveraged ETFs: Admissible leverage and risk horizon. *Journal of Investment Strategies*, 2(1):39–61.

Leung, T. and Santoli, M. (2014). Accounting for earnings announcements in the pricing of equity options. *Journal of Financial Engineering*, 01(04):1450031.

Leung, T. and Sircar, R. (2015). Implied volatility of leveraged ETF options. *Applied Mathematical Finance*, 22:126–188.

Lord, R., Fang, F., Bervoets, F., and Oosterlee, C. W. (2008). A fast and accurate FFT-based method for pricing early-exercise options under Lévy processes. *SIAM Journal of Scientific Computing*, 30(4):1678–1705.

Madan, D. and Unal, H. (1998). Pricing the risks of default. *Review of Derivatives Research*, 2:121–160.

Maheu, J. and McCurdy, T. (2004). News arrival, jump dynamics and volatility components for individual stock returns. *Journal of Finance*, 59:755–793.

Mehra, A., Kolanovic, M., and Kaplan, B. (2014). Earnings and option volatility monitor. Technical report, J.P. Morgan.

Merton, R. (1976). Option pricing when underlying stock returns are discontinuous. *Journal of Financial Economics*, 3:125–144.

Merton, R. C. (1973). Theory of rational option pricing. *The Bell Journal of Economics and Management Science*, 4(1):141–183.

Øksendal, B. (2003). *Stochastic Differential Equations: An Introduction with Applications*. Springer.

Patell, J. and Wolfson, M. (1981). The ex ante and ex post price effect of quarterly earnings announcements reflected in option and stock prices. *Journal of Accounting Research*, 19:434–458.

Patell, J. and Wolfson, M. (1984). The intraday speed of adjustment of stock prices to earnings and dividend announcements. *Journal of Financial Economics*, 13:223–252.

Piazzesi, M. (2005). Bond yields and the Federal Reserve. *Journal of Political Economy*, 113:311–344.

Raible, S. (2000). *Lévy processes in finance: Theory, numerics, and empirical facts*. PhD thesis, Univ. Freiburg.

Rogers, J., Skinner, D., and Van Buskirk, A. (2009). Earnings guidance and market uncertainty. *Journal of Accounting and Economics*, 48:90–109.

Russell, M. (2009). Long-term performance and option pricing of leveraged ETFs. Senior Thesis, Princeton University.

Zhang, J. (2010). *Path dependence properties of leveraged exchange-traded funds: compounding, volatility and option pricing.* PhD thesis, New York University.

Appendix A

In this Appendix, we provide a number of detailed proofs and formulas related to the results of Chapter 2.

A.1 Details for Formula (2.4.2)

In this section we write the expression of the function Υ in (2.4.2) explicitly. For ease of notation, we refer to the parameters given as input to Υ as a vector $\Theta \equiv (\theta_1, ..., \theta_{13})$. In addition, let $\tilde{\Theta}$ be a permutation of the vector Θ where only the 8th and 9th components (the parameters for the randomly timed jumps) are switched. The function Υ is given by

$$\Upsilon(\Theta) = \sum_{n=0}^{\infty} \frac{(\theta_6\theta_4)^n e^{-\theta_6\theta_4}}{n!} Z_n(\Theta), \tag{A.1.1}$$

where

$$\begin{aligned} Z_n(\Theta) &= \theta_{10} \textstyle\sum_{l=0}^{n} \left(P_{n,l} T_{1,n}(k,\Theta) + Q_{n,l} T_{2,n}(k,\Theta)\right) + \\ &\quad \theta_{11} \textstyle\sum_{l=0}^{n} \left(P_{n,l} T_{3,n}(k,\Theta) + Q_{n,l} T_{4,n}(k,\Theta)\right), \end{aligned}$$

$$k = \log\left(\frac{\theta_2}{\theta_1}\right) - \left(\theta_3 - \frac{\theta_5^2}{2} - m\kappa\right)\theta_4 - \alpha, \quad m = p\frac{\lambda_1}{\lambda_1 - 1} + q\frac{\lambda_2}{\lambda_2 + 1} - 1,$$

$$\begin{aligned} T_{1,n+1}(s,\Theta) = \frac{\theta_8}{\theta_8 - \theta_{12}} \Bigg(& T_{1,n}(s,\Theta) - \theta_{12} \frac{e^{\frac{(\theta_5\theta_8)^2\theta_4}{2}}}{\sqrt{2\pi}} \left(\theta_5\sqrt{\theta_4}\theta_8\right)^n \cdot \\ & I_n\left(s; -\theta_8, -\frac{1}{\theta_5\sqrt{\theta_4}}, -\theta_8\theta_5\sqrt{\theta_4}\right)\Bigg), \end{aligned}$$

$$T_{2,n+1}\left(s,\Theta\right)=\frac{\theta_9}{\theta_9+\theta_{12}}\left(T_{2,n}\left(s,\Theta\right)+\theta_{12}\frac{e^{\frac{\left(\theta_5\theta_8\right)^2\theta_4}{2}}}{\sqrt{2\pi}}\left(\theta_5\sqrt{\theta_4}\theta_9\right)^n\cdot I_n\left(s;\theta_9,\frac{1}{\theta_5\sqrt{\theta_4}},-\theta_9\theta_5\sqrt{\theta_4}\right)\right),$$

$$T_{3,n+1}\left(s,\Theta\right)=\quad 1-T_{2,n+1}\left(-s,\tilde{\Theta}\right),\quad T_{4,n+1}\left(s,\Theta\right)=\quad 1-T_{1,n+1}\left(-s,\tilde{\Theta}\right),$$

$$T_{1,0}\left(s,\Theta\right)=T_{2,0}\left(s,\Theta\right)=\theta_{12}\frac{e^{\left(\theta_5\theta_{12}\right)^2\theta_4/2}}{\sqrt{2\pi}}I_0\left(s;-\theta_{12},-\frac{1}{\theta_5\sqrt{\theta_4}},-\theta_{12}\theta_5\sqrt{\theta_4}\right),$$

$$T_{1,1}\left(s,\Theta\right)=\frac{1}{\frac{1}{\theta_8}-\frac{1}{\theta_{12}}}\left(\frac{e^{\frac{\left(\theta_5\theta_8\right)^2\theta_4}{2}}}{\sqrt{2\pi}}I_0\left(s;-\theta_8,\frac{-1}{\theta_5\sqrt{\theta_4}},-\theta_8\theta_5\sqrt{\theta_4}\right)-\frac{e^{\frac{\left(\theta_5\theta_{12}\right)^2\theta_4}{2}}}{\sqrt{2\pi}}I_0\left(s;-\theta_{12},\frac{-1}{\theta_5\sqrt{\theta_4}},-\theta_{12}\theta_5\sqrt{\theta_4}\right)\right),$$

$$T_{2,1}\left(s,\Theta\right)=\frac{1}{\frac{1}{\theta_9}-\frac{1}{\theta_{12}}}\left(\frac{e^{\frac{\left(\theta_5\theta_9\right)^2\theta_4}{2}}}{\sqrt{2\pi}}I_0\left(s;-\theta_9,\frac{-1}{\theta_5\sqrt{\theta_4}},-\theta_9\theta_5\sqrt{\theta_4}\right)-\frac{e^{\frac{\left(\theta_5\theta_{12}\right)^2\theta_4}{2}}}{\sqrt{2\pi}}I_0\left(s;-\theta_{12},\frac{-1}{\theta_5\sqrt{\theta_4}},-\theta_{12}\theta_5\sqrt{\theta_4}\right)\right),$$

$$P_{n,m}=\sum_{i=m}^{n-1}\binom{n-m-1}{i-m}\binom{n}{i}\left(\frac{\theta_8}{\theta_8+\theta_9}\right)^{i-m}\left(\frac{\theta_9}{\theta_8+\theta_9}\right)^{n-i}\theta_7^i(1-\theta_7)^{n-i},$$

$$Q_{n,m}=\sum_{i=m}^{n-1}\binom{n-m-1}{i-m}\binom{n}{i}\left(\frac{\theta_8}{\theta_8+\theta_9}\right)^{n-i}\left(\frac{\theta_9}{\theta_8+\theta_9}\right)^{i-m}\theta_7^{n-i}(1-\theta_7)^i,$$

$$P_{n,n}=\theta_7^n,Q_{n,n}=(1-\theta_7)^n,P_{0,0}=1,Q_{0,0}=0,$$

$$Hh_n(x)=\frac{1}{n}\left(Hh_{n-2}(x)-xHh_{n-1}(x)\right),$$

$$Hh_0(x)=\int_{-\infty}^{-x}e^{-t^2/2}dt,I_n\left(k;\alpha,\beta,\delta\right)=-\frac{e^{\alpha k}}{\alpha}Hh_n\left(\beta k-\delta\right)+\frac{\beta}{\alpha}I_{n-1},$$

$$I_{-1}(k;\alpha,\beta,\delta)=\frac{\sqrt{2\pi}}{\beta}e^{\frac{\alpha\delta}{\beta}+\frac{\alpha^2}{2\beta^2}}\begin{cases}\Phi\left(-\beta k+\delta+\frac{\alpha}{\beta}\right) & if\ \beta>0\ \alpha\neq 0,\\ -\Phi\left(\beta k-\delta-\frac{\alpha}{\beta}\right) & if\ \beta<0\ \alpha<0.\end{cases}$$

As suggested by these definitions, the implementation of the formula involves successive computation of functions, followed by a summation in (A.1.1) that must be truncated. In order to control the error, we notice that[1] $Z_n \leq 2$, and the error bound

$$\begin{aligned}\Upsilon(\Theta)-\sum_{n=0}^{M}\frac{(\theta_6\theta_4)^n e^{-\theta_6\theta_4}}{n!}Z_n(\Theta) &\leq 2\sum_{n=M+1}^{\infty}\frac{(\theta_6\theta_4)^n e^{-\theta_6\theta_4}}{n!}\\ &= 2-2\sum_{n=0}^{M}\frac{(\theta_6\theta_4)^n e^{-\theta_6\theta_4}}{n!}\equiv\epsilon(\theta_6\theta_4,M).\end{aligned}$$

Therefore, if we truncate the summations in (2.4.2) at the Mth term, the upper bound for the truncation error is given by

$$e^{-\alpha}S\epsilon\left((m+1)\kappa T,M\right)+e^{-rT}K\epsilon\left(\kappa T,M\right).$$

This can be computed quickly and used to limit the error to the a priori desired decimal place. For example, take $S=K=100$, $T=1$ and an error tolerance of 0.01. Then, with $\kappa\approx 100$, and $m,\alpha<0.001$, we obtain $M=143$.

A.2 Proof of Propositions 2.4.1

In order to price the European call option, we need to evaluate the terms $\mathbb{Q}\{S_T>K\}$ and $\mathbb{E}\left\{e^{S_T}1_{\{S_T>K\}}\right\}$. We first state some useful facts (see Kou (2002) for proofs).

Lemma A.2.1. *Define two i.i.d. exponential r.v.'s, namely, $J_i^+\sim Exp(\lambda_1)$, $J_i^-\sim Exp(\lambda_2)$. For every $n\geq 1$, we have*

$$\sum_{i=1}^{n}J_i\ \overset{d}{=}\ \begin{cases}\sum_{i=1}^{m} & J_i^+\text{, w.p. } P_{n,m},\\ \sum_{i=1}^{m} & J_i^-\text{, w.p. } Q_{n,m},\end{cases}$$

[1] This can be verified directly from the proof of Proposition 2.4.1 presented in A.2.

where

$$P_{n,m}=\sum_{i=m}^{n-1}\binom{n-m-1}{i-m}\binom{n}{i}\left(\frac{\lambda_1}{\lambda_1+\lambda_2}\right)^{i-m}\left(\frac{\lambda_2}{\lambda_1+\lambda_2}\right)^{n-i}p^iq^{n-i},$$

$$Q_{n,m}=\sum_{i=m}^{n-1}\binom{n-m-1}{i-m}\binom{n}{i}\left(\frac{\lambda_1}{\lambda_1+\lambda_2}\right)^{n-i}\left(\frac{\lambda_2}{\lambda_1+\lambda_2}\right)^{i-m}p^{n-i}q^i,$$

$$P_{n,n}=p^n,\ Q_{n,n}=q^n,\ P_{0,0}=1,\ Q_{0,0}=0,\ q=1-p.$$

Next, for every $n\geq 0$, we define the functions[2]

$$Hh_n(x)=\int_x^\infty Hh_{n-1}(y)\,dy=\frac{1}{n!}\int_x^\infty (t-x)^n e^{-\frac{t^2}{2}}dt,$$

$$Hh_{-1}(x)=e^{-x^2/2},\ \ Hh_0(x)=\int_x^\infty e^{-\frac{t^2}{2}}dt=\sqrt{2\pi}\Phi(-x),$$

where $\Phi(x)$ denotes the standard normal c.d.f. In addition, for $n\geq 0$, define the integral

$$I_n(k,\alpha,\beta,\delta)=\int_k^\infty e^{\alpha x}Hh_n(\beta x-\delta)\,dx.$$

Lemma A.2.2. *(i) If $\beta>0$ and $\alpha\neq 0$, then for all $n\geq -1$, we have*

$$I_n(k,\alpha,\beta,\delta)=\frac{-e^{\alpha k}}{\alpha}\sum_{i=0}^{n}\left(\frac{\beta}{\alpha}\right)^{n-i}Hh_i(\beta k-\delta)+\left(\frac{\beta}{\alpha}\right)^{n+1}\frac{\sqrt{2\pi}}{\beta}e^{\frac{\alpha\delta}{\beta}+\frac{\alpha^2}{2\beta^2}}\Phi\left(-\beta k+\delta+\frac{\alpha}{\beta}\right).$$

(ii) If $\beta<0$ and $\alpha<0$, then for all $n\geq -1$, we have

$$I_n(k,\alpha,\beta,\delta)=\frac{-e^{\alpha k}}{\alpha}\sum_{i=0}^{n}\left(\frac{\beta}{\alpha}\right)^{n-i}Hh_i(\beta k-\delta)-\left(\frac{\beta}{\alpha}\right)^{n+1}\frac{\sqrt{2\pi}}{\beta}e^{\frac{\alpha\delta}{\beta}+\frac{\alpha^2}{2\beta^2}}\Phi\left(\beta k-\delta-\frac{\alpha}{\beta}\right).$$

In particular,

$$I_{-1}(k;\alpha,\beta,\delta)=\frac{\sqrt{2\pi}}{\beta}e^{\frac{\alpha\delta}{\beta}+\frac{\alpha^2}{2\beta^2}}\begin{cases}\Phi\left(-\beta k+\delta+\frac{\alpha}{\beta}\right) & if\ \beta>0,\ \alpha\neq 0,\\ -\Phi\left(\beta k-\delta-\frac{\alpha}{\beta}\right) & if\ \beta<0\,,\alpha<0.\end{cases}$$

---

[2]The Hh functions can be calculated using either of the following facts:

$$Hh_n=2^{-\frac{n}{2}}\sqrt{\pi}e^{-\frac{x^2}{2}}\left(\frac{{}_1F_1\left(\frac{n+1}{2},\frac{1}{2},\frac{x^2}{2}\right)}{\sqrt{2}\Gamma\left(1+\frac{n}{2}\right)}-x\frac{{}_1F_1\left(\frac{n}{2}+1,\frac{3}{2},\frac{x^2}{2}\right)}{\Gamma\left(\frac{n+1}{2}\right)}\right),$$

$$nHh_n(x)=Hh_{n-2}(x)-xHh_{n-1}(x)\ \ ,\ n\geq 1,$$

where ${}_1F_1$ denotes the confluent hypergeometric function and Γ is the gamma function.

In addition, under either assumption (i) or (ii) over the parameters α and β given above, the functions (I_n) satisfy the recursive relation

$$I_n(k;\alpha,\beta,\delta) = -\frac{e^{\alpha k}}{\alpha} H h_n(\beta k - \delta) + \frac{\beta}{\alpha} I_{n-1}(k;\alpha,\beta,\delta).$$

In our extended Kou model, we need to understand the distribution of the sum of double exponentially distributed randomly timed and EA jumps. Hence, we consider the associated p.d.f.'s.

Lemma A.2.3. *Let Z_e^+, Z_e^- be i.i.d. exponential r.v.'s, $Z_e^+, \sim Exp(\eta_1)$, $Z_e^-, \sim Exp(\eta_2)$. In addition, let J_i^+, J_i^-, Z_e^+, Z_e^- be independent. Then, we have*

$$f_{\sum_1^n J_i^+ + Z_e^+}(t) = \left(\frac{1}{\frac{1}{\lambda_1} - \frac{1}{\eta_1}}\right)^n \left(A_n(t)\, e^{-\lambda_1 t} + B_n(t)\, e^{-\eta_1 t}\right), \quad t > 0, \lambda_1 \neq \eta_1, \tag{A.2.1}$$

$$f_{-\sum_1^n J_i^- + Z_e^+}(t) = \left(\frac{1}{\frac{1}{\lambda_2} + \frac{1}{\eta_1}}\right)^n C_n(t)\, e^{\lambda_2 min(0,t) - \eta_1 \max(0,t)}, \quad t \in \mathbb{R}, \lambda_2 \neq \eta_1, \tag{A.2.2}$$

where f_Y denotes the p.d.f. of Y, and

$$B_n(t) = -\eta_1^{-(n-1)}, A_n(t) = 1 + \sum_i^{n-1} \eta_1^{-(i-1)} \left(\frac{1}{\lambda_1} - \frac{1}{\eta_1}\right)^{n-i} \lambda_1^{n-i} \frac{(t)^{n-i}}{(n-i)!}, \quad t > 0,$$

$$C_n(t) = \frac{C_{n-1}(t)}{\lambda_2} + \lambda_2^{n-1} \frac{(\max(0,t) - t)^{n-1}}{(n-1)!}, \quad t \in \mathbb{R}.$$

In addition, they satisfy the following recursive relations:

$$f_{\sum_1^{n+1} J_i^+ + Z_e^+}(t) = \frac{\lambda_1}{(\lambda_1 - \eta_1)} \left(f_{\sum_1^n J_i^+ + Z_e^+}(t) - \lambda_1^n \frac{(t)^n}{n!} \eta_1 e^{-\lambda_1 t}\right), \tag{A.2.3}$$

$$f_{-\sum_1^{n+1} J_i^- + Z_e^+}(t) = \frac{\lambda_2}{\lambda_2 + \eta_1} \left(f_{-\sum_1^n J_i^- + Z_e^+}(t) + \lambda_2^n \frac{(\max(0,t) - t)^n}{n!} \eta_1 e^{\lambda_2 t} e^{-(\lambda_2 + \eta_1)\max(0,t)}\right). \tag{A.2.4}$$

Proof. We first notice that the positive r.v., $J_i^+ + Z_e^+$, has the p.d.f.

$$\begin{aligned}\int_0^t \lambda_1 e^{-\lambda_1(t-x)} \eta_1 e^{-\eta_1 x} dx &= \frac{1}{\frac{1}{\lambda_1} - \frac{1}{\eta_1}} \left(e^{-\lambda_1 t} - e^{-\eta_1 t}\right) \\ &\equiv \left(\frac{1}{\frac{1}{\lambda_1} - \frac{1}{\eta_1}}\right) \left(A_1(t) e^{-\lambda_1 t} + B_1(t) e^{-\eta_1 t}\right), \quad t > 0, \lambda_1 \neq \eta_1.\end{aligned}$$

Now suppose for a fixed $n \geq 1$, $f_{\sum_1^n J_i^+ + Z_e^+}(t) = \left(\frac{1}{\frac{1}{\lambda_1}-\frac{1}{\eta_1}}\right)^n \left(A_n(t)e^{-\lambda_1 t} + B_n(t)e^{-\eta_1 t}\right)$, we obtain

$$\begin{aligned} f_{\sum_1^n J_i^+ + Z_e^+}(t) &= \int_0^t \lambda_1^n \frac{(t-x)^{n-1}}{(n-1)!} e^{-\lambda_1(t-x)} \eta_1 e^{-\eta_1 x} dx \\ &= \lambda_1^n \frac{(t)^n}{n!} \eta_1 e^{-\lambda_1 t} + \frac{(\lambda_1 - \eta_1)}{\lambda_1} f_{\sum_1^{n+1} J_i^+ + Z_e^+}(t), \\ \implies \quad f_{\sum_1^{n+1} J_i^+ + Z_e^+}(t) &= \frac{\lambda_1}{(\lambda_1 - \eta_1)} \left(f_{\sum_1^n J_i^+ + Z_e^+}(t) - \lambda_1^n \frac{(t)^n}{n!} \eta_1 e^{-\lambda_1 t} \right) \\ &= \left(\frac{1}{\frac{1}{\lambda_1}-\frac{1}{\eta_1}}\right)^{n+1} \left(A_{n+1}(t)e^{-\lambda_1 t} + B_{n+1}(t)e^{-\eta_1 t}\right), \end{aligned}$$

where the coefficients satisfy

$$\begin{aligned} B_{n+1} &= \frac{1}{\eta_1} B_n, \quad A_{n+1} = \frac{A_n}{\eta_1} - C_{n+1}, \quad C_{n+1} = \left(\frac{1}{\lambda_1} - \frac{1}{\eta_1}\right)^n \lambda_1^n \frac{(t)^n}{n!}, \\ B_n &= -\eta_1^{-(n-1)}, \quad A_n = 1 + \sum_i^{n-1} \eta_1^{-(i-1)} \left(\frac{1}{\lambda_1} - \frac{1}{\eta_1}\right)^{n-i} \lambda_1^{n-i} \frac{(t)^{n-i}}{(n-i)!}, \end{aligned}$$

and this yields (A.2.1). Next, we note that the real-valued r.v. $-J_i^- + Z_e^+$ has the p.d.f.

$$\int_{\max(0,t)}^{\infty} \lambda_2 e^{\lambda_2(t-x)} \eta_1 e^{-\eta_1 x} dx = \frac{e^{\lambda_2 \min(0,t) - \eta_1 \max(0,t)}}{\frac{1}{\lambda_2} + \frac{1}{\eta_1}}, \quad t \in \mathbb{R}, \lambda_2 \neq \eta_1.$$

For a fixed $n \geq 1$, assume that $f_{-\sum_1^n J_i^- + Z_e^+}(t) = \left(\frac{1}{\frac{1}{\lambda_2}+\frac{1}{\eta_1}}\right)^n C_n(t) e^{\lambda_2 \min(0,t) - \eta_1 \max(0,t)}$, then we get

$$\begin{aligned} f_{-\sum_1^n J_i^- + Z_e^+}(t) &= \int_{\max(0,t)}^{\infty} \lambda_2^n \frac{(-t+x)^{n-1}}{(n-1)!} e^{\lambda_2(t-x)} \eta_1 e^{-\eta_1 x} dx \\ &= -\lambda_2^n \frac{(\max(0,t) - t)^n}{n!} \eta_1 e^{\lambda_2 t} e^{-(\lambda_1+\eta_1)\max(0,t)} + \frac{(\lambda_2 + \eta_1)}{\lambda_2} f_{-\sum_1^{n+1} J_i^- + Z_e^+}(t), \end{aligned}$$

$$\begin{aligned} \implies f_{-\sum_1^{n+1} J_i^- + Z_e^+}(t) &= \frac{\lambda_2}{\lambda_2 + \eta_1} \left(f_{-\sum_1^n J_i^- + Z_e^+}(t) + \lambda_2^n \frac{(\max(0,t) - t)^n}{n!} \eta_1 e^{\lambda_2 t} e^{-(\lambda_1+\eta_1)\max(0,t)} \right) \\ &\equiv \left(\frac{1}{\frac{1}{\lambda_2}+\frac{1}{\eta_1}}\right)^{n+1} C_{n+1}(t) e^{\lambda_2 \min(0,t) - \eta_1 \max(0,t)}. \end{aligned}$$

Matching terms yields $C_{n+1}(t) = \frac{C_n(t)}{\lambda_2} + \lambda_2^n \frac{(\max(0,t)-t)^n}{n!}$. □

We now calculate the distribution of the sum of a normal r.v. and double-exponentials.

Proposition A.2.4. *Let $W \sim N\left(0, \sigma^2\right)$. Then, we have the p.d.f.'s:*

$$f_{W+\sum_{i=1}^{n+1} J_i^+ + Z_e^+}(t) = \left(\frac{\lambda_1}{\lambda_1 - \eta_1}\right)^n \eta_1 \frac{e^{\frac{(\sigma\eta_1)^2}{2}}}{\sqrt{2\pi}} e^{-\eta_1 t} Hh_0\left(-\frac{t}{\sigma} + \sigma\eta_1\right) - \tag{A.2.5}$$
$$\sum_{i=1}^{n} \left(\frac{\lambda_1}{\lambda_1 - \eta_1}\right)^{n-i+1} \eta_1 \frac{e^{\frac{(\sigma\lambda_1)^2}{2}}}{\sqrt{2\pi}} \left(\sigma^i \lambda_1^i\right) e^{-\lambda_1 t} Hh_i\left(\frac{-t}{\sigma} + \sigma\lambda_1\right) \ , \ t > 0, \ \lambda_1 \neq \eta_1,$$

$$f_{W-\sum_{i=1}^{n+1} J_i^- + Z_e^+}(t) = \left(\frac{\lambda_2}{\lambda_2 + \eta_1}\right)^n \eta_1 \frac{e^{\frac{(\sigma\eta_1)^2}{2}}}{\sqrt{2\pi}} e^{-\eta_1 t} Hh_0\left(-\frac{t}{\sigma} + \sigma\eta_1\right) + \tag{A.2.6}$$
$$\sum_{i=1}^{n} \left(\frac{\lambda_2}{\lambda_2 + \eta_1}\right)^{n-i+1} \eta_1 \frac{e^{\frac{(\sigma\lambda_2)^2}{2}}}{\sqrt{2\pi}} \left(\sigma^i \lambda_2^i\right) e^{\lambda_2 t} Hh_i\left(\frac{t}{\sigma} + \sigma\lambda_2\right) \ , \ t \in \mathbb{R}, \ \lambda_2 \neq \eta_1.$$

Moreover, they admit the recursive relations:

$$f_{W+\sum_{i=1}^{n+1} J_i^+ + Z_e^+}(t) = \frac{\lambda_1}{\lambda_1 - \eta_1} \left(f_{W+\sum_{i=1}^{n} J_i^+ + Z_e^+}(t) - \right.$$
$$\left. \eta_1 \frac{e^{\frac{(\sigma\lambda_1)^2}{2}}}{\sqrt{2\pi}} \left(\sigma^n \lambda_1^n\right) e^{-\lambda_1 t} Hh_n\left(\frac{-t}{\sigma} + \sigma\lambda_1\right)\right), \tag{A.2.7}$$

$$f_{W-\sum_{i=1}^{n+1} J_i^- + Z_e^+}(t) = \frac{\lambda_2}{\lambda_2 + \eta_1} \left(f_{W-\sum_{i=1}^{n+1} J_i^- + Z_e^+}(t) + \right.$$
$$\left. \eta_1 \frac{e^{\frac{(\sigma\lambda_2)^2}{2}}}{\sqrt{2\pi}} \left(\sigma^n \lambda_2^n\right) e^{\lambda_2 t} Hh_n\left(\frac{t}{\sigma} + \sigma\lambda_2\right)\right). \tag{A.2.8}$$

Proof. We start with the p.d.f. for $W + Z_e^+$:

$$f_{W+Z_e^+}(t) = \eta_1 \frac{e^{\frac{(\sigma\eta_1)^2}{2}}}{\sqrt{2\pi}} e^{-\eta_1 t} Hh_0\left(-\frac{t}{\sigma} + \sigma\eta_1\right).$$

Using (A.2.3), we also write

$$f_{W+\sum_{i=1}^{n+1} J_i^+ + Z_e^+}(t) = \int_{-\infty}^{t} f_{\sum_1^{n+1} J_i^+ + Z_e^+}(t - x) \frac{e^{-\frac{x^2}{2\sigma^2}}}{\sqrt{2\pi\sigma^2}} dx$$
$$= \frac{\lambda_1}{\lambda_1 - \eta_1} \left(f_{W+\sum_{i=1}^{n} J_i^+ + Z_e^+}(t) - \eta_1 \frac{e^{\frac{(\sigma\lambda_1)^2}{2}}}{\sqrt{2\pi}} \left(\sigma^n \lambda_1^n\right) e^{-\lambda_1 t} Hh_n\left(\frac{-t}{\sigma} + \sigma\lambda_1\right)\right),$$

which leads directly to

$$f_{W+\sum_{i=1}^{n+1} J_i^+ + Z_e^+}(t) = \left(\frac{\lambda_1}{\lambda_1-\eta_1}\right)^n \eta_1 \frac{e^{\frac{(\sigma\eta_1)^2}{2}}}{\sqrt{2\pi}} e^{-\eta_1 t} Hh_0\left(-\frac{t}{\sigma}+\sigma\eta_1\right) + - \sum_{i=1}^{n}\left(\frac{\lambda_1}{\lambda_1-\eta_1}\right)^{n-i+1} \eta_1 \frac{e^{\frac{(\sigma\lambda_1)^2}{2}}}{\sqrt{2\pi}} \left(\sigma^i \lambda_1^i\right) e^{-\lambda_1 t} Hh_i\left(\frac{-t}{\sigma}+\sigma\lambda_1\right).$$

To prove (A.2.6), we apply (A.2.4) to get the recursive expression

$$f_{W-\sum_{i=1}^{n+1} J_i^- + Z_e^+}(t) = \int_{\mathbb{R}} f_{-\sum_{i=1}^{n+1} J_i^- + Z_e^+}(t-x)\frac{e^{-\frac{x^2}{2\sigma^2}}}{\sqrt{2\pi\sigma^2}}dx$$
$$= \frac{\lambda_2}{\lambda_2+\eta_1}\left(f_{W-\sum_{i=1}^{n+1} J_i^- + Z_e^+}(t) + \eta_1 \frac{e^{\frac{(\sigma\lambda_2)^2}{2}}}{\sqrt{2\pi}}\left(\sigma^n\lambda_2^n\right) e^{\lambda_2 t} Hh_n\left(\frac{t}{\sigma}+\sigma\lambda_2\right)\right),$$

which can be written explicitly as

$$f_{W-\sum_{i=1}^{n+1} J_i^- + Z_e^+}(t) = \left(\frac{\lambda_2}{\lambda_2+\eta_1}\right)^n \eta_1 \frac{e^{\frac{(\sigma\eta_1)^2}{2}}}{\sqrt{2\pi}} e^{-\eta_1 t} Hh_0\left(-\frac{t}{\sigma}+\sigma\eta_1\right) + + \sum_{i=1}^{n}\left(\frac{\lambda_2}{\lambda_2+\eta_1}\right)^{n-i+1} \eta_1 \frac{e^{\frac{(\sigma\lambda_2)^2}{2}}}{\sqrt{2\pi}} \left(\sigma^i \lambda_2^i\right) e^{\lambda_2 t} Hh_i\left(\frac{t}{\sigma}+\sigma\lambda_2\right).$$

□

We can now calculate the tail probabilities that will allow us to price the call option.

Proposition A.2.5. *Let $F_X(z) \equiv \mathbb{Q}\{X \le z\}$. Then,*

$$F_{W+\sum_{i=1}^{n+1} J_i^+ + Z_e^+}(z) = \left(\frac{\lambda_1}{\lambda_1-\eta_1}\right)^n \eta_1 \frac{e^{\frac{(\sigma\eta_1)^2}{2}}}{\sqrt{2\pi}} I_0\left(z; -\eta_1, -\frac{1}{\sigma}, -\eta_1\sigma\right) - \tag{A.2.9}$$
$$\sum_{i=1}^{n}\left(\frac{\lambda_1}{\lambda_1-\eta_1}\right)^{n-i+1} \eta_1 \frac{e^{\frac{(\sigma\lambda_1)^2}{2}}}{\sqrt{2\pi}} \left(\sigma^i\lambda_1^i\right) I_i\left(z; -\lambda_1, -\frac{1}{\sigma}, -\lambda_1\sigma\right), \quad z>0,\ \lambda_1 \ne \eta_1,$$

$$F_{W-\sum_{i=1}^{n+1} J_i^- + Z_e^+}(z) = \left(\frac{\lambda_2}{\lambda_2+\eta_1}\right)^n \eta_1 \frac{e^{\frac{(\sigma\eta_1)^2}{2}}}{\sqrt{2\pi}} I_0\left(z, -\eta_1, -\frac{1}{\sigma}, -\sigma\eta_1\right) + \tag{A.2.10}$$
$$\sum_{i=1}^{n}\left(\frac{\lambda_2}{\lambda_2+\eta_1}\right)^{n-i+1} \eta_1 \frac{e^{\frac{(\sigma\lambda_2)^2}{2}}}{\sqrt{2\pi}} \left(\sigma^i\lambda_2^i\right) I_n\left(z, \lambda_2, \frac{1}{\sigma}, -\sigma\lambda_2\right), \quad z\in\mathbb{R},\ \lambda_2 \ne \eta_1,$$

In addition, these c.d.f.'s admit the following recursive relations:

$$F_{W+\sum_{i=1}^{n+1} J_i^+ + Z_e^+}(z) = \frac{\lambda_1}{(\lambda_1 - \eta_1)} \left(F_{W+\sum_{i=1}^{n} J_i^+ + Z_e^+}(z) - \eta_1 \frac{e^{\frac{(\sigma\lambda_1)^2}{2}}}{\sqrt{2\pi}} \left(\sigma^n \lambda_1^n\right) I_n \left(z; -\lambda_1, -\frac{1}{\sigma}, -\lambda_1\sigma \right) \right), \tag{A.2.11}$$

$$F_{W-\sum_{i=1}^{n+1} J_i^- + Z_e^+}(z) = \frac{\lambda_2}{\lambda_2 + \eta_1} \left(F_{W-\sum_{i=1}^{n+1} J_i^- + Z_e^+}(z) + \eta_1 \frac{e^{\frac{(\sigma\lambda_2)^2}{2}}}{\sqrt{2\pi}} \left(\sigma^n \lambda_2^n\right) I_n \left(z, \lambda_2, \frac{1}{\sigma}, -\sigma\lambda_2 \right) \right). \tag{A.2.12}$$

Proof. The above expressions can all be derived by integrating the corresponding densities given in (A.2.5), (A.2.6), (A.2.7), (A.2.8) and taking into account the definitions of the Hh and I functions. □

We remark that although we did not provide the tail probability formulas $F_{\sigma W_T + \sum_{i=1}^{m} \hat{J}_i^+ - \hat{Z}_e^-}$ and $F_{\sigma W_T - \sum_{i=1}^{m} \hat{J}_i^- - \hat{Z}_e^-}$ we point out that they can be derived by symmetry. For example, we have

$$F_{\sigma W_T + \sum_{i=1}^{m} \hat{J}_i^+ - \hat{Z}_e^-}(s) = 1 - F_{\sigma W_T - \sum_{i=1}^{m} \hat{J}_i^+ + \hat{Z}_e^-}(-s).$$

In fact, these c.d.f.'s appear in the pricing formula as the functions $T_{i,j}$'s, defined in Section A.1. We now give the formula for the call option price. Recall the call price can be written as

$$C(S) = S\mathbb{E}\left\{ e^{(-\frac{\sigma^2}{2} - \frac{\alpha}{T} - \kappa\zeta)T + \sigma W_T + \sum_{i=1}^{N_T} J_i + Z_e} \mathbf{1}_{\{S_T > K\}} | S_0 = S \right\} - e^{-rT} K \mathbb{Q}\left\{ S_T > K | S_0 = S \right\}. \tag{A.2.13}$$

Using the results above, we can write

$$\begin{aligned}
& \mathbb{Q}\left\{S_T > K | S_0 = S\right\} && \text{(A.2.14)}\\
= & \sum_{n=1}^{\infty} \mathbb{Q}\left\{N_T = n\right\} \mathbb{Q}\left\{\sigma W_T + \sum_{i}^{n} J_i + Z_e > \log\left(\frac{K}{S}\right) - \left(r - \frac{\sigma^2}{2} - \frac{\alpha}{T} - \kappa\zeta\right) T\right\}\\
= & \sum_{n=1}^{\infty} \frac{\kappa^n e^{-\kappa}}{n!} \Bigg[u \sum_{m=1}^{n} \Bigg(P_{n,m} \mathbb{Q}\left\{\sigma W_T + \sum_{i}^{m} J_i^+ + Z_e^+ > k\right\} +\\
& Q_{n,m} \mathbb{Q}\left\{\sigma W_T - \sum_{i}^{m} J_i^- + Z_e^+ > k\right\}\Bigg) + w \sum_{m=1}^{n} \Bigg(P_{n,m} \mathbb{Q}\left\{\sigma W_T + \sum_{i}^{m} J_i^+ - Z_e^- > k\right\} +\\
& Q_{n,m} \mathbb{Q}\left\{\sigma W_T - \sum_{i}^{m} J_i^- - Z_e^- > k\right\}\Bigg)\Bigg]\\
= & \sum_{n=1}^{\infty} \frac{\kappa^n e^{-\kappa}}{n!} \Bigg[u \sum_{m=1}^{n} \left(P_{n,m} T_{1,n}(k,\Theta) + Q_{n,m} T_{2,n}(k,\Theta)\right) +\\
& w \sum_{m=1}^{n} \left(P_{n,m} T_{3,n}(k,\Theta) + Q_{n,m} T_{4,n}(k,\Theta)\right)\Bigg],
\end{aligned}$$

where $k \equiv \log\left(\frac{K}{S}\right) - \left(r - \frac{\sigma^2}{2} - \kappa\zeta\right) T - \alpha$.

It remains to compute

$$\begin{aligned}
& \mathbb{E}\left\{e^{\sigma W_T + \sum_{i=1}^{N_T} J_i + Z_e} \mathbf{1}_{\{S_T > K\}} | S_0 = S\right\} && \text{(A.2.15)}\\
& = \sum_{n=1}^{\infty} \frac{(\kappa T)^n e^{-\kappa T}}{n!} \Bigg[u \sum_{m=1}^{n} P_{n,m} \mathbb{E}\left\{e^{\sigma W_T + \sum_{i=1}^{m} J_i^+ + Z_e^+} \mathbf{1}_{\{\sigma W_T + \sum_{i=1}^{m} J_i^+ + Z_e^+ > k\}}\right\} + && \text{(A.2.16)}\\
& + u \sum_{k=1}^{n} Q_{n,k} \mathbb{E}\left\{e^{\sigma W_T - \sum_{i=1}^{m} J_i^- + Z_e^+} \mathbf{1}_{\{\sigma W_T - \sum_{i=1}^{m} J_i^- + Z_e^+ > k\}}\right\} + && \text{(A.2.17)}\\
& + w \sum_{k=1}^{n} P_{n,k} \mathbb{E}\left\{e^{\sigma W_T + \sum_{i=1}^{m} J_i^+ - Z_e^-} \mathbf{1}_{\{\sigma W_T + \sum_{i=1}^{m} J_i^+ - Z_e^- > k\}}\right\} + && \text{(A.2.18)}\\
& + w \sum_{k=1}^{n} Q_{n,k} \mathbb{E}\left\{e^{\sigma W_T - \sum_{i=1}^{m} J_i^- - Z_e^-} \mathbf{1}_{\{\sigma W_T - \sum_{i=1}^{m} J_i^- - Z_e^-\}}\right\}\Bigg]. && \text{(A.2.19)}
\end{aligned}$$

In order to compute the expectation in (A.2.16), we apply the p.d.f. from Prop. A.2.4 to

write

$$\begin{aligned}
&\mathbb{E}\left\{e^{\sigma W_T+\sum_{i=1}^m J_i^+ + Z_e^+}\mathbf{1}_{\{\sigma W_T+\sum_{i=1}^m J_i^+ + Z_e^+ > k\}}\right\} = \\
&= \int_k^\infty \int_{\mathbb{R}} \frac{e^{t-x}e^{-\frac{(t-x)^2}{2\sigma^2 T}}}{\sqrt{2\pi\sigma^2 T}} \int_{\mathbb{R}} e^{x-y} f_{\sum_{i=1}^m J_i^+}(x-y)\, e^y f_{Z_e^+}(y)\, dydxdt \\
&= \int_k^\infty \int_{\mathbb{R}} e^{\frac{\sigma^2 T}{2}} \frac{e^{-\frac{\left(t-x-\sigma^2 T\right)^2}{2\sigma^2 T}}}{\sqrt{2\pi\sigma^2 T}} \int_{\mathbb{R}} \left(\frac{\lambda_1}{\lambda_1-1}\right)^m f_{\sum_{i=1}^m \hat{J}_i^+}(x-y)\, \frac{\eta_1}{\eta_1-1} f_{\hat{Z}_e^+}(y)\, dydxdt \\
&= e^{\frac{\sigma^2 T}{2}} \left(\frac{\lambda_1}{\lambda_1-1}\right)^m \frac{\eta_1}{\eta_1-1} \mathbb{Q}\left(\sigma W_T + \sum_{i=1}^m \hat{J}_i^+ + \hat{Z}_e^+ > k - \sigma^2 T\right) \\
&= e^{\frac{\sigma^2 T}{2}} \left(\frac{\lambda_1}{\lambda_1-1}\right)^m \frac{\eta_1}{\eta_1-1} F_{\sigma W_T+\sum_{i=1}^m \hat{J}_i^+ + \hat{Z}_e^+}\left(k-\sigma^2 T\right), \qquad \text{(A.2.20)}
\end{aligned}$$

where $\hat{J}_i^+ \sim Exp\,(\lambda_1 - 1)$ and $\hat{Z}_e^+ \sim Exp\,(\eta_1 - 1)$. Expressions analogous to (A.2.20) can be found for the terms (A.2.17), (A.2.18) and (A.2.19). Substituting these expressions and rearranging terms, we get

$$\begin{aligned}
&\mathbb{E}\left\{e^{(-\frac{\sigma^2}{2}-\frac{\alpha}{T}-\kappa\zeta)T+\sigma W_T+\sum_{i=1}^N J_i+Z_e}\mathbf{1}_{\{S_T>K\}}|S_0=S\right\} \\
&= e^{-\alpha}\sum_{n=1}^\infty \frac{(\hat{\kappa}T)^n e^{-\hat{\kappa}T}}{n!}\left(\hat{u}\sum_{k=1}^n \left(\hat{P}_{n,k}T_{1,n}(k,\Theta) + \hat{Q}_{n,k}T_{2,n}(k,\Theta)\right) + \right. \\
&\left. \hat{w}\sum_{k=1}^n \left(\hat{P}_{n,k}T_{3,n}\left(\hat{k},\Theta\right) + \hat{Q}_{n,k}T_{4,n}\left(\hat{k},\Theta\right)\right)\right),
\end{aligned}$$

where $\hat{P}_{n,k}$, $\hat{Q}_{n,k}$ are calculated as $P_{n,k}$, $Q_{n,k}$ but with the parameters $\hat{\eta}_{1,2}, \hat{\lambda}_{1,2}$ in place of $\eta_{1,2}$ and $\lambda_{1,2}$. In addition, the Poisson intensity parameter has also been transformed to $\hat{\kappa} \equiv (m+1)\kappa$, with $m = p\frac{\lambda_1}{\lambda_1-1} + q\frac{\lambda_2}{\lambda_2+1} - 1$. Finally, substituting the expressions for (A.2.14) and (A.2.15) into (A.2.13) concludes the proof.

A.3 Proof of Propositions 2.5.1 and 2.5.2

The first part of Proposition 2.5.1 follows from Jensen's inequality, namely,

$$\begin{aligned}
C(t,S) &\geq \mathbb{E}\left\{e^{-r\tau}\left(Se^{r\tau+Z_e}-K\right)^+\right\} \\
&= \int_{\mathbb{R}^+} C_{BS}\left(\tau, S; \frac{\hat{\sigma}}{\sqrt{\tau}}, K, r\right)\mathbb{G}(d\hat{\sigma}) \geq C_{BS}\left(\tau, S; \frac{\hat{\sigma}_{min}}{\sqrt{\tau}}, K, r\right), \qquad \text{(A.3.1)}
\end{aligned}$$

where $\tau \equiv T - t$. In (A.3.1), the equality follows from the tower property of the conditional expectation and the last inequality follows from the monotonicity of C_{BS} w.r.t. the volatility parameter σ. The second part of the proposition is proved in a similar fashion.

To prove Proposition 2.5.2, we first observe that

$$C(t,S) = \int_{\mathbb{R}^+\times\mathbb{R}^+} C_{BS}\left(\tau, S; \sqrt{\frac{\tilde{\sigma}^2+\hat{\sigma}^2}{\tau}}, K, r\right) \mathbb{H}(d\tilde{\sigma})\,\mathbb{G}(d\hat{\sigma}).$$

For an ATM-forward option, i.e. $K = e^{r\tau}S$, we notice that the Black-Scholes price C_{BS} is concave in its volatility parameter σ. Consequently, by Jensen's inequality, we obtain the upper bound

$$C(t,S) \leq C_{BS}\left(\tau, S; \sqrt{\int_{\mathbb{R}^+}\frac{\tilde{\sigma}^2}{\tau}\mathbb{H}(d\tilde{\sigma}) + \int_{\mathbb{R}^+}\frac{\hat{\sigma}^2}{\tau}\mathbb{G}(d\hat{\sigma})}, K, r\right).$$

A.4 Proof of Propositions 2.5.4 and 2.5.5

Propositions 2.5.4 and 2.5.5 are applications of the more general results developed in Benaim and Friz (2008). Denote by $M(\omega) \equiv \mathbb{E}\left\{e^{\omega X}\right\}$ the m.g.f. of the r.v. X, and with F its c.d.f. As mentioned in Section 2.5, if $r^* \equiv \inf\{\omega \; s.t. \; M(\omega) < \infty\}$ is finite, than it follows that $\limsup_{x\to\infty}\frac{-\log(1-F(x))}{x} = r^*$. In turn, if F is well-behaved, the lim sup can be replaced by a lim and the tail asymptotics $\frac{-\log(1-F(x))}{x} \sim r^*x$, along with the condition $r^* > 1$ are sufficient to provide the asymptotics for the implied volatility

$$\frac{I^2(t;K,T)(T-t)}{\log\left(\frac{K}{S_t}\right)} \sim \xi\,(p^*), \quad \text{as } K \to \infty;$$

see Theorems 9 and 10 of Benaim and Friz (2008) for this result and the associated technical conditions. A symmetric argument holds for the negative tails of F and of the implied volatility. Therefore, given that the log stock price under the extended Kou and Heston models admits a m.g.f, it remains to prove that $\frac{-\log(1-F(x))}{x} \sim r^*x$. Theorem 7 and Theorem 8 in Benaim and Friz (2008) provide sufficient conditions for models admitting a m.g.f. to ensure that such condition holds.

The m.g.f. M of $X \equiv \log\left(\frac{S_T}{S_t}\right)$ under the extended Heston model (2.4.3), given $\sigma_t = \sigma$,

satisfies[3]

$$\begin{aligned}\log M(\omega) &= C + \omega D - \frac{\nu\vartheta}{\zeta^2}\left(2\log\left(\frac{1-ge^{-d(T-t)}}{1-g}\right) + d(T-t)\right) + \\ &\quad \frac{\nu-\rho\zeta\omega-d}{\zeta^2}\frac{1-e^{-d(T-t)}}{1-ge^{-d(T-t)}}\sigma^2 + \psi_e(\omega), \\ \text{with}\quad g &= \frac{\nu-\rho\zeta\omega-d}{\nu-\rho\zeta\omega+d}, \quad d = \sqrt{(\nu-\rho\zeta\omega)^2 + \zeta^2(\omega-\omega^2)}, \\ \psi_e(\omega) &= \log\left(u\frac{\eta_1}{\eta_1-\omega} + w\frac{\eta_2}{\eta_2+\omega}\right),\end{aligned}$$

where C and D are constants. Clearly, we have $r^* = \min\{p, \eta_1\}$, where p is the smallest positive solution of $1 - ge^{-d(T-t)}|_{\omega=p} = 0$. In turn, the last equation is equivalent to

$$\nu - \rho\zeta p + \sqrt{(\nu-\rho\zeta p)^2 + \zeta^2(p-p^2)}\coth\left(\frac{(T-t)}{2}\sqrt{(\nu-\rho\zeta p)^2 + \zeta^2(p-p^2)}\right) = 0.$$

Notice that, when $r^* = p$, the dominating term for $\omega \to p$ is $\frac{\nu-\rho\zeta\omega i-d}{\zeta^2}\frac{1-e^{-d(T-t)}}{1-ge^{-d(T-t)}}\sigma^2$. Using l'Hopital's rule, it follows that

$$\frac{p-\omega}{1-ge^{-d(T-t)}} \to \text{constant}, \quad \text{as } \omega \to p^-.$$

This means that $\frac{\nu-\rho\zeta\omega-d}{\zeta^2}\frac{1-e^{-d(T-t)}}{1-ge^{-d(T-t)}}\sigma_t^2$ is regularly varying of index 1 as a function of $\frac{1}{p-\omega}$ and Criterion II of Theorem 8 in Benaim and Friz (2008) is satisfied. When $r^* = \eta_1$, we have

$$M(\eta_1 - z) \sim u\eta_1 z^{-1} \text{ as } z \to 0^+,$$

and thus Criterion I of Theorem 7 in Benaim and Friz (2008) is satisfied. A similar argument holds for the negative tail.

Now consider the m.g.f. of $X \equiv \log\left(\frac{S_T}{S_t}\right)$ under the extended Kou model:

$$\log M(\omega) = \mu\omega + \frac{\sigma^2\omega^2}{2} + \kappa\left(p\frac{\lambda_1}{\lambda_1-\omega} + (1-p)\frac{\lambda_2}{\lambda_2+\omega} - 1\right) + \log\left(u\frac{\eta_1}{\eta_1-\omega} + (1-u)\frac{\eta_2}{\eta_2+\omega}\right),$$

where μ is a constant. This m.g.f. satisfies the tail asymptotics condition with $r^* = \min\{\lambda_1, \eta_1\}$, and

$$\begin{cases}\log M(\lambda_1 - z) \sim \kappa p\lambda_1 z^{-1} \text{ as } z \to 0^+ & if\ \lambda_1 \le \eta_1, \\ M(\eta_1 - z) \sim u\eta_1 z^{-1} \text{ as } z \to 0^+ & if\ \lambda_1 > \eta_1.\end{cases}$$

[3]For the derivation of the Heston m.g.f., see, e.g. del Baño Rollin et al. (2009).

Hence, M satisfies either Criterion I or II (depending on whether $\lambda_1 > \eta_1$ or not) of Theorems 7 and 8 in Benaim and Friz (2008). A similar argument holds for the negative tail.

A.5 Proof of Proposition 2.7.1

Let $A(t,S;u)$ be the American put price when the earnings announcement is scheduled at time $T_e = u,\ t < u \leq T$. Our goal is to show that $A(t,S;u) \geq A(t,S;l)$, for $t < u \leq l$. W.l.o.g., let $t = 0$ and write $A(S;l) \equiv A(0,S;l)$. Let $X_s = \log(S_s/S_0) - 1_{\{s \geq T_e\}} Z_e$ be the log stock price excluding the EA jump, and denote by $(\mathcal{F}^u_s)_{0 \leq s \leq T}$ (resp. $(\mathcal{F}^l_s)_{0 \leq s \leq T}$) the filtration generated by S with $T_e = u$ (resp. $T_e = l$). Notice that $\mathcal{F}^l_s = \mathcal{F}^u_s$ for $s < u$ or $s \geq l$, and $\mathcal{F}^l_s \subset \mathcal{F}^u_s$, for $u \leq s < l$. Therefore, the sets of stopping times w.r.t to $\mathcal{F}^u$ and $\mathcal{F}^l$, denoted respectively by $\mathcal{T}^u$ and $\mathcal{T}^l$, satisfy $\mathcal{T}^l \subset \mathcal{T}^u$. Thus, for any candidate stopping time $\tau \in \mathcal{T}^l$, we have

$$\mathbb{E}\left\{e^{-r\tau}\left(K - Se^{X_\tau + 1_{\{\tau \geq u\}} Z_e}\right)^+ | \mathcal{F}^l_{l-}\right\} \tag{A.5.1}$$

$$= \mathbb{E}\left\{1_{\{\tau < l\}} e^{-r\tau}\left(K - Se^{X_\tau + 1_{\{\tau \geq u\}} Z_e}\right)^+ | \mathcal{F}^l_{l-}\right\} +$$

$$\mathbb{E}\left\{1_{\{\tau \geq l\}} e^{-r\tau}\left(K - Se^{X_\tau + 1_{\{\tau \geq u\}} Z_e}\right)^+ | \mathcal{F}^l_{l-}\right\} \tag{A.5.2}$$

$$\geq \mathbb{E}\left\{1_{\{\tau < l\}} e^{-r\tau}\left(K - Se^{X_\tau}\right)^+ | \mathcal{F}^l_{l-}\right\} +$$

$$\mathbb{E}\left\{1_{\{\tau \geq l\}} e^{-r\tau}\left(K - Se^{X_\tau + 1_{\{\tau \geq l\}} Z_e}\right)^+ | \mathcal{F}^l_{l-}\right\} \tag{A.5.3}$$

$$= \mathbb{E}\left\{e^{-r\tau}\left(K - Se^{X_\tau + 1_{\{\tau \geq l\}} Z_e}\right)^+ | \mathcal{F}^l_{l-}\right\}. \tag{A.5.4}$$

The inequality holds as follows. In the first term of (A.5.2), given the information in $\mathcal{F}^l_{l-}$ and on $\{\tau < l\}$ the values of τ and X_τ are known, we apply Jensen's inequality to get the first term in (A.5.3). In addition, since $\tau \geq l$ implies that $\tau \geq u$, the second terms of (A.5.2) and (A.5.3) are equal. The last equality follows from the fact that $1_{\{\tau \geq l\}} = 0$ on $\{\tau < l\}$.

In turn, taking expectations in (A.5.1) and (A.5.4) and maximizing both sides over $\mathcal{T}^l$, we get

$$A(S;u) \geq \sup_{\tau \in \mathcal{T}^l} \mathbb{E}\left\{e^{-r\tau}\left(K - Se^{X_\tau + 1_{\{\tau \geq u\}} Z_e}\right)^+\right\} \geq A(S;l),$$

where the first inequality follows from the inclusion $\mathcal{T}^l \subset \mathcal{T}^u$.

A.6 Barone-Adesi Approximation

Here we give a sketch of the derivation of the approximation formula (2.7.7). The arguments are adapted from Barone-Adesi and Whaley (1987) and Kou and Wang (2004). We start by writing

$$A(t,S) = P_E(t,S) + \epsilon(t,S),$$

where P_E is the European put price with an EA jump, and ϵ is a correction term. Note that P_E is computed using the results in Proposition 2.4.1. In the continuation region, ϵ must satisfy the same PIDE as that of P_E and A, namely

$$r\epsilon(t,S) - \partial_t \epsilon(t,S) - \mathcal{L}\epsilon(t,S) = 0, \tag{A.6.1}$$

where the operator $\mathcal{L}$ is defined in (2.7.5). The idea of the approximation in Barone-Adesi and Whaley (1987) is to remove the term ϵ_t in (A.6.1). This involves letting $\epsilon(t,S) \equiv g(z,S)\,z$, with $z \equiv 1 - e^{-r(T-t)}$, substituting in the above PIDE, and ignoring the term $(1-z)\,g_z$. This results in the OIDE

$$\frac{r}{z}\epsilon(t,S) - \mathcal{L}\epsilon(t,S) = 0. \tag{A.6.2}$$

While (A.6.2) holds in the continuation region, in the exercise reason we have $\epsilon(t,S) = K - S - P_E(t,S)$. Following Kou and Wang (2004), we consider the ansatz

$$\epsilon(t,S) = \begin{cases} \gamma_1(t)\,S^{-\beta_1} + \gamma_2(t)\,S^{-\beta_2} & , \quad S > \alpha(t), \\ K - S - P_E(t,S) & , \quad S \le \alpha(t), \end{cases}$$

where $\alpha(t)$ is the boundary at time t. One can directly verify that the ansatz solves the OIDE (A.6.2) if $\beta_{1,2}$ are two positive solutions to 2.7.10, and if

$$\frac{K}{\lambda_2} - \frac{\alpha(t)}{1+\lambda_2} - \int_{-\infty}^{0} P_E(t,\alpha e^y)\,e^{\lambda_2 y}dy = \gamma_1(t)\,\frac{\alpha^{-\beta_1}}{\lambda_2-\beta_1} + \gamma_2(t)\,\frac{\alpha^{-\beta_2}}{\lambda_2-\beta_2}, \tag{A.6.3}$$

In turn, we impose the continuous-fit and smooth-pasting conditions. The first condition yields (2.7.11) while the second condition, altogether with (A.6.3), yields the constants γ_1 and γ_2 in (2.7.8) and (2.7.9).